

Luminescent Silver Sulfide Clusters in Zeolite A

Inauguraldissertation
der Philosophisch-naturwissenschaftlichen Fakultät
der Universität Bern

vorgelegt von

Claudia Leiggener

von Ausserberg (VS)

Leiter der Arbeit:

Prof. Dr. G. Calzaferri

Departement für Chemie und Biochemie
der Universität Bern

Luminescent Silver Sulfide Clusters in Zeolite A

Inauguraldissertation
der Philosophisch-naturwissenschaftlichen Fakultät
der Universität Bern

vorgelegt von

Claudia Leiggener

von Ausserberg (VS)

Leiter der Arbeit:

Prof. Dr. G. Calzaferri

Departement für Chemie und Biochemie
der Universität Bern

Von der Philosophisch-naturwissenschaftlichen Fakultät angenommen

Bern, den 27. Januar 2005

Der Dekan

Prof. Dr. Paul Messerli

Thanks

First I thank my supervisor Prof. Dr. Gion Calzaferri for giving me the opportunity to work on such an interesting topic and for always encouraging me in my work. I enjoyed the positive work climate in his group and the freedom he gave me in my research project.

I would like to thank Prof. Dr. Daniel Vanmaekelbergh who was so kind to read my PhD thesis and to act as co-referee.

Thanks to everybody who helped me to realize my experiments, namely René Schraner and Kurt von Escher for the electronics, René Bühler for his assistance in the lab, and Ueli Kindler and his team for repairing everything.

Special thanks go to Beatrice Frey for the SEM and the EDX analysis.

I thank all former and current group members for the pleasant atmosphere. Special thanks go to Dominik Brühwiler who introduced me into the world of luminescent silver sulfide clusters, and to Arantzazu Zabala Ruiz, Olivia Bossart, Claudia Minkowski, and Stefan Huber for the inspiring coffee breaks.

I also want to thank my fellow students with whom I had a great time during all my studies, especially Claudia Loosli, Regina Schreier, Sandra Soverna, and Timo Barrelet for the lunches we spent together.

Last but not least, a big thank-you goes to my boyfriend Emanuel Stoll and to my parents who always supported my decisions.

Contents

1. Introduction	1
1.1 Molecules, clusters, and nanoparticles	1
1.2 Silver sulfide clusters	2
2. The Zeolite A - Ag₂S/ Host-Guest System	5
2.1 Zeolite A - structure, morphology, and ion exchange	5
2.2 Ag ⁺ -exchanged zeolite A	9
2.2.1 Chapter of the Publication	9
<i>"The electronic structure of Cu⁺, Ag⁺, and Au⁺ zeolites"</i>	
2.2.2 Ag ⁺ -exchange in K ⁺ -zeolite A	11
2.3 Silver sulfide	13
2.4 The "ship-in-a-bottle" synthesis	13
2.5 Summary	15
3. Optical Properties of Ag₂S-Zeolite A Materials	17
3.1 Ag ₂ S-CaA-x	17
3.1.1 Influence of the silver loading	17
3.1.2 Influence of the environment	27
3.1.3 Summary	28
3.1.4 Publication	29
<i>"Luminescence properties of Ag₂S and Ag₄S₂ in zeolite A"</i>	
3.2 Ag ₂ S-MA-x	44
3.2.1 Absorption	46
3.2.1 Luminescence	46
3.2.3 Stability	50
3.3 Conclusions	52
4. Monolayers of Zeolite A Containing Luminescent Silver Sulfide Clusters	55
4.1 Publication	56
4.2 Luminescence thermochromism of Ag ₂ S-KA-x	63
4.3 Laser action	64

4.4 Monolayers on different substrates	65
4.5 Conclusions	69
5. Silver Sulfide Clusters in other Zeolites	71
5.1 Zeolite L	71
6. Experimental	75
6.1 Synthesis of zeolite A	75
6.2 Synthesis of silver sulfide clusters	79
6.3 Spectroscopy	81
6.3.1 Sample preparation	81
6.3.2 Absorption spectra	81
6.3.3 Luminescence spectra	81
6.3.4 Time-resolved luminescence spectra	82
6.3.5 Laser experiments	86
6.4 Preparation of zeolite A monolayers	87
6.4.1 Size separation of zeolite A crystals	87
6.4.2 Preparation of monolayers	89
6.5 Ag ⁺ /K ⁺ ion exchange isotherms	89
6.5.1 Experimental	89
7. Conclusions and Outlook	91
8. References	95
9. Summary	99
Appendix	
List of Publications	101
Conference Contributions	103
Curriculum Vitae	105

1. Introduction

1.1 Molecules, clusters, and nanoparticles

Materials properties change if one goes from single atoms or molecules to solids. Clusters or nanoparticles present a state of matter which lies between the smallest element of the material (atom or molecule) and its bulk phase. In general the name “cluster” is used for an aggregate of a small number of atoms, while a nanoparticle lies in the nanometer size regime and often consists of several hundreds of atoms. One property, which can change with particle size, is the color of the material. This phenomenon is called quantum size effect and is often observed in semiconductors.

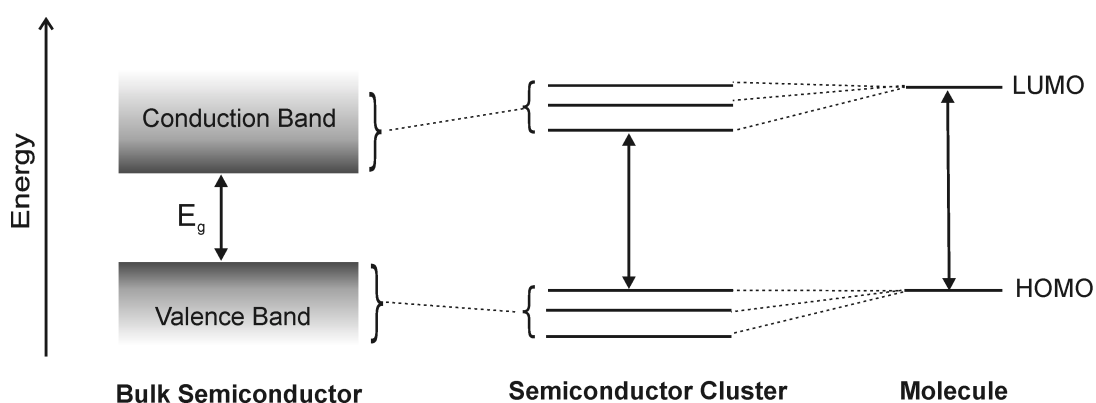


Figure 1.1.1: Correlation scheme relating the energy levels of the bulk phase, of clusters and of the monomer of a semiconductor.

The development of the energy levels from a molecule to a cluster to the bulk phase of a semiconductor is illustrated in Figure 1.1.1. By aggregation of molecules into a cluster, the HOMO and the LUMO of the monomer split into several delocalized molecular orbitals, the number of which depends on the cluster size. In the bulk phase continuous bands of energy levels instead of discrete levels are formed. The energy gap between valence band and conduction band is called band gap E_g . Depending on the band gap of the semiconductor the electrons of the valence band can be thermally or electronically excited to the conduction band. By exciting an electron to the conduction band one creates a hole in the valence band. The electron and the hole are bound together by a screened Coulomb interaction to form a so-called Mott-Warnier exciton with a materials dependent exciton Bohr radius.^[1,2] Quantum size effects occur when the radius of the

semiconductor cluster becomes comparable to the bulk exciton radius. The energy of the first excited state of the cluster is shifted by

$$\Delta E = \frac{h^2}{8m_{\text{eff}}r^2} \quad (1.1.1)$$

from its energy in the bulk material, where h is the Planck constant, m_{eff} is the effective mass of the electrons and holes, and r is the cluster radius. This means that the band gap increases with decreasing cluster size as $1/r^2$. The electronic spectra of clusters are then blue-shifted compared to the bulk resulting in a color change of the material.

Quantum size effects have been observed on a number of semiconductors such as Zn- and Pb-chalcogenides,^[3-5] while a lot of work has been done on Cd-chalcogenide compounds. Cd-chalcogenide nanoparticles show a large quantum size effect (exciton Bohr radius 5.6 nm for CdSe^[1]) and are well studied objects with fascinating properties such as photo-, electro- and chemiluminescence.^[6-8] The color of the emitted light can be tuned over a large spectral range by selecting nanoparticles of different size. This makes them interesting for applications in LEDs and display devices.

1.2 Silver sulfide clusters

Silver sulfide is a semiconductor as well and thus is expected to show quantum size effects in small enough clusters. The electronic transition from the valence band to the conduction band of bulk α -Ag₂S is essentially a charge transfer from 3p(S) to 5s(Ag) states. This property is kept for the HOMO-LUMO transition of Ag₂S monomers.^[9] Extended Hückel molecular orbital calculations of Ag₂S monomers were carried out by Dominik Brühwiler^[10] and Stephan Glaus^[11] and are summarized in Figure 1.2.1. The model Ag₂S has a bond angle of 112° and an Ag-S bond length of 2.42 Å. There are 4 strong transitions between 300 nm and 400 nm which are expected to be observed in the absorption spectrum, while the HOMO-LUMO transition has a very weak oscillator strength.

Until recently there were no spectroscopic data available for small (Ag₂S)_n-clusters and especially the Ag₂S molecule. This may be due to the fact that Ag₂S shows a strong tendency for aggregation into bulk. Several methods have been developed for the synthesis of silver sulfide clusters. By using different kind of polymers as stabilizing agents^[12-15] or by implantation into silica glass^[16] silver sulfide clusters of a few nanometers were synthesized. However, the first silver sulfide clusters showing a significant blue-shift in the absorption spectra were synthesized by Dominik Brühwiler.^[9,10] He developed a

method for synthesizing silver sulfide clusters in zeolite A. Due to the small dimensions of the zeolite cages the size of the clusters is limited to less than 15 Å. The silver sulfide clusters stay after the synthesis as guests inside the zeolite cages yielding very stable materials. This means that small silver sulfide clusters in the molecular dimension can be stabilized and investigated. These host-guest systems were found to reveal interesting photoluminescence properties depending on the cluster size. The aim of this thesis was to deeper investigate these luminescence properties and to study the influence of different factors on the synthesis and properties of the silver sulfide clusters.

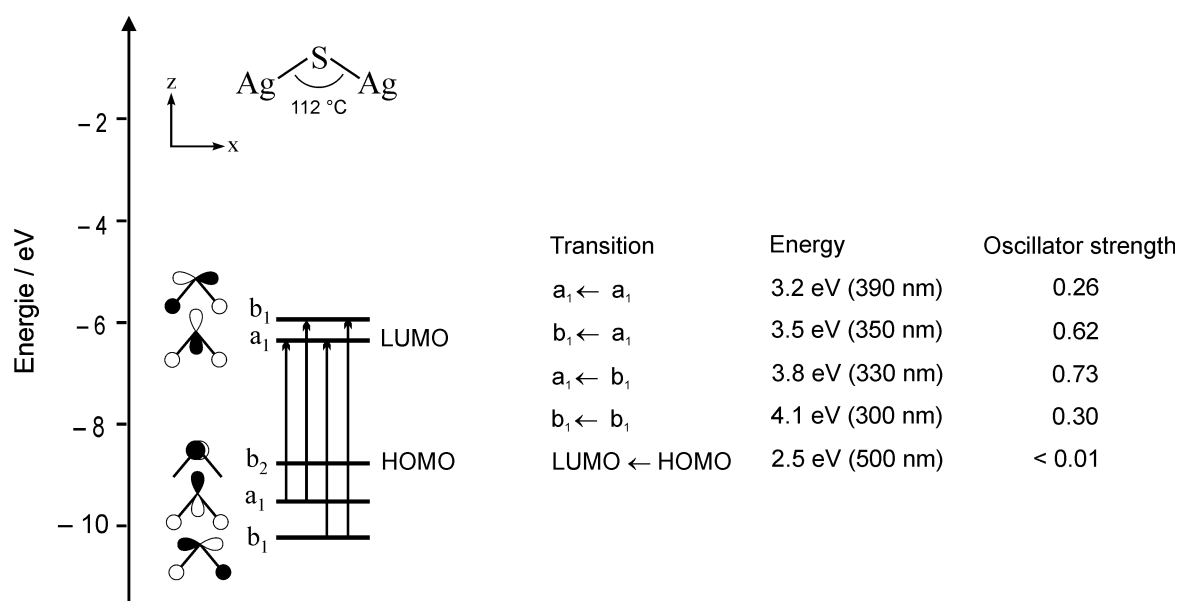


Figure 1.2.1: Energy level diagram of a Ag_2S molecule with the calculated transition energy and oscillator strengths.^[17]

2. The Zeolite A - Ag₂S / Host-Guest System

Zeolites are porous crystalline materials which are used in a broad field of applications. Due to their ion exchange capability they can act as water softeners and their well defined cavities allow size-selective reactions, for example in catalysis, or removal of pollutants. Some examples are given in Refs. [18-22]. Zeolites are also suitable hosts for supramolecular organization of different kinds of molecules, clusters, and metal complexes.^[23] The cages of zeolite A turned out to be convenient for hosting small ions and semiconductor clusters.^[24-26] In this work zeolite A was chosen as a host for the synthesis of silver sulfide clusters in the size regime of a few Å. The zeolite prevents the small silver sulfide particles from aggregation into larger clusters or bulk.

The optical properties of zeolite A - Ag₂S / host-guest materials strongly depend on the amount of silver sulfide inside the zeolite and will be discussed in chapter 3. In this chapter some properties of zeolite A are introduced and the principle of the “ship-in-a-bottle” synthesis of silver sulfide clusters is described.

2.1 Zeolite A - structure, morphology, and ion exchange

The framework of zeolite A is built up by SiO₄ and AlO₄ tetrahedra. The tetrahedra are connected over the oxygen atoms in the corners resulting in a larger building unit called β-cage (or sodalite cage) which is shown in Figure 2.1.1B. The oxygen bridges are represented as black lines where the blue dots stand for Si and Al atoms. Eight β-cages are linked together over the 4-membered rings giving rise to a larger cavity called α-cage. The diameter of the α-cage is 11.4 Å while the largest window (8-ring, see Figure 2.1.1C) has a diameter of 4.1 Å. The negative charge of the framework is compensated by cations which are located at different positions in the framework. Under ambient conditions the cations are coordinated to water molecules, which are also present inside the zeolite cages. In dehydrated zeolites the cations have three different possibilities for coordination to the oxygen atoms of the framework. Either they coordinate to a 4-membered ring (18 sites/α-cage), or to a 6-membered ring (8 sites/α-cage), or to a 8-membered ring (3 sites/α-cage). In the case of the 4-membered ring one can distinguish between two different positions, position S 4S in the β-cage (12 sites) and position S 4L in the α-cage (6 sites). In common zeolite A the amounts of Si and Al are equal and the corresponding tetrahedra alternate. So, for charge compensation 12 monovalent or 6 divalent cations per α-cage are needed, leading to the formula M₁₂[(AlO₂)₁₂(SiO₂)₁₂] or M₆[(AlO₂)₁₂(SiO₂)₁₂], respectively, where M stands for the cations.

This formula is also named pseudo unit cell and is more convenient than the crystallographic unit cell, which consists of eight pseudo unit cells.

A typical synthesis procedure yields cubic crystals with the composition Na₁₂[(AlO₂)₁₂(SiO₂)₁₂]·27 H₂O and chamfered edges as shown in Figure 2.1.1D. Other cation forms can be prepared by ion exchange in aqueous solution. For small cations like Na⁺ and Ca²⁺ ions the most occupied position is S 6 in the 6-membered ring. In one pseudo unit cell eight Na⁺ are located at S 6, three Na⁺ at S 8, and one Na⁺ at S 4S. In the case of Ca₆[(SiO₂)₁₂(AlO₂)₁₂] all six Ca²⁺ are coordinated to S 6.

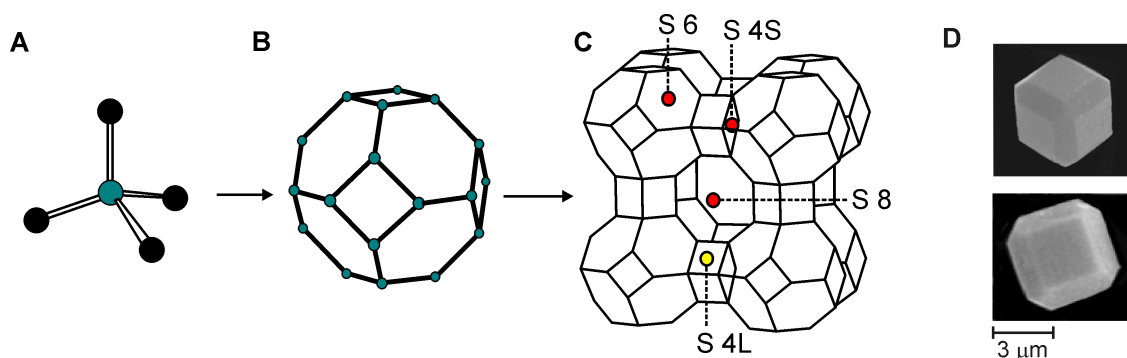
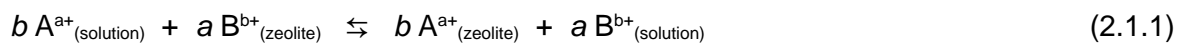


Figure 2.1.1: Scheme of the building units of zeolite A (A-C) and electronmicrographic image of typical zeolite A crystals (D). In C the framework of zeolite A with its crystallographically identified cation positions is shown.

All Na⁺ ions be can be exchanged with other monovalent or divalent cations at room temperature. In a suspension of zeolite A in water the cations inside the zeolites are in equilibrium with the cations in solution:^[27]



The equivalent fractions of the exchanging cation *A* in the solution *S*(*A*) and in the zeolite *Z*(*A*) are defined by:

$$S(A^{a+}) = \frac{a A^{a+}_{(\text{solution})}}{b B^{b+}_{(\text{solution})} + a A^{a+}_{(\text{solution})}} \quad (2.1.2)$$

$$Z(A^{a+}) = \frac{n_A}{N_A} \quad (2.1.3)$$

where n_A is the number of equivalents of the exchanging cation A^{a+} and N_A is the total number of equivalents in the zeolite according to the stoichiometric composition. For zeolite A $N_A = 12$ for monovalent cations and $N_A = 6$ for divalent cations.

The order of decreasing selectivity for monovalent cations in zeolite A is according to Ref. [27]:

$Ag > Tl > Na > K > NH_4 > Rb > Li > Cs$

For divalent cations, the order of decreasing selectivity is:

$Zn > Sr > Ba > Ca > Co > Ni > Cd > Hg > Mg$

The ion exchange properties are often described by means of ion exchange isotherms. The ion exchange isotherm is a plot of $Z(A^{a+})$ as a function of $S(A^{a+})$ at a given total concentration in the equilibrium solution and at a constant temperature. Depending on the ion pair one can classify different types of exchange isotherms.^[27] As an example the ion exchange isotherms of the ion pair Ag^+/K^+ in zeolite A measured at different temperatures are shown in Figure 2.1.2.^[28] It demonstrates that the entering cation Ag^+ is initially preferred over the leaving cation K^+ .

In practice, one can use ion exchange isotherms for calculating the precise amount of the exchanging cation needed for a specific exchange degree (Z). Complete ion exchange can be achieved for a lot of ion pairs by suspending the zeolites several times in an excess of the corresponding aqueous salt solution.

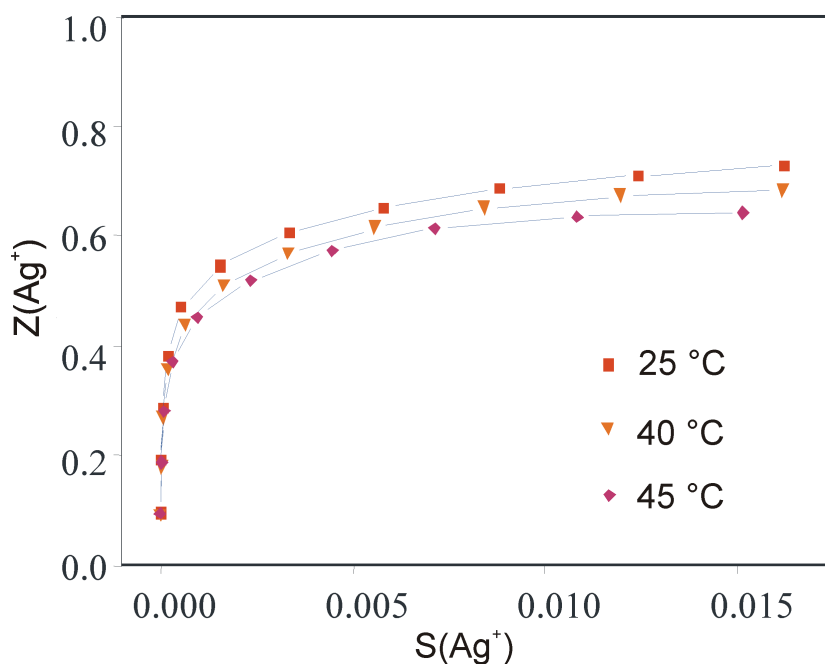


Figure 2.1.2: Ion exchange isotherms of the system Ag^+/K^+ -zeolite A at different temperatures. The isotherms were measured in 0.1 M aqueous KNO_3 solution.

Depending on the charge compensating cations the effective pore size of zeolite A changes. This can be tested by gas adsorption (e.g. N₂, Ar) on dehydrated zeolites. The gas adsorption isotherms give information about the occupation of the S 8 sites. It was found that Ca²⁺-zeolite A adsorbs molecules up to a size of 5 Å while Na⁺-zeolite A only adsorbs molecules smaller than 4 Å.^[29] The difference is due to the occupation of the S 8 site by three Na⁺ per pseudo unit cell. In K⁺-zeolite A the S 8 position is occupied as well, resulting in an effective pore size of 3 Å, because the ionic radius of K⁺ is larger than the ionic radius of Na⁺. The different effective pore size of these three cation-forms of zeolite A gave them the names Linde type 5A, 4A, and 3A, respectively.

Zeolite ZK-4 has the same framework as zeolite A but the Si/Al ratio is > 1 and thus the number of cations per pseudo unit cell is smaller than 12. The typical synthesis procedure used in this work yields crystals with the composition Na₉[(AlO₂)₁₅(SiO₂)₉]·nH₂O. This means that the less favored cation positions are not occupied. Gas adsorption experiments showed that the S 8 positions are free.^[30]

2.2 Ag⁺-exchanged zeolite A

In this chapter the electronic properties of Ag⁺-exchanged zeolite A will be discussed. It will be shown that they depend on the amount of exchanged silver ions (silver loading x) and the co-cations which influence the occupation probability of Ag⁺ at specific cation sites. The silver loading x expresses the number of Ag⁺ per α -cage and can take any value between 0 and 12. The abbreviations Ag⁺ _{x} Na⁺_{12- x} A, and Ag⁺ _{x} Ca²⁺_{6-0.5 x} A, and so on are used for differently loaded samples where A stands for the framework of zeolite A.

2.2.1 Chapter of the Publication: “The electronic structure of Cu⁺, Ag⁺, and Au⁺ zeolites” *Chem. Soc.Rev.* **2003**, *32*, 29-37.

Gion Calzaferri^{a)}*, Claudia Leiggner^{a)}, Stephan Glaus^{a)}, David Schürch^{a)}, Ken’ichi Kuge^{b)}

^{a)} Department of Chemistry and Biochemistry,
University of Bern, Freiestrasse 3, CH-3000 Bern 9, Switzerland

^{b)} Faculty of Engineering, Chiba University, 1-33 Yayoi-cho, Inage-ku, Chiba 263, Japan

A variety of procedures have been used to prepare d¹⁰-zeolite materials. The electronic structure of these materials can be regarded in a first approximation as a superposition of the framework, of the charge compensating ions, of solvent molecules and of guest species. Zeolite oxygen to d¹⁰-ion charge transfer transitions dominate the electronic spectra if the ions coordinate to the zeolite oxygens. Specific coordination sites can influence the energy and the intensity of these transitions remarkably. Intra guest transitions dominate in quantum dot materials, as discussed in detail for luminescent Ag₂S zeolite A. The zeolite is not needed for the photocatalytic water oxidation on Ag⁺/AgCl photo anodes with visible light. It can, however, be used to increase the active surface area substantially.

4 The electronic structure of Ag⁺ zeolite A

Rálek et al. reported in 1962 that hydrated colorless zeolite Ag⁺ _{x} Na⁺_{12- x} A turns yellow to brick-red on activation [31]. No explanation of this phenomenon was given at that time. Later it was believed that the color change was due to formation of silver clusters (Ag⁰ _{n}) in the cavities of silver zeolite A. These neutral silver species were assumed to be formed at elevated temperatures via an auto-reduction process in which O₂ from the zeolite framework was released [32]. We studied the vibrational spectra of Ag⁺ zeolite A materials in some detail [33], and we showed that activation at room temperature under high vacuum is already sufficient to produce the yellow form of Ag⁺ _{x} Na⁺_{12- x} A. The fully reversible

color change, which depends on the hydration state of the silver zeolite, was attributed to electronic charge transfer transitions from the oxygen lone pairs of the zeolite framework to the empty 5s orbital of the Ag⁺ ions, denoted as Ag⁺(5s)←O(n) [34]. Silver containing sodium zeolite A is colorless in its fully hydrated form. In activated silver zeolite A materials, the Ag⁺ is forced to coordinate zeolite oxygen because an insufficient number of available water molecules is present. The question remained if specific coordination sites which act as yellow and/or red „color centers” can be identified. We answered this question by studying the UV/vis spectra of Ag⁺ _{x} Na⁺_{12- x} A and of Ag⁺ _{x} Ca²⁺_{6-0.5 x} A materials in their fully hydrated, in HV room temperature dehydrated, and in HV elevated

temperature dehydrated states. The possible ion positions in $\text{Ag}_x^+\text{Ca}^{2+}_{6-0.5x}\text{A}$, probed by gas adsorption experiments, offered the unique possibility of investigating different coordination sites of Ag^+ ions in zeolite A [35]. Pure sodium and calcium zeolite A do not absorb light within the spectral range from 200 - 1000 nm we have investigated. This means that any absorption band or colors observed in silver zeolite A materials are due to the presence of silver ions. Figure 9 shows the different colors of a $\text{Ag}_6^+\text{Na}_6^+\text{A}$ zeolite in its fully hydrated state (white), after activation under high vacuum (2×10^{-7} mbar) at room temperature (deep yellow) and after heating in the vacuum to 200 °C (red). The spectrum of the yellow sample is fully reversible. After readsorption of water the yellow samples turn white again and the absorption spectrum is the same as before the activation.

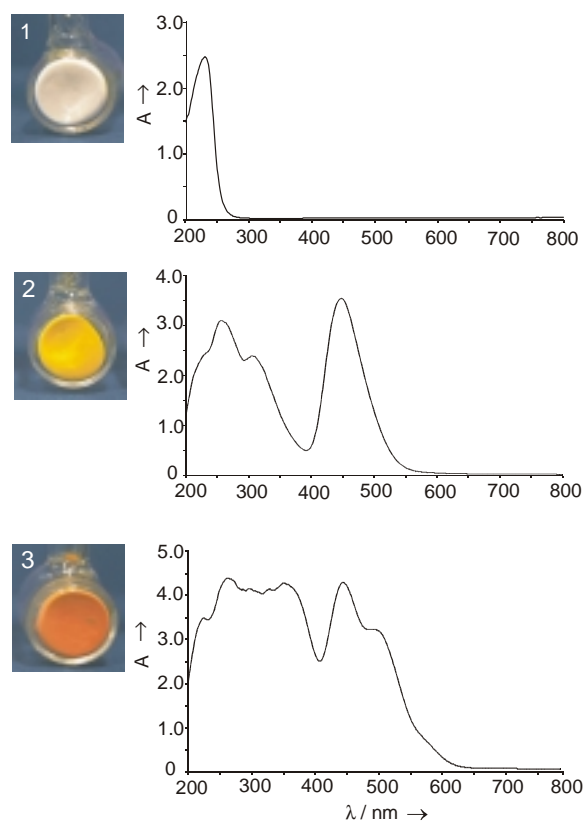


Figure 9: Samples (left) and the corresponding UV/Vis spectra (right) of $\text{Ag}_6^+\text{Na}_6^+\text{A}$ in its fully hydrated state (1), after activation in high vacuum at room temperature (2), and after activation in high vacuum at 200 °C (3).

We found that 6- and 8-ring coordinated Ag^+ give rise to electronic transitions in the near UV region. An absorption in the visible, namely at 450 nm, was only observed in materials where 4-ring coordinated Ag^+ was present and only they showed the typical deep yellow color. We also observed that Ag^+ avoids the 4-ring sites as long as possible in $\text{Ag}_x^+\text{Ca}^{2+}_{6-0.5x}\text{A}$, namely as long as x is smaller than 10. In the case of $\text{Ag}_x^+\text{Na}^{12-x}\text{A}$ either a Na^+ or a Ag^+ is forced to coordinate a 4-ring site because all other places are occupied. The presence of the 450 nm absorption responsible for the yellow color, already at $x < 0.2$, proves that isolated Ag^+ ions are sufficient to cause it and that the 4-ring coordination of Ag^+ is significantly stronger than that of the Na^+ . The red color of elevated temperature activated samples is caused by a strong absorption band at 520 nm. We observed that samples which remained colorless after room temperature activation never turned red, that samples with lower silver content than one Ag^+ per α -cage never turn red, and that room temperature dehydration under our experimental conditions was not sufficient to produce red colored samples. These observations strongly indicate that only samples with 4-ring coordinated Ag^+ can give rise to the 520 nm band and this only occurs if a second Ag^+ is not too far away at a 6-ring site, so that they can interact to develop a corresponding low lying state.

Molecular orbital calculations carried out on a sufficiently large zeolite part consisting of 1296 atoms allowed us to address questions about the nature of the HOMO and of the LUMO region, about the contributions of the zeolite framework atoms to the electronic transitions, about the influence of the local symmetry of the Ag^+ at 4- and at 6-ring sites, and about the importance of $\text{Ag}^+ - \text{Ag}^+$ interactions.

We found that 6-ring coordinated Ag^+ give rise to electronic transitions in the near UV and that the 4-ring coordinated Ag^+

is responsible for the deep yellow color of the room temperature activated material. This implies that similar $\text{Ag}^+(5s) \leftarrow \text{O}(n)$ LMCT transitions are to be expected in other Ag^+ exchanged zeolites. Ag^+ exchanged zeolite Y can be used as a test. We therefore measured UV/vis spectra of pure Na^+_{69}Y , of room temperature HV dehydrated Ag^+_{69}Y , and rehydrated Ag^+_{69}Y . The main result is that an intense band at about $34'000 \text{ cm}^{-1}$ appears upon dehydration which vanishes upon rehydration [35]. Analogously one would expect a similar type of LMCT transitions in Cu^+ zeolite materials. $\text{Cu}^+(4s) \leftarrow \text{O}(n)$ LMCT transition, reversible upon HV hydration/dehydration, have indeed been observed in Cu^+ zeolite A and X [36].

Based on all the information which has been collected over the last few years, we can now draw the schematic state diagram in Figure 10 for Ag^+ containing zeolites.

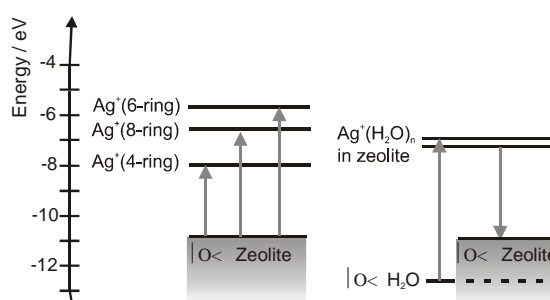


Figure 10: State diagram of Ag^+ -loaded zeolite A. On the left side we show the levels observed in room temperature activated zeolites in which all three sites are occupied by silver ions, while the scheme on the right side corresponds to situations typically observed in $\text{Ag}^+_x\text{Ca}^{2+}_{6-0.5x}\text{A}$ materials containing some water.

2.2.2 Ag^+ -exchange in K^+ -zeolite A

K^+ -zeolite A has the same amount of cations as Na^+ -zeolite A and the K^+ ions are expected to occupy the same coordination sites in the dehydrated zeolite as the Na^+ do. However, the affinity for specific sites is different. The observation that $\text{Ag}^+_x\text{Na}^+_{12-x}\text{A}$ turns yellow on dehydration already at very low silver loading ($x < 0.2$) led to the conclusion that first the Na^+ ions in the 4-membered ring are exchanged with Ag^+ , because only 4-ring coordinated Ag^+ give rise to transitions in the visible, while 6-ring and 8-ring coordinated Ag^+ are responsible for transitions in the UV. This means that the affinity of the 4-membered ring is higher for Ag^+ than for Na^+ , or the affinity of the 6- and 8-membered rings is higher for Na^+ than for Ag^+ . I observed that the situation changes if one uses K^+ -zeolite A instead of Na^+ -zeolite A. At a silver loading of $x = 2$ dehydrated K^+ -zeolite A is still brilliant white. Only at higher silver loadings ($x > 3$) the samples start slowly to turn yellow on dehydration. At a silver loading of $x = 6$ the color is as intense as in the corresponding $\text{Ag}^+_x\text{Na}^+_{12-x}\text{A}$ samples. Figure 2.2.1 shows a photographic picture of dehydrated $\text{Ag}^+_x\text{K}^+_{12-x}\text{A}$ samples with different silver loading.

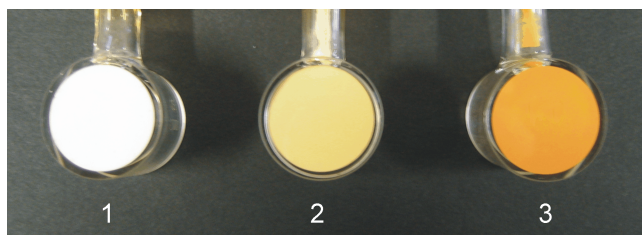


Figure 2.2.1: Photographic picture of dehydrated $\text{Ag}^+_x\text{K}^{12-x}\text{A}$ samples with different x . 1) $x = 2$, 2) $x = 5$, 3) $x = 6$. The samples are sealed in airtight quartz ampoules.

This observation also corresponds to the absorption spectra in Figure 2.2.2. Samples with a silver loading of $x < 3$ only reveal absorption bands in the UV which can be assigned to charge transfer transitions of 6-ring coordinated Ag^+ ions.^[30] The band at 450 nm which is responsible for the yellow color starts to rise at a silver loading of $x = 4$ and becomes intense at $x \geq 6$. Its position is the same as in $\text{Ag}^+_x\text{Na}^{12-x}\text{A}$. These results indicate that first three to four K^+ in 6-ring positions are exchanged with Ag^+ before the K^+ in the 4-ring is exchanged.

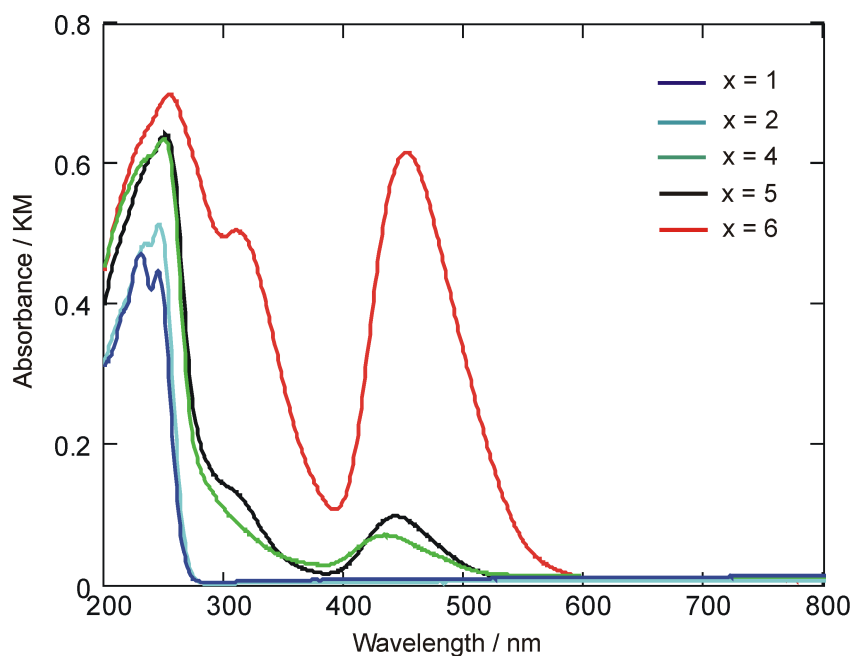


Figure 2.2.2: Diffuse reflectance spectra of dehydrated $\text{Ag}^+_x\text{K}^{12-x}\text{A}$ with different x . KM stands for the Kubelka-Munk formula.

On the first sight it is astonishing that not all of the eight 6-ring positions are occupied by silver ions before they occupy 8-ring and 4-ring positions. An explanation can be given by considering the results of Pluth and Smith^[37] who found two differently coordinated K⁺ in the 6-ring with different bond lengths and thus different binding energies. These two possibilities of coordination to the 6-ring are explained to be caused by electrostatic repulsion between neighboring K⁺. For the smaller Na⁺ ions one cannot distinguish between two different coordination sites in the 6-ring.^[38] Ag⁺ ions are expected to have a similar affinity to specific sites as K⁺ ions due to the similar ionic radii ($r_{\text{Ag}^+} = 1.26 \text{ \AA}$, $r_{\text{K}^+} = 1.33 \text{ \AA}$), while the Na⁺ ions are smaller ($r_{\text{Na}^+} = 0.95 \text{ \AA}$).

These results of dehydrated silver-exchanged K⁺-zeolite A also helped to understand the different thermodynamic data obtained by measuring the ion exchange isotherms of Ag⁺/Na⁺ and Ag⁺/K⁺ in zeolite A. The data predict a different exchange behavior of silver ions in K⁺-zeolite A than in Na⁺-zeolite A and are discussed in Ref. [28].

2.3 Silver sulfide

Silver sulfide crystallizes in two different forms, α and β , having the stoichiometry Ag₂S. The low-temperature α -form named acanthite is monoclinic and stable up to 173 °C. Above this temperature the cubic β -form named argentite appears. With its band gap of about 1 eV at 20 °C silver sulfide is a semiconductor. Due to its photoconductivity silver sulfide has also been used in photoelectric cells.^[39,40] Thin layers of silver sulfide have been considered for photoimaging and photodetection in the IR.^[41] In photography sulfur compounds are used to increase the photographic efficiency of silver halide microcrystals. This process is known as sulfur sensitization and small (Ag₂S)_n-clusters such as Ag₄S₂ on the surface of the silver halide crystals are expected to play a central role.^[42,43]

2.4 The “ship-in-a-bottle” synthesis

There are several interesting compounds obtained by means of a so called “ship-in-a-bottle” synthesis in zeolites.^[44-46] The name is due to artistic bottles containing a ship that is larger than the bottle neck. In chemistry it means the in situ synthesis of compounds occluded in a host material. This is done by insertion of sufficiently small molecules and ions into the cavities of the host and further reaction until the product is too large to leave the cavities. Zeolite A is a suitable host material for this kind of synthesis of guest species because the diameter of the α -cage is much larger than the largest entrance (see chapter 2.1).

The synthesis of silver sulfide clusters in the cavities of zeolite A is based on the knowledge that Ag⁺-exchanged zeolite A can be reversibly dehydrated at room temperature. The dehydrated Ag⁺-zeolites are then exposed to H₂S gas which reacts with the Ag⁺ inside the zeolite yielding AgSH and a proton:



Equation (2.4.1) predicts that the amount of protons produced during this reaction depends on the silver loading. Protons are known to destabilize the lattice of zeolite A and at a certain amount of protons the zeolite will be destroyed. So if one wants to go to high silver loading ($x > 6$) it is better to do the synthesis in two steps. This means first a sample with a small or medium silver sulfide content is synthesized, then the protons are exchanged with other cations (e.g. Na⁺, Ca²⁺, etc.), and then the whole synthesis procedure is repeated starting with silver ion exchange. In fact materials with $x = 6$ produced in a two-step-synthesis have a higher luminescence quantum yield than the corresponding products of the one-step-synthesis.^[47]

After the reaction with H₂S according to Equation (2.4.1) the samples are allowed to take up water again. Rehydration of the zeolite causes solvation and mobilization of AgSH which is small enough to pass the 8-ring windows. Diffusion of AgSH is followed by the reaction of two AgSH to Ag₂S and H₂S according to Equation (2.4.2).



H₂S is displaced by water and leaves the zeolite, which can be easily recognized by the smell of freshly synthesized samples. Ag₂S is expected to be less mobile than AgSH due to sterical hindrance of the diffusion through the zeolite, but further reaction with AgSH can occur leading to the formation of larger silver sulfide clusters.



Particles having the stoichiometry (Ag₂S)_n are stable in the hydrated zeolite because their solubility product in water is very low, while particles like Ag₃S₂H are expected to be less stable. Once the stable particles are built, further aggregation is prevented by the zeolite. The largest (Ag₂S)_n cluster that would fit into the α-cage would approximately be Ag₈S₄.^[17]

The nomenclature used in the following for zeolite A - Ag₂S / host-guest materials is Ag₂S-MA-x, where M stands for the charge compensating cations (co-cations), A for the framework of zeolite A, and x denotes the silver loading.

2.5 Summary

The cavities of zeolite A provide a suitable environment to host silver ions and small silver sulfide clusters. The silver ions are introduced by means of ion exchange. On dehydration of silver-exchanged zeolite A, the silver ions are forced to coordinate to oxygen atoms of the zeolite lattice resulting in a change of the absorption spectra. While the absorption spectrum of fully hydrated Ag⁺-zeolite A corresponds to Ag⁺ in water, the absorption spectra of dehydrated Ag⁺-zeolite A reveals Ag⁺(5s)←O(n) LMCT transitions in the UV and in the visible. The position of the absorption bands depends on the coordination site of the silver ions. 4-ring coordinated Ag⁺ absorbs at 450 nm and is thus responsible for the yellow color of some dehydrated Ag⁺-zeolite A samples. The order of the occupation of different coordination sites by silver ions is influenced by the exchanging cation. This could be demonstrated by comparing the ion pairs Na⁺/Ag⁺ and K⁺/Ag⁺. All color changes due to dehydration/rehydration of silver-exchanged zeolite A at room temperature are reversible.

Silver-exchanged zeolite A is the starting material for the „ship-in-a-bottle” synthesis of silver sulfide clusters in zeolite A. The silver sulfide clusters are expected to have the stoichiometry (Ag₂S)_n and to be located in the α-cages. The size of the particles can theoretically range from the Ag₂S molecule to the Ag₈S₄ cluster or even arrays of clusters in different α-cages, and is given by the initial amount of silver ions per α-cage (silver loading x). Tuning the size of the silver sulfide clusters leads to different and fascinating optical properties of these host-guest materials, which will be discussed in the following chapters.

3. Optical Properties of Ag₂S-Zeolite A Materials

The optical properties of Ag₂S-zeolite A systems depend on the silver sulfide content and to a certain extent on the charge compensating cations (co-cations) present during and after the silver sulfide synthesis. The influence of the silver loading (x) on the size of the silver sulfide clusters is exemplified in chapter 3.1 for Ca²⁺-exchanged zeolite A. Systems with other cations will be discussed in chapter 3.2.

3.1 Ag₂S-CaA-x

The Ca²⁺-exchanged form of zeolite A (CaA) turned out to be very suitable for investigating optical changes of the samples as a function of increasing silver sulfide content. The color of these materials is brilliant and not grayish as sometimes observed for Ag₂S-NaA-x. Also the luminescence is quite intense and in most cases even visible at room temperature. In this chapter the influence of the silver loading (x) on the optical properties of Ag₂S-CaA-x will be discussed. It was found that this kind of material is sensitive to specific environmental changes. Especially the influence of water, of the temperature, and of additional silver ions on the optical properties of Ag₂S-CaA-x will be presented. The main conclusions of the work on the Ag₂S-CaA-x system is summarized in the publication "*Luminescence properties of Ag₂S and Ag₄S₂ in zeolite A*" at the end of this chapter.

3.1.1 Influence of the silver loading

Pure zeolite A does not absorb light in the visible part of the spectrum (200 - 1000 nm), so the color of all samples is due to absorbing silver sulfide species. Figure 3.1.1 shows the absorption spectra of differently colored Ag₂S-CaA-x samples. The colorless sample (A) reveals transitions in the UV, while the spectra of yellow colored samples (B and C) have a shoulder at 450 nm. With increasing x the samples start to become brown and absorb in the whole visible region (D and E). The spectra lose their structure and the absorption in the UV gets so strong that saturation effects occur. In comparison the absorption spectrum of bulk silver sulfide is shown in (F).

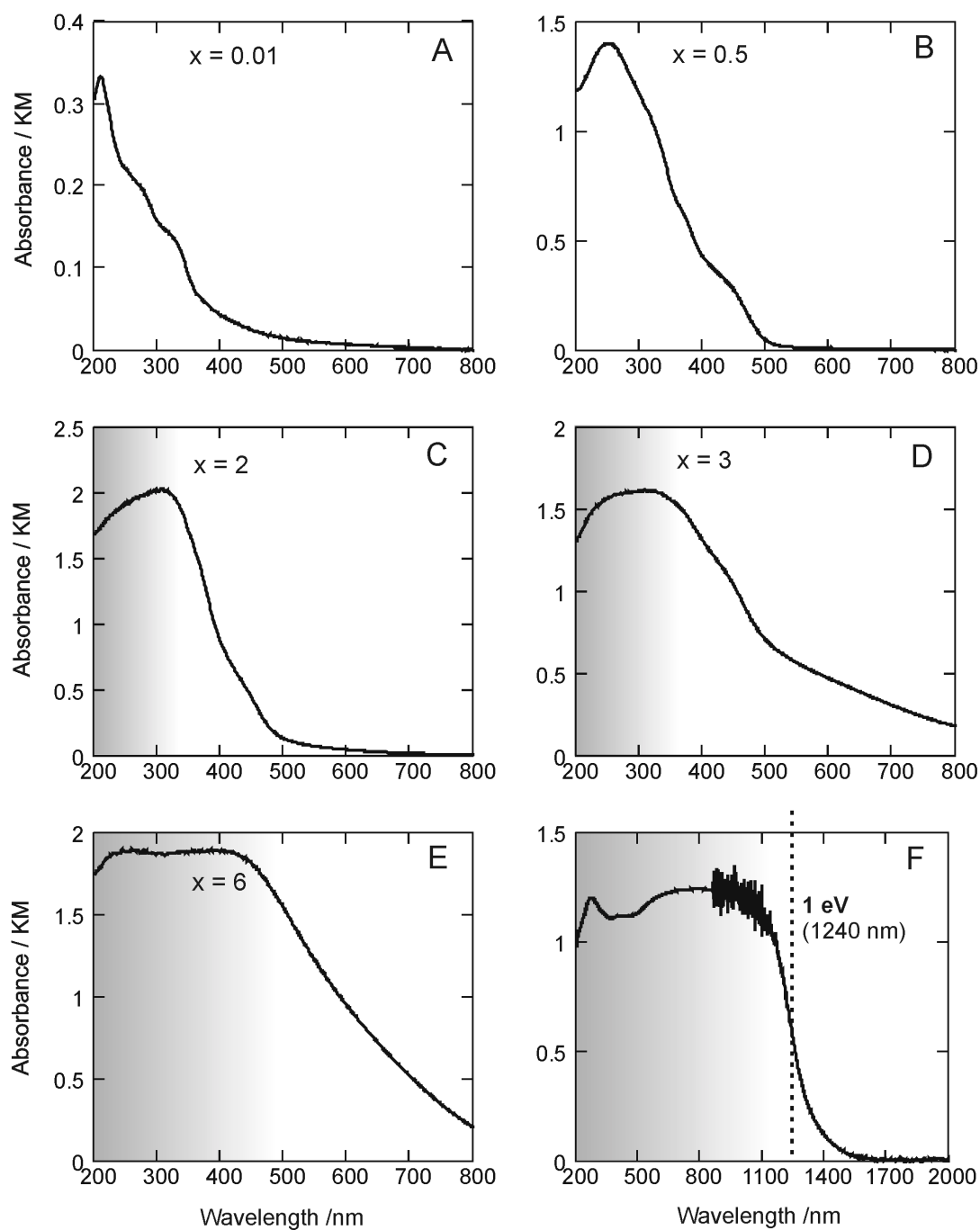


Figure 3.1.1: Diffuse reflectance spectra of Ag₂S-CaA-x with different x (A - E) and of bulk silver sulfide (F). KM stands for the Kubelka-Munk function. The shaded part shows the spectral region where saturation effects occur.

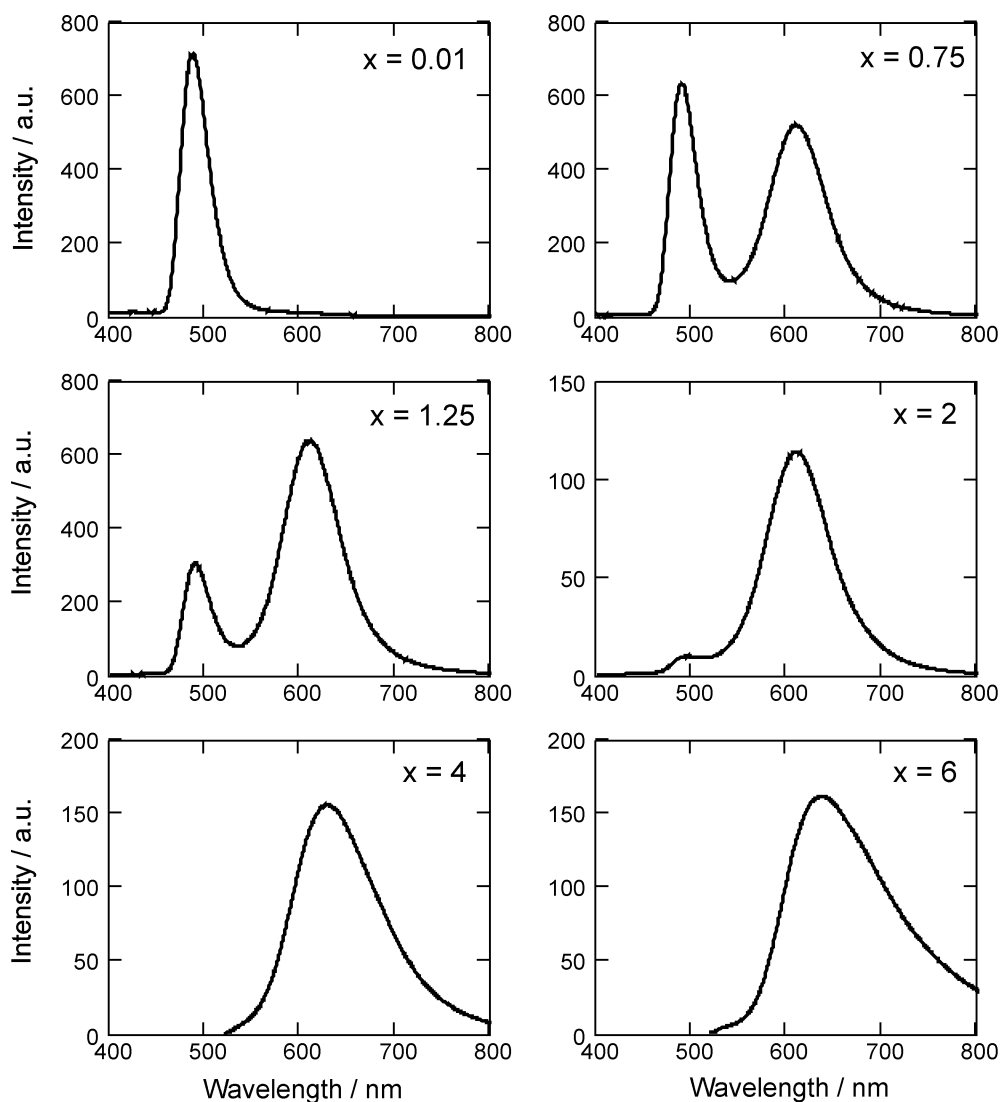


Figure 3.1.2: Luminescence spectra of Ag₂S-CaA-x at -190 °C upon excitation at 320 nm.

The color of the luminescence changes from green to orange with increasing silver sulfide content. The development of the luminescence bands as a function of x can be seen in the spectra in Figure 3.1.2. Over a large range of different silver loading (x) the luminescence spectra consist of one or two emission bands, one “green” band at 490 nm and one “orange” band at 610 nm. At $x > 2$ there is a shoulder in the red part of the “orange” luminescence band. This shoulder becomes stronger with increasing silver sulfide content.

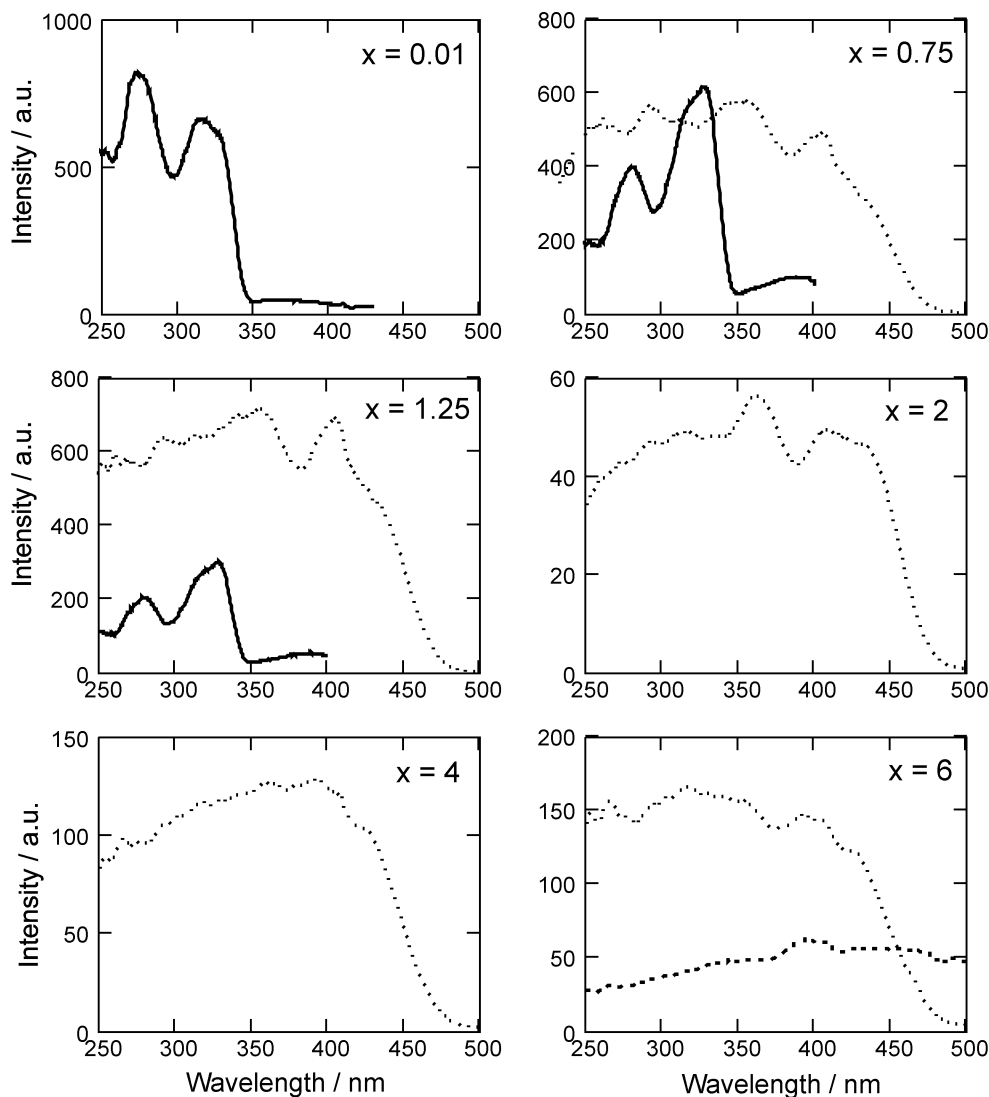


Figure 3.1.3: Excitation spectra of the same samples observed at 490 nm (solid), at 610 nm (dots), and at 780 nm (dash).

The excitation spectra of the same samples are shown in Figure 3.1.3. Up to $x = 2$ one can distinguish again between two different spectra with more or less structure. At higher x the spectra become unstructured and the excitation spectrum at 780 nm is very broad.

It seems that samples with $0.01 \leq x \leq 2$ contain always the same two luminescent species in variable ratio. The rise of the luminescence band at 610 nm goes simultaneously with the decrease of the relative luminescence at 490 nm. This is illustrated in the plot in Figure 3.1.4. The relative luminescence intensities are calculated as follows:

$$I_1 = \frac{I_{490}}{I_{490} + I_{610}} \quad (3.1.1)$$

$$I_2 = \frac{I_{610}}{I_{610} + I_{490}} \quad (3.1.2)$$

where I_{490} is the luminescence intensity at 490 nm and I_{610} is the luminescence intensity at 610 nm.

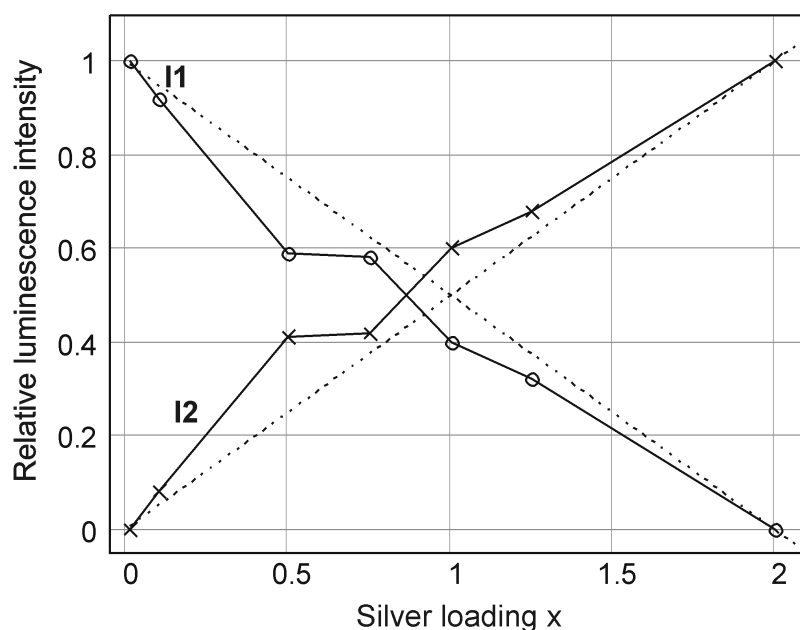


Figure 3.1.4: Plot of the relative luminescence intensities at 490 nm (I_1) and at 610 nm (I_2) as a function of silver loading.

These results indicate that in a defined loading range of $0.01 \leq x \leq 2$ Ag₂S-CaA-x samples contain only two different silver sulfide species. At low silver loading green luminescent species are preferentially built which are then replaced by orange luminescent species with increasing silver loading. From experimental and theoretical reasons it can be concluded that the luminescence at 490 nm is due to single Ag₂S molecules.^[17] The calculated electronic transitions of Ag₂S (see chapter 1) can be recognized in the absorption spectrum of Ag₂S-CaA-0.01 (Figure 3.1.1) and in all excitation spectra of the green luminescence (Figure 3.1.3). The formation of Ag₄S₂ by linking together two Ag₂S molecules is discussed in Ref. [17] and in chapter 3.1.4. The main conclusion out of that work is that the LUMO of Ag₄S₂ lies lower than the LUMO of Ag₂S while the HOMO stays at the same energy, resulting in a red shift of the

luminescence. So it is fair to assume that the luminescence at 610 nm is due to Ag₄S₂. The shoulder in the red part of the spectrum at higher silver loading is probably caused by larger silver sulfide clusters. Energy Dispersive X-ray analysis (EDX) gives a Ag/S ratio of 2 up to a silver loading of $x = 6$. This means that up to $x = 6$ the stoichiometry of the silver sulfide species is still (Ag₂S)_n. Possible candidates are Ag₃S₆ and Ag₄S₈ that still fit into an α -cage. In highly loaded samples one may also consider interactions between clusters in different α -cages which form some kind of supercluster.

The luminescence lifetimes lie all in the order of magnitude of several microseconds. They were studied as a function of silver loading and of temperature. The longest luminescence lifetime in Ag₂S-CaA-x have isolated Ag₂S molecules with about 300 μ s. The luminescence decay of Ag₂S can be fitted in a good approximation to a single-exponential function. However, as soon as Ag₄S₂ clusters are present in the same zeolite crystal, the decay is no longer single-exponential. It can be then fitted to a bi-exponential function and the average luminescence lifetime was found to decrease with increasing amount of Ag₄S₂. The data of a series of measurements of samples containing different ratios of Ag₂S and Ag₄S₂ are summarized in Table 1 of chapter 3.1.4. The explanation given there is that energy transfer from excited Ag₂S to Ag₄S₂ occurs. Actually, we have in our system an analogue situation as Förster describes in Ref. [48], where the donor and the acceptor molecules are assumed to be at fixed positions. In our case the donors are Ag₂S and the acceptors are Ag₄S₂, which are spatially separated from each other by the zeolite framework as illustrated in Figure 3.1.5.

The rate constant for energy transfer k_{EnT} strongly depends on the distance between donor and acceptor and can be expressed as follows:

$$k_{\text{EnT}}(i) = \frac{1}{\tau_{D^*}} \left(\frac{R_0}{R_i} \right)^6 \quad (3.1.3)$$

τ_{D^*} is the luminescence lifetime of the donor without acceptor, R_0 is the Förster radius, and R_i is the distance between donor and acceptor. With increasing donor-acceptor distance the probability of radiative relaxation of the donor increases. In the situation shown in Figure 3.1.5 the probability that the excitation energy of Ag₂S is transferred to the nearest Ag₄S₂ (distance R_1) is therefore much higher than to the diagonal lying Ag₄S₂ (distance R_2).

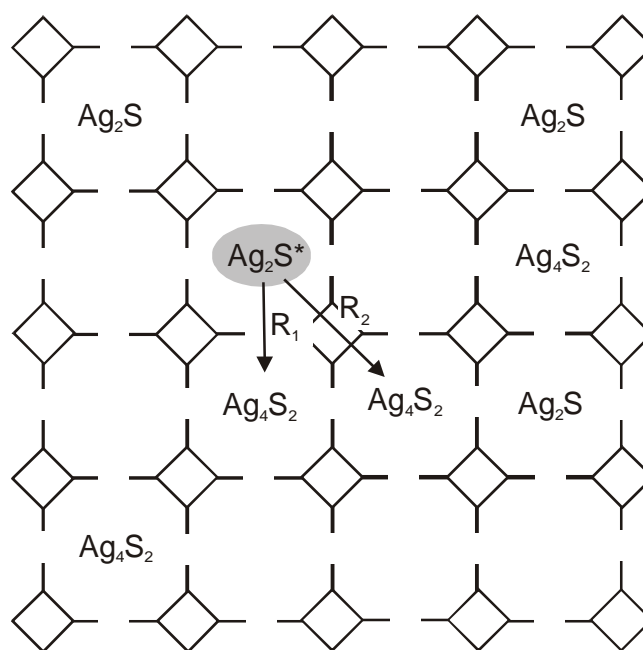


Figure 3.1.5: Scheme of Ag₂S and Ag₄S₂ in the α -cages of a zeolite A crystal. An excited Ag₂S can transfer its excitation energy to a neighboring Ag₄S₂.

The luminescence decay of the donor can then be described by a so called stretched exponential function:

$$\langle \rho_{D^*}(t) \rangle = \exp\left(-\frac{t}{\tau_{D^*}}\right) \cdot \exp\left(-2\gamma\sqrt{\frac{t}{\tau_{D^*}}}\right) \quad (3.1.4)$$

ρ_{D^*} is the luminescence intensity of the donor as a function of time, and γ is defined as follows

$$\gamma = \frac{\sqrt{\pi}}{2} c_A \frac{4\pi}{3} R_0^3 \quad (3.1.5)$$

where c_A is the concentration of acceptors.

Theoretically, the luminescence decay of Ag₂S is expected to fit to Equation (3.1.4), and γ should become larger with increasing silver loading because the concentration of the acceptors (Ag₄S₂) increases with increasing silver loading. In practice, we noticed that such a fit is not possible. As an example the luminescence decay of a Ag₂S-CaA-0.5 sample containing Ag₂S and Ag₄S₂ will now be discussed. The time-resolved luminescence spectra of Ag₂S-CaA-0.5 are shown in Figure 3.1.6.

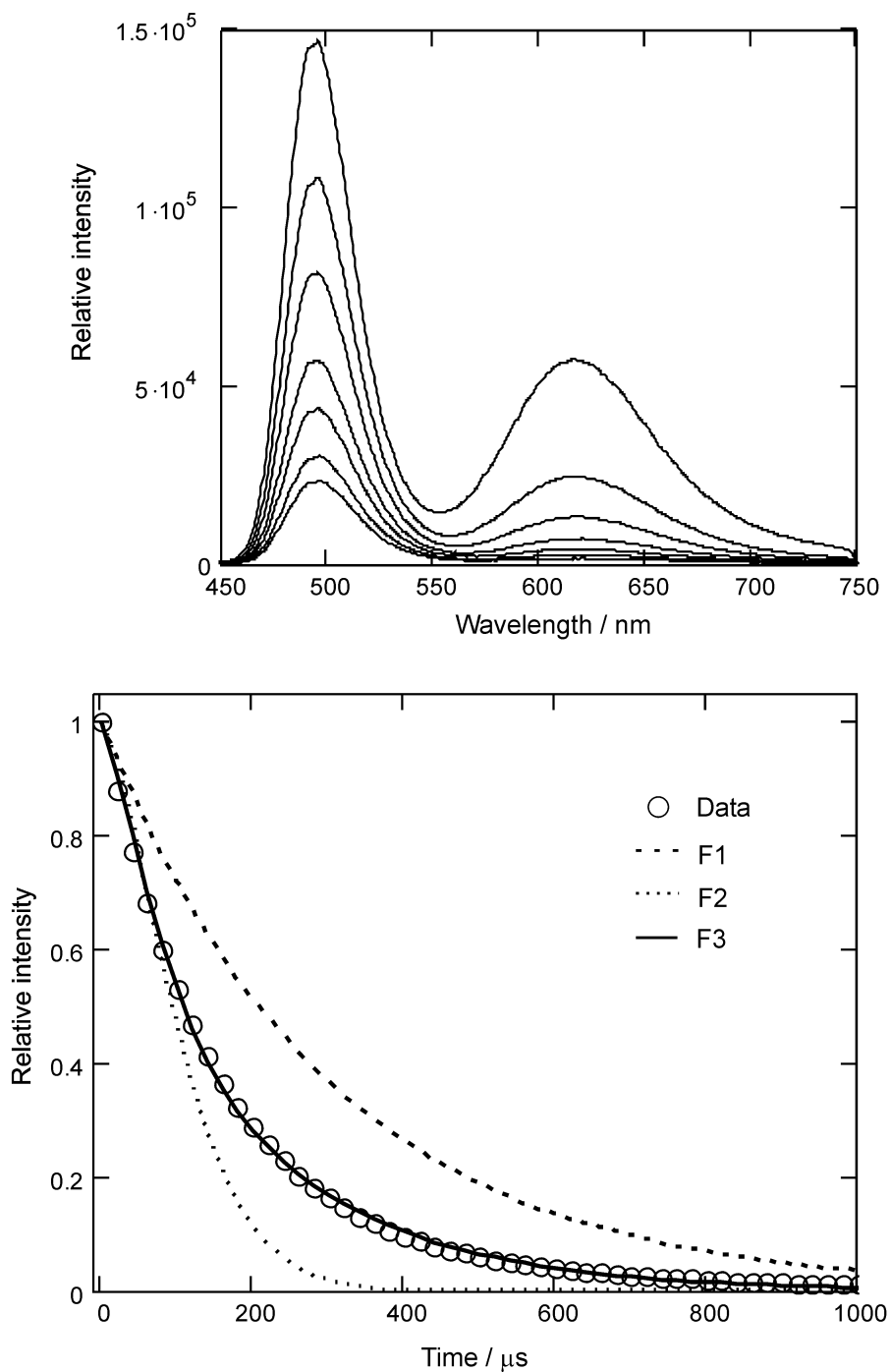


Figure 3.1.6: *Top*: Time-resolved luminescence spectra of Ag₂S-CaA-0.5 at -150 °C. The first six spectra after the excitation pulse are shown. Excitation was performed at 320 nm and the time-window for detection (gate) was 100 μs . *Bottom*: Corresponding decay curve at 490 nm (Data). The functions F1 (single-exponential), F2 (stretched-exponential), and F3 (adapted model function) are explained in the text.

The luminescence decay of Ag₂S can be fitted to a bi-exponential function with the parameters $a_1 = 0.894$, $a_2 = 0.106$, $\tau_1 = 143 \mu\text{s}$, and $\tau_2 = 423 \mu\text{s}$.

$$I(t) = a_1 \cdot \exp\left(-\frac{t}{\tau_1}\right) + a_2 \cdot \exp\left(-\frac{t}{\tau_2}\right) \quad (3.1.6)$$

For comparison a single-exponential function (F1 with $\tau = 300 \mu\text{s}$) and a stretched-exponential function (F2 with $\tau = 300 \mu\text{s}$ and $\gamma = 2$) are plotted in the same Figure 3.1.6. It can be seen that the data better fit to F2 at the beginning of the decay, but later the decay is slower. One can also see that an approach to get the model function closer to the data is by taking the sum of F1 and F2. This means that we have again a bi-exponential function similar to Equation (3.1.6), but the new function is constructed out of the decay function of the donor without acceptor (j_1) and the decay function of the donor in the presence of the acceptor (j_2).

$$\text{F3: } I(t) = j_1(t) + j_2(t) = c_1 \cdot \exp\left(-\frac{t}{\tau_1}\right) + c_2 \cdot \exp\left(-2\gamma \frac{\sqrt{t^3}}{\sqrt{\tau_2^3}}\right) \quad (3.1.7)$$

τ_1 and τ_2 are in the ideal case equal to τ_{D^*} , but in the following procedure they were varied within a reasonable range. For the model function F3 in Figure 3.1.6 the following parameters were used: $\tau_1 = 210 \mu\text{s}$, $\tau_2 = 300 \mu\text{s}$, $c_1 = 0.7$, $c_2 = 0.3$, and $\gamma = 3$.

The same procedure was also applied on other samples with different silver loading and thus different Ag₂S/Ag₄S₂ ratios. The parameters used for the model functions are listed in Table 3.1 and the corresponding decay curves are shown in Figure 3.1.7.

Table 3.1: Parameters for the luminescence decay of Ag₂S in Ag₂S-CaA-x.

x	$\tau_1 / \mu\text{s}$	$\tau_2 / \mu\text{s}$	c_1	c_2	γ
0.1	265	300	0.8	0.2	2.5
0.75	210	300	0.55	0.45	3.5
1.25	200	300	0.32	0.68	7

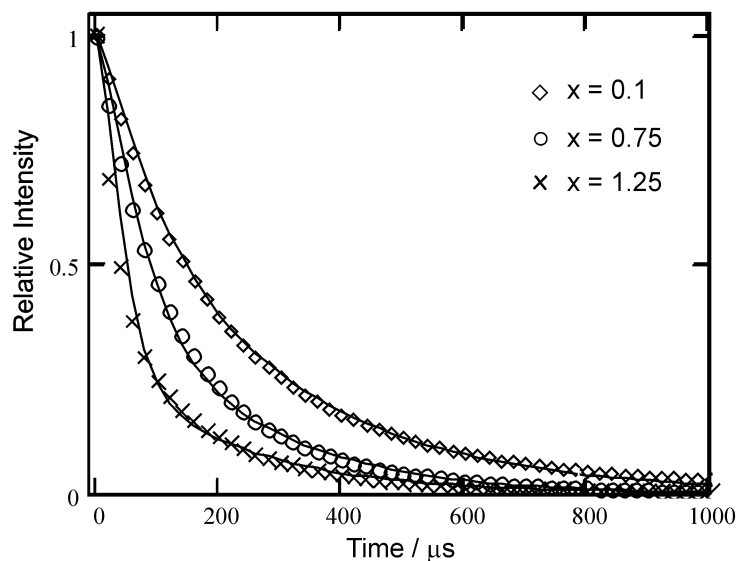


Figure 3.1.7: Decay curves of the luminescence of Ag_2S in Ag_2S -CaA- x with different x and the corresponding model functions.

The parameters in Table 3.1 have arbitrary values and they are not independent from each other. The idea is just trying to find suitable values to get the model function as close as possible to the real decay curve. However, two important points have to be mentioned. First, the value of γ has to increase with increasing silver loading. Second, the stretched exponential function has to be more weighted with increasing silver loading (larger c_2). Both is fulfilled and indicates that energy transfer from excited Ag_2S to Ag_4S_2 is favored at higher silver loading due to a higher concentration of the acceptor Ag_4S_2 .

The reason why the $\text{Ag}_2\text{S}/\text{Ag}_4\text{S}_2$ -zeolite A system cannot be described only by the stretched-exponential model probably lies in the heterogeneous nature of the samples. Within one sample not every crystal contains the same amount of Ag_2S and Ag_4S_2 . One may expect to find crystals with a distribution of Ag_2S and Ag_4S_2 which favors energy transfer and others where most of the Ag_2S relax radiatively.

Another problem by investigating energy transfer between Ag_2S and Ag_4S_2 is that the donor Ag_2S cannot be selectively excited. By exciting Ag_2S one always excites Ag_4S_2 as well, so it is difficult to say which part of the Ag_4S_2 luminescence is due to direct excitation and which part is due to energy transfer. Only the other way around is possible, namely selective excitation of Ag_4S_2 . The luminescence decay of Ag_4S_2 was also studied as a function of silver loading and is always multi-exponential. Best fits were achieved by using three exponents. The luminescence lifetimes of Ag_4S_2 are always shorter than the

luminescence lifetimes of Ag₂S and stay the same up to a silver loading of $x = 2$. At $x > 2$ they become shorter with increasing silver loading. This observation correlates with the broadening and the red-shift of the orange luminescence band at $x > 2$. An explanation is that the presence of larger cluster and cluster-cluster interaction at higher silver loading give rise to new pathways for radiationless relaxation.

3.1.2 Influence of the environment

All Ag₂S-CaA- x samples are very stable under ambient conditions. During the first few weeks after the synthesis the color of the samples still becomes more intense, but then the spectra do not change for years. Water has no effect on the absorption, but strongly influences the luminescence. After dehydration of Ag₂S-CaA- x samples in high vacuum the absorption properties do not change. However, dehydrated samples do not show luminescence at all. The dehydration/rehydration process is completely reversible. After 6 h storage of the dehydrated samples under ambient conditions the luminescence spectra are again identical to fully hydrated samples. This observation is on the first sight astonishing because water is usually known to favor radiationless relaxation. The interpretation of this phenomenon is the following: in the dehydrated state the silver sulfide particles are stronger attached to the zeolite lattice than in the hydrated state. The interaction between the silver sulfide particle and the zeolite is not strong enough to cause spectral shifts but it quenches the luminescence.

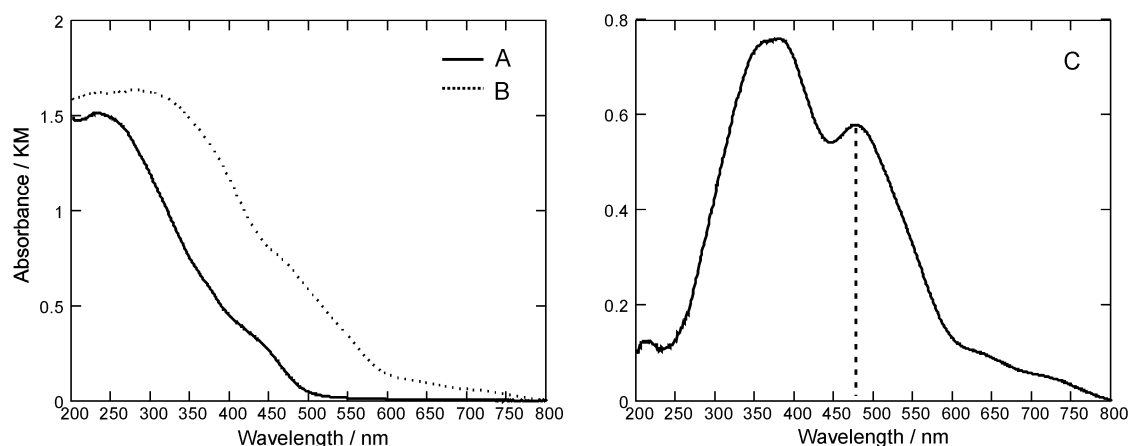


Figure 3.1.8: A: absorption spectrum of Ag₂S-CaA-1, B: absorption spectrum of Ag⁺/Ag₂S-CaA-1, C: difference spectrum of A and B.

Exchangeable cations also influence the optical properties to a certain extent. Alkaline and earth alkaline ions will be discussed in chapter 3.2. The strongest effect is observed when Ag₂S-CaA-x is suspended in a aqueous solution containing silver ions. A yellow sample (e.g. Ag₂S-CaA-1) turns orange within seconds. This indicates a very fast exchange of cations from the inside of the zeolite (Ca²⁺ and H⁺) with Ag⁺ from solution and a strong electronic interaction between Ag⁺ and silver sulfide. The color change is shown in the spectra in Figure 3.1.8. The difference spectrum demonstrates that there are new transitions at 480 nm and in the UV due to the additional Ag⁺. These transitions are not observed in pure Ag⁺-CaA and can therefore be assigned to Ag⁺(Ag₂S)_n species.

The luminescence properties also strongly depend on the temperature. The decreasing luminescence intensity with increasing temperature correlates with simultaneously decreasing luminescence lifetimes and can be explained by thermally favored radiationless relaxation. Detailed results are reported in the publication in chapter 3.1.4. An interesting aspect is that the luminescence of Ag₄S₂ is more affected by temperature than the luminescence of Ag₂S and that samples containing both particles therefore change their luminescence color with temperature.

3.1.3 Summary

Using CaA as a host material and choosing silver loadings between $x = 0.01$ and $x = 2$ leads to systems with Ag₂S and Ag₄S₂ as the only silver sulfide species. The luminescence properties of these species were studied in detail and are summarized in the following publication "*Luminescence properties of Ag₂S and Ag₄S₂ in zeolite A*" (chapter 3.1.4). At higher silver loading than $x = 2$ the formation of larger clusters than Ag₄S₂ is favored. This is revealed in a broadening and a red shift of the luminescence spectrum and is related to a brown color of the material. However, an assignment to a specific particle is more difficult than in the case of Ag₂S and Ag₄S₂. All samples are sensitive to environmental influences such as water, cations and temperature which makes them interesting for applications in specific sensor devices.

3.1.4 Publication

"Luminescence properties of Ag₂S and Ag₄S₂ in zeolite A"

J. Mater. Chem. **2003**, *13*, 1969-1977.

Claudia Leiggenger, Dominik Brühwiler, and Gion Calzaferri*

Department of Chemistry and Biochemistry, University of Bern, Freiestrasse 3, CH-3000 Bern 9, Switzerland

Silver sulfide particles of different size are synthesized in the cavities of zeolite A and ZK-4 by exposing the Ag⁺-exchanged dehydrated zeolites to H₂S. The two smallest stable particles synthesized by this method are the Ag₂S molecule and the Ag₄S₂ cluster. Both show photoluminescence in the visible. The luminescence properties of the samples are studied as a function of temperature, of the silver sulfide content, and of the co-cations. By using the Ca²⁺-exchanged form of zeolite A it is possible to synthesize silver sulfide-zeolite systems which contain Ag₂S and Ag₄S₂ in the same zeolite crystal. After excitation with UV light energy transfer from the excited Ag₂S to Ag₄S₂ most probably occurs. These systems are potential materials for thermometry because their luminescence properties strongly depend on the temperature.

1 Introduction

Several methods have been developed for the synthesis of nanosized silver sulfide particles. By using different kind of polymers as stabilizing agents¹⁻⁴ or by implantation into silica glass⁵ silver sulfide particles of a few nanometers were synthesized. Zeolites can act as hosts for the synthesis of even smaller semiconductor quantum dots or arrays.⁶ Their well defined cavities allow to synthesize particles in a specific size regime and prevent them from aggregation. In previous communications we reported the synthesis of the first luminescent silver sulfide clusters in zeolite A.^{7,8} The procedure is based on the knowledge that Ag⁺-exchanged zeolite A can be reversibly activated in vacuum at room temperature.^{9,10} A scheme of the synthesis is shown in Figure 1. After ion exchange and dehydration of the zeolite the silver ions occupy some of the cation positions so that they are coordinated to the oxygens of the zeolite lattice. The formation of silver sulfide can then be described as follows: 1) Reaction with H₂S yields AgSH and a proton, the AgSH molecules still being coordinated to the

zeolite lattice. 2) Rehydration of the zeolite causes solvation and mobilization of AgSH. 3) Diffusion of AgSH is followed by the reaction of two AgSH to Ag₂S and H₂S. H₂S is displaced by water and leaves the zeolite, which can be easily recognized by the smell of freshly synthesized samples.

The optical properties of Ag₂S-zeolite A are influenced by the initial amount of exchanged silver ions. This observation led to the conclusion that the size of the silver sulfide clusters can be tuned by using different Ag⁺ loading densities. At a very low Ag⁺ loading single Ag₂S molecules are formed which exhibit a blue-green luminescence. With increasing silver sulfide content the color of the samples changes from colorless over light yellow to deep yellow to orange-brown or brown (the specific coloring depends on the co-cations). The color of the luminescence was found to change as well (see Figure 2). The red shift of the absorption and of the luminescence is caused by larger (Ag₂S)_n clusters.

The environment inside the zeolite cages is expected to play a role in the formation and stabilization of different kind of silver sulfide clusters. It is known that the charge

compensating cations influence the amount and the arrangement of water molecules inside the zeolite cavities.^{11,12} Generally zeolites with small cations contain more water, with stronger localization around bivalent cations compared to monovalent cations. Because of their different pK_a values the cations also to a certain extent determine the pH inside the cavities.¹³ We have investigated the influence of the co-cations on the properties of silver sulfide clusters in zeolite A. For that purpose we exchanged the Na⁺ ions of zeolite A with other cations (Li⁺, K⁺, Mg²⁺, Ca²⁺, Sr²⁺) before loading the zeolite with silver sulfide. In an additional experiment we synthesized silver sulfide clusters in ZK-4 which has the same structure as zeolite A but a higher Si content and thus less charge compensating cations.

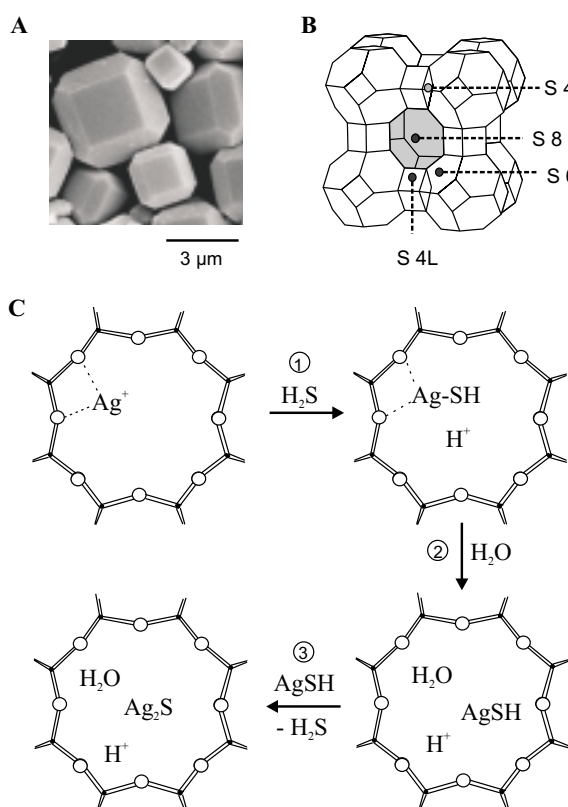


Fig. 1 A: SEM picture of typical zeolite A crystals. B: Framework of zeolite A showing the crystallographically identified cation positions. C: Scheme of the silver sulfide formation inside the zeolite cages.

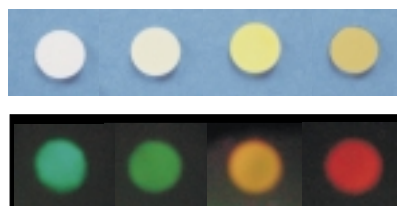


Fig. 2 Photographic pictures of zeolite A samples containing silver sulfide with increasing silver sulfide content from the left to the right. *Upper*: Color seen in reflection. *Lower*: Luminescence of the same samples at -10° C upon excitation at 360 nm.

2 Experimental

Synthesis

Zeolite A ($\text{Na}_{12}[(\text{AlO}_2)_{12}(\text{SiO}_2)_{12}]$) and ZK-4 ($\text{Na}_9[(\text{AlO}_2)_9(\text{SiO}_2)_{15}]$) were synthesized and characterized according to ref. 14 and ref. 9, respectively. The ion exchanged samples were prepared by suspending 500 mg NaA or NaZK-4 in 20 ml 0.5 M $\text{M}(\text{NO}_3)_n$ solution ($\text{M} = \text{Li}^+, \text{K}^+, \text{Mg}^{2+}, \text{Ca}^{2+}, \text{Sr}^{2+}$) for 15 min at room temperature. After repeating two times, the samples were washed three times with bidistilled water. Completely exchanged samples were obtained by this procedure except for Mg^{2+} which can only reach an exchange level of 85% in zeolite A.¹⁵ The synthesis of Ag₂S in zeolites consists of four steps and is described in detail in ref. 8: 1. Insertion of a defined amount of Ag⁺ by means of ion exchange, 2. dehydration of the Ag⁺-zeolite in vacuum at room temperature, 3. reaction of Ag⁺ with H₂S, 4. rehydration and cluster growth. Only freshly exchanged Ag⁺-samples were used for the synthesis of silver sulfide clusters.

Nomenclature

The following abbreviations are used: NaA for sodium zeolite A ($\text{Na}_{12}[(\text{AlO}_2)_{12}(\text{SiO}_2)_{12}]$), CaA for calcium zeolite A ($\text{Ca}_6[(\text{AlO}_2)_{12}(\text{SiO}_2)_{12}]$) and so on, as well as Na-ZK4 for sodium ZK-4 ($\text{Na}_9[(\text{AlO}_2)_9(\text{SiO}_2)_{15}]$), Ca-ZK4 for calcium ZK-4 ($\text{Ca}_{4.5}[(\text{AlO}_2)_9(\text{SiO}_2)_{15}]$) and so on. The stoichiometry of the silver sulfide-zeolite

composites is $\text{Ag}_x\text{S}_{0.5x}\text{M}_{12-x}\text{H}_x\text{Si}_{12}\text{Al}_{12}\text{O}_{48} \cdot n\text{H}_2\text{O}$ for zeolite A with monovalent cations M^+ and $\text{Ag}_x\text{S}_{0.5x}\text{M}_{6-0.5x}\text{H}_x\text{Si}_{12}\text{Al}_{12}\text{O}_{48} \cdot n\text{H}_2\text{O}$ for zeolite A with divalent cations M^{2+} . We use the abbreviations $\text{Ag}_2\text{S-MA-x}$ ($\text{M} = \text{Na}, \text{Li}, \text{K}, \text{Mg}, \text{Ca}, \text{Sr}$) for differently loaded samples, where x denotes the number of silver ions per α -cage of zeolite A.

Optical Measurements

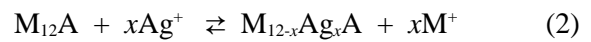
All samples were prepared on quartz plates and were measured in their fully hydrated state. For that purpose the samples were suspended in bidistilled water, dropped on a clean quartz plate and then let dry on air at room temperature. Diffuse reflectance spectra (DRS) were recorded at room temperature using a Perkin-Elmer Lambda 900 spectrophotometer with an integrating sphere. The data were converted using the Kubelka-Munk formula. Since the scattering coefficient of zeolites is gradual in the wavelength region of interest, the Kubelka-Munk function is expected to be a good representation of the absorption spectrum.⁸ Steady-state luminescence spectra were taken on a Perkin-Elmer LS 50B spectrofluorometer equipped with a nitrogen cryostat (Oxford Instruments PE 1704). Time-resolved luminescence measurements were performed by exciting the samples with a pulsed laser. The system used for this purpose consists of a Nd:YAG laser (Quantel Brilliant), an OPO (Opotek MagicPrism Vibrant Vis) which is pumped by the third harmonic and an UV-Mixer Module for excitation in the UV. The energy of the laser pulse is around 4 mJ per pulse for visible light and around 0.5 mJ per pulse for UV light on a surface of about 0.5 cm². To determine the luminescence decay curves, the time-dependent spectra were integrated over the wavelength region of interest. The data were then fitted with a n -exponential function which gives n luminescence lifetimes (τ_n) and their corresponding amplitudes (a_n). The average luminescence

lifetime was calculated by the following formula:

$$\langle \tau \rangle = \frac{\sum a_n \cdot \tau_n^2}{\sum a_n \cdot \tau_n} \quad (1)$$

3 Ion exchange and cluster growth

The stoichiometry of ion exchange of zeolite A containing monovalent alkali ions M^+ by silver ions is described as follows:



where A stands for $[(\text{AlO}_2)_{12}(\text{SiO}_2)_{12}]^{12-}$ and $0 \leq x \leq 12$. In a crystal of 1 μm^3 size consisting of $n_\alpha = 5 \cdot 10^8$ α -cages x can take any value between n_α^{-1} ($= 2 \cdot 10^{-9}$) and 12. The lowest silver loading we used for the synthesis of silver sulfide clusters is $x = 0.01$ which means that a crystal of 1 μm^3 size contains $5 \cdot 10^6$ silver ions or $2.5 \cdot 10^6$ Ag_2S molecules. Figure 3 shows the calculated distribution of silver ions in zeolite A after the exchange of monovalent cations by Ag^+ .¹⁶ p_J is the relative number of α -cages containing a specific number ($J = 0, 1, \dots, 12$) of Ag^+ . If there is no Ag^+ -exchange ($x = 0$), p_0 is 1 while all other p_J are zero. This means that 100 % of the α -cages are empty (0 Ag^+ , 12 M^+). With increasing x the number of empty α -cages decreases and the probability of finding α -cages with 1 and more Ag^+ increases. At a silver loading of $x = 0.5$ for example p_0 is 0.6, p_1 is 0.3, and p_2 is 0.1. The relative number p_J of α -cages with a higher number of Ag^+ then drops rapidly with increasing J . At a silver loading of $x = 1.5$ the distribution is significantly different: most of the α -cages contain 1 Ag^+ ($p_1 = 0.35$), around 30 % of the α -cages contain 2 Ag^+ ($p_2 = 0.3$), 20 % of the α -cages contain 0 Ag^+ ($p_0 = 0.2$), 15 % of the α -cages contain 3 Ag^+ ($p_3 = 0.15$), and around 10 % of the α -cages contain 4 Ag^+ ($p_4 = 0.1$).

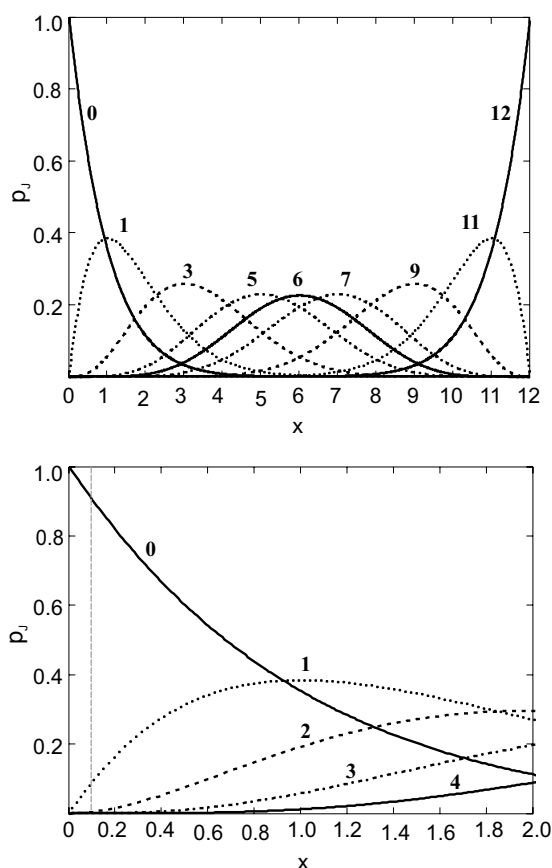
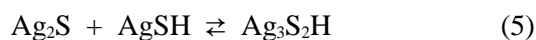
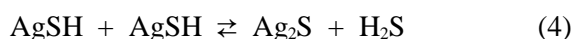


Fig. 3 Distribution p_j of Ag^+ in zeolite A after exchange of monovalent cations. x is the average number of Ag^+ per α -cage (= Ag^+ loading) and p_j is the relative number of α -cages containing $J = 0, 1, 2, \dots, 12$ Ag^+ for a given exchange x .

Up to a silver loading of $x = 0.1$ there are only α -cages with 0 or 1 silver ions. Therefore the reaction of H_2S with Ag^+ in a sample with such a low silver loading leads only to the formation of AgSH as shown in equation (3). Rehydration of the zeolite causes solvation and diffusion of AgSH molecules which become mobile at room temperature. They can then react to Ag_2S and H_2S according to equation (4). For $x = 0.1$ we then find one Ag_2S per 20 α -cages. Experimental evidence for this mechanism was reported in ref. 8. The reversibility of reactions (4) and (6) was confirmed by adding an excess of H_2S to dehydrated samples containing silver sulfide. For reaction (5) we assume that $\text{Ag}_3\text{S}_2\text{H}$ is less stable than Ag_2S and Ag_4S_2 so that the

formation of Ag_2S and Ag_4S_2 is favored. Indeed, Energy Dispersive X-ray Analysis (EDX) gives a Ag/S ratio of 2 up to a silver loading of 6 Ag^+ per α -cage. This means that after rehydration most of the silver sulfide clusters have the stoichiometry $(\text{Ag}_2\text{S})_n$. The equilibria (4) and (6) can be shifted towards Ag_2S and Ag_4S_2 , respectively, by removing H_2S after the reaction.



Ag_2S molecules have a very low diffusion rate in hydrated zeolites at room temperature so that they are stable for years if they are in isolated α -cages and no reaction with AgSH according to equation (5) occurs. An explanation for the low diffusion rate at room temperature gives the size and geometry of the Ag_2S molecule. Figure 4 illustrates the dimensions of a Ag_2S molecule compared to an α -cage of zeolite A. For the calculation of the size of the Ag_2S molecule we used a bond angle of 112° and a bond length of 2.42 \AA from previous calculations⁸ and the ionic radii $r(\text{Ag}^+) = 1.26 \text{ \AA}$ and $r(\text{S}^{2-}) = 1.84 \text{ \AA}$. The 8-ring window of zeolite A has a structural diameter of 4.1 \AA . However, the effective pore size of zeolite A varies with exchanged cations. It was found that Ca^{2+} -exchanged zeolite A adsorbs molecules up to a size of 5 \AA while the Na^+ -exchanged form only adsorbs molecules smaller than 4 \AA .¹⁷ The difference is due to the occupation of the cation sites in the 8-ring. Diffusion of Ag_2S from one α -cage to another should be possible especially in cases where the 8-ring cation site is vacant. The diffusion rate is expected to increase at elevated temperature,

mainly because of the activation of ring-breathing vibrations.^{18,19}

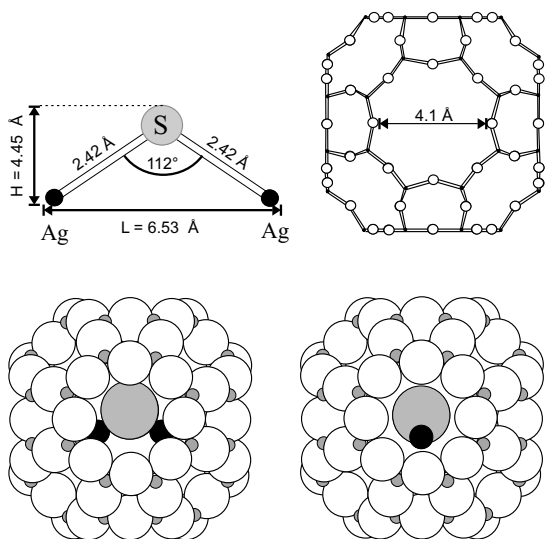


Fig. 4 *Top*: Geometries of the Ag₂S molecule and of the framework of zeolite A, respectively. The height and the length of the Ag₂S molecule include the interatomic distances and the ionic radii of Ag⁺ (1.26 Å) and of S²⁻ (1.84 Å). The structural diameter of the 8-ring of zeolite A is known from crystallographic data.²⁰ *Bottom*: Space-fill model of a Ag₂S molecule in an α -cage. For the orientation on the right hand-side it appears to be possible that the Ag₂S molecule can leave the α -cage through the 8-ring window.

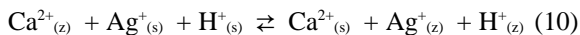
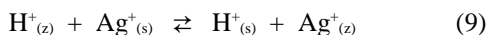
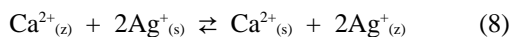
It is most likely that in samples with a silver loading smaller than 0.1 (the exact value depends on the co-cations) the cluster growth stops after reaction (4) since after some time no AgSH is left and the distance between the isolated Ag₂S molecules is too large so that they cannot reach each other by diffusion. This means that samples with a low silver loading contain to a great extent single Ag₂S molecules.

The reactions (5)-(7) mainly play a role in higher loaded samples where the Ag⁺ content of the individual α -cages varies to a certain extent (see Figure 3). The formation of Ag₂S proceeds much faster because AgSH molecules do not have to diffuse through several cages until they can react with other particles. Free AgSH reacts with Ag₂S to form larger silver sulfide particles as

described by equation (5) and (6). Reaction (7) is likely to take place if two Ag₂S are either in the same or in neighboring α -cages or if the samples are heated so that the diffusion rate of Ag₂S is increased. This process is observed upon heating hydrated Ag₂S-CaA-*x* samples for 1 h at 90° C in toluene. Figure 5 shows the luminescence spectra of Ag₂S-CaA-0.01 and of Ag₂S-CaA-0.75 before and after heating. In both cases there is an increase of the luminescence band at 610 nm after heating. Additionally a color change of Ag₂S-CaA-0.75 from bright yellow to darker yellow was observed. Slightly less pronounced changes were observed after heating the samples at 80° C for 1.5 h in air. Considering the distribution of the silver ions in the zeolite and the cluster growth mechanism described above we can assign the luminescence band at 490 nm to isolated Ag₂S molecules.

We will now discuss the exchange of divalent cations by silver ions. One divalent cation is always exchanged by two silver ions according to equation (8) (*z* = zeolite, *s* = solution). This means that at low silver loading there would only be α -cages containing 0 or 2 silver ions. To obtain only one silver ion per α -cage, ion exchange according to equation (9) or (10) would be required. However, these reactions play a less important role than reaction (8). On the one hand there is no evidence for Ca²⁺ exchange by H⁺ under our reaction conditions. There is always a higher Ag⁺ concentration than H⁺ concentration in a neutral solution (for example to achieve a silver loading of *x* = 0.01, 120 mg zeolite are suspended in 10 ml of 5·10⁻⁴ M Ag⁺ solution). The exchange of one Ca²⁺ by two Ag⁺ is an explanation for the observation that the formation of larger silver sulfide particles at low silver loading is more favorable in CaA than in NaA (see Figure 6 in ref. 8). Nevertheless it seems that at a low enough silver loading (*x* = 0.01) only single Ag₂S are

formed also in CaA. At such a low silver loading one Ca²⁺ is exchanged by two Ag⁺ according to equation (8). This results in a loading density of 2 Ag⁺ per 200 α-cages. Since the two silver ions are in the same α-cage occupying two different cation sites, the reaction with H₂S leads to the formation of two AgSH in the same α-cage. During rehydration of the zeolite both AgSH become mobile and form Ag₂S and H₂S (equation (4)). Thus one out of 200 α-cages contains one Ag₂S molecule and the probability for aggregation of two Ag₂S molecules as a result of diffusion is very low at room temperature.



The occupation of specific cation sites by Ag⁺ in dehydrated zeolites and the thereby determined position of AgSH after the reaction with H₂S affect the cluster growth. Zeolite A samples with Ag⁺ in the 4-ring position turn yellow upon dehydration. The yellow color is due to a charge transfer transition from the oxygen atoms of the zeolite lattice to the empty 5s orbital of the silver ions.^{9,10} Silver ions generally avoid the 4-ring position. Ag⁺-NaZK4 samples and Ag⁺-exchanged zeolite A samples with divalent co-cations and a silver loading of $x < 10$ do not turn yellow upon dehydration because there are enough other free cation sites which can be occupied by Ag⁺ so that all 4-ring positions stay free. In NaA the Na⁺ at the less favorable position in the 4-ring is exchanged by Ag⁺ first. This is the reason why Ag⁺-NaA samples turn yellow at a silver loading of as low as $x < 1$. In contrast to Ag⁺-NaA, Ag⁺-LiA and Ag⁺-KA show a yellow coloring upon dehydration only at higher silver loading (approximately $x = 4$ for Ag⁺-KA). This indicates that first some K⁺ and Li⁺ at the 8-ring or 6-ring positions

are exchanged by Ag⁺. K⁺ in a 4-ring is replaced by a Ag⁺ only after three of these positions have been occupied. These effects are caused by the different size of the cations and thus their different preference for coordination to the zeolite lattice.

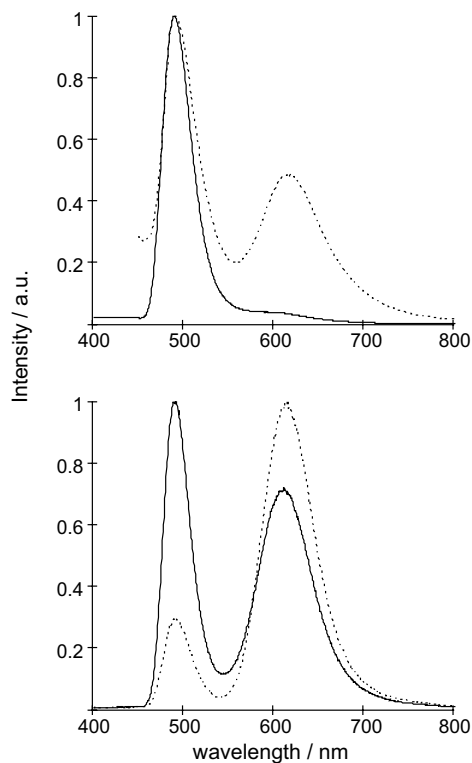


Fig. 5 Luminescence spectra of Ag₂S-CaA-0.01 (top) and Ag₂S-CaA-0.75 (bottom) at 80 K after excitation at 320 nm. The solid line is the spectrum before heating and the dotted line is the spectrum after heating the fully hydrated samples for 1 h at 363 K in toluene.

4 Diffuse Reflectance Spectra

The color of Ag₂S-MA-x samples strongly depends on the silver loading and on the co-cations and varies between colorless, yellow, orange and brown. Colorless samples which contain only Ag₂S molecules absorb in the UV (see Figure 6). Compared to Ag⁺-exchanged zeolite A the absorption of Ag₂S-CaA-0.01 consists of more than one absorption band. The color of Ag₂S-CaA-x

samples changes from light yellow to dark yellow to brown with increasing silver loading. The yellow color is typical for Ag₂S-CaA-*x* samples with $0.1 < x \leq 2$ and is related to an absorption between 400 and 500 nm while brown samples ($x > 2$) absorb almost in the whole visible region. The absorption of the colored samples in the UV is very strong so that saturation occurs.

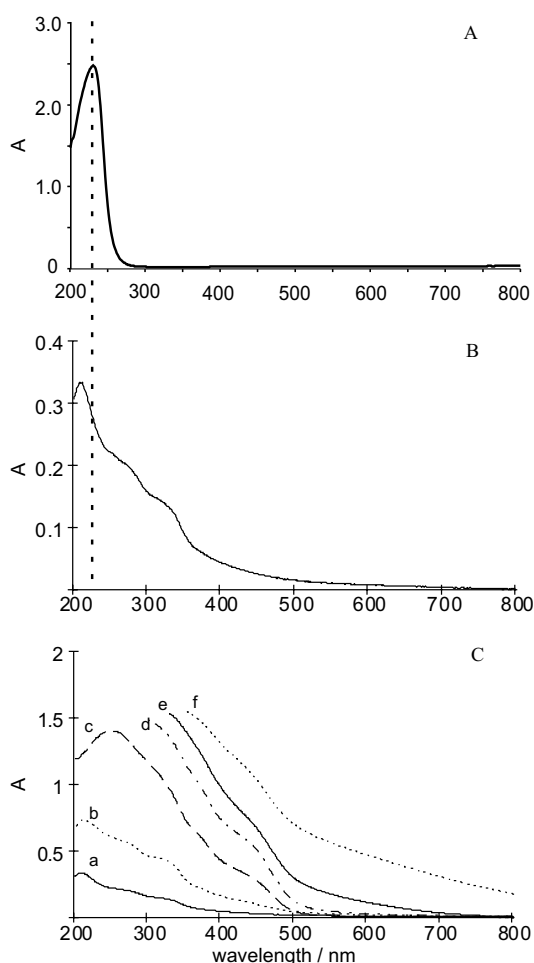


Fig. 6 DRS (Kubelka-Munk) of fully hydrated Ag₆Na₆A (A) and Ag₂S-CaA-*x* (B and C). B: *x* = 0.01, C: a) *x* = 0.01, b) *x* = 0.1, c), *x* = 0.5, d) *x* = 1.25, e) *x* = 2, and f) *x* = 3. Strong absorption in the UV causes saturation for samples of high Ag⁺ loading.

The co-cations affect the optical properties of Ag₂S-zeolite materials. We synthesized a series of samples with similar silver sulfide content but with different co-cations (Li⁺, Na⁺, K⁺, Mg²⁺, Ca²⁺, Sr²⁺). All samples with a silver loading around 1 Ag⁺ per α -cage show

an intense color. In the case of Ag₂S-CaA-1 and Ag₂S-SrA-1 the color is bright yellow. Ag₂S-MgA-1 is yellow-orange due to an absorption between 500 nm and 600 nm which is missing in the corresponding Ca²⁺ and Sr²⁺ samples (see Figure 7, right hand-side). The color of Ag₂S-KA-1 is orange and this is in contrast to Ag₂S-NaA-1 and Ag₂S-LiA-1 which are brown.

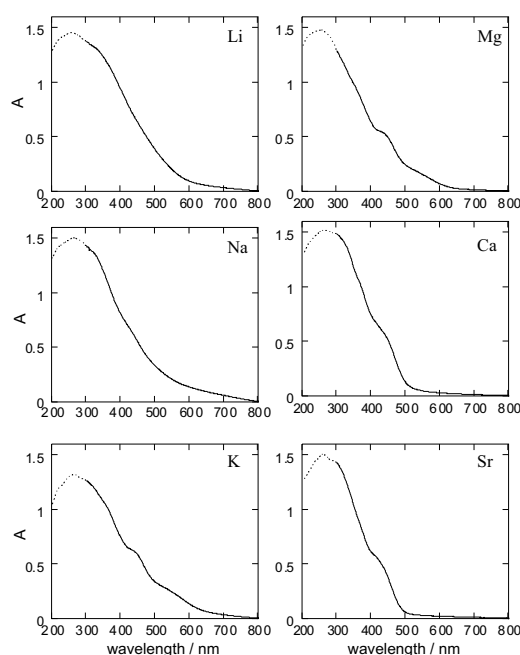


Fig. 7 DRS (Kubelka-Munk) of Ag₂S-MA-1 samples with M = Li⁺, Na⁺, K⁺, Mg²⁺, Ca²⁺, and Sr²⁺. The dotted line below 300 nm means that in this wavelength region saturation effects may occur.

5 Photoluminescence

Luminescence of Ag⁺-zeolite A

The luminescence properties of Ag⁺-zeolite A strongly depend on the amount of water and on the cations present in the cavities. The Ag⁺-luminescence can be clearly distinguished from the luminescence of silver sulfide containing zeolites. The luminescence of fully hydrated Ag⁺-zeolite samples considered here is always much weaker and at higher energies than the luminescence of Ag₂S-zeolite samples. Ca²⁺ and Mg²⁺ exchanged zeolites containing Ag⁺

show luminescence in their fully hydrated state while in the case of fully hydrated Na⁺-exchanged samples no luminescence could be observed. Figure 8 shows the luminescence spectra of a Ag⁺ exchanged CaA sample (1 Ag⁺ per α -cage) in its fully hydrated state directly after the ion exchange and one year later after storage in a closed vessel under ambient conditions. A state diagram of Ag_xCa_{6-0.5x}A containing some water is also shown in Figure 8. The absorption of UV-light leads to a charge transfer transition from the oxygen lone pairs of water to the 5s orbitals of Ag⁺. From there radiative relaxation to the lone pairs of the zeolite oxygens can take place.²¹ The color of Ag⁺-exchanged samples changes from brilliant white to grayish white after several weeks and a red shift of the emission and of the excitation spectrum is observed. This could be due to some migration of the silver ions and further reactions inside or outside the zeolite cages. Previous work about Ag⁺-exchanged zeolites showed that the luminescence properties of partially dehydrated Ag_xNa_{12-x}A irreversibly changed under intense illumination with UV light.²² These changes might be due to photochemical reduction and formation of silver clusters.

Luminescence properties of Ag₂S-CaA-x as a function of silver loading

By varying the silver loading the color of the luminescence of Ag₂S-CaA-x changes from green over different kinds of yellow and orange to red. Looking at the luminescence spectra in Figure 9 it can be seen that the green luminescence is related to an emission band at 490 nm, the orange luminescence is related to an emission band at 610 nm, and the yellow luminescence is caused by a mixture of both bands. At high silver loading ($x > 2$) the orange luminescence band shifts to lower energies which results in a dark red luminescence.

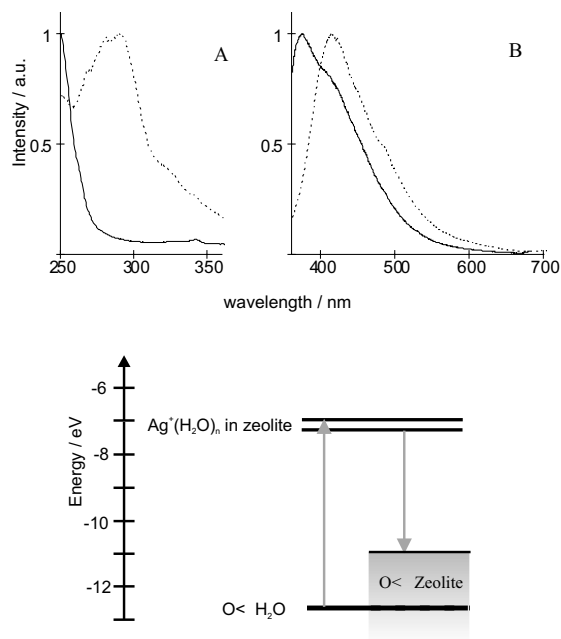


Fig. 8 Top: Excitation (A) and emission (B) spectra of Ag_xCa_{5.5}A in its fully hydrated state at 80 K. *Solid line*: freshly exchanged sample, *dotted line*: after one year storage under ambient conditions. Bottom: State diagram of Ag_xCa_{6-0.5x}A containing some water. |O< symbolizes the oxygen lone pairs of water and the zeolite lattice, respectively.

In the case of Ag₂S-CaA-x with $0.01 < x < 2$ the luminescence spectra can be broken down into two components, at 490 nm and 610 nm. Time resolved measurements show that the two components decay with different rates (see Figure 10, bottom). Considering the low silver loading and the distinct absorption bands in the excitation spectrum of the green luminescence we can assign the band at 490 nm to single Ag₂S molecules. This assignment is supported by MO calculations.⁸ The band at 610 nm can therefore be assigned to larger clusters. We propose that the luminescence at 610 nm is caused by the presence of Ag₄S₂ clusters. The structure of Ag₄S₂ clusters was theoretically studied by Bagatur'yants et al.²³

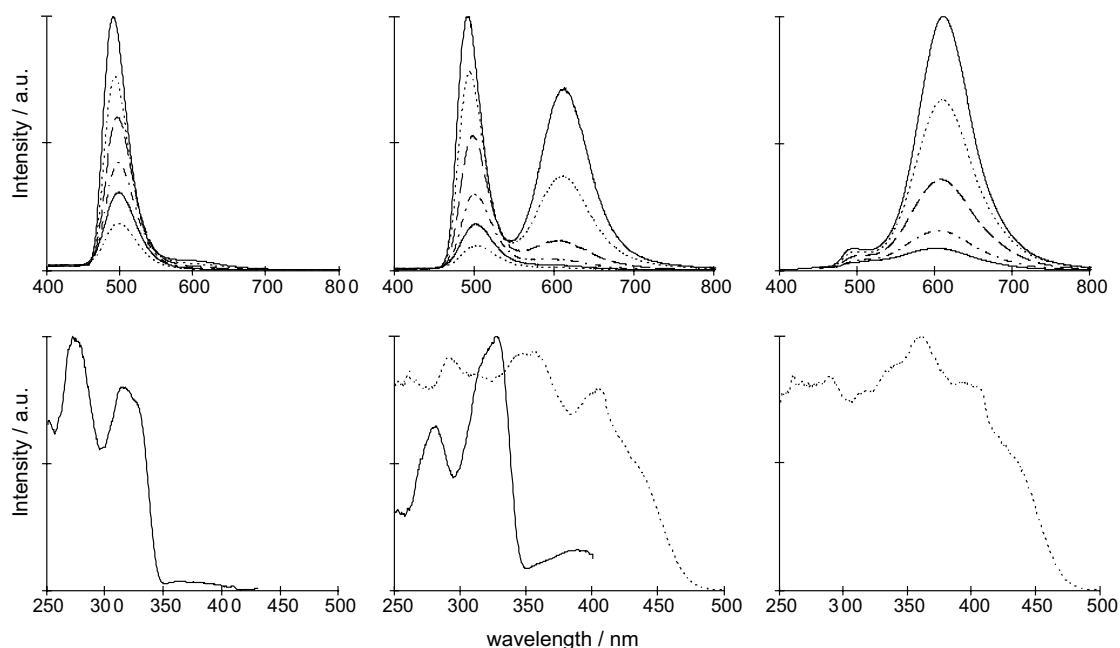


Fig. 9 *Top*: Luminescence spectra of Ag₂S-CaA- x with $x = 0.01, 0.75,$ and 2 from the left to the right at different temperatures (80 K, 123 K, 173 K, 223 K, 273 K, and 293 K). The luminescence intensity increases with decreasing temperature. Excitation was performed at 320 nm. *Bottom*: Excitation spectra at 490 nm (solid line) and at 610 nm (dotted line) at 80 K.

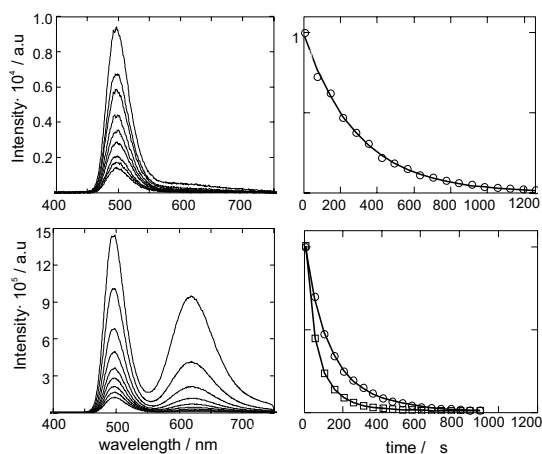


Fig. 10 *Left*: Time resolved luminescence spectra of Ag₂S-CaA-0.01 (top) and Ag₂S-CaA-0.75 (bottom) at 123 K. Excitation was performed at 320 nm and the time window for detection was 100 μ s. *Right*: The corresponding decay curves at 490 nm (points) and 610 nm (squares). The luminescence lifetime of Ag₂S-CaA-0.01 is 295 μ s. The average luminescence lifetimes of Ag₂S-CaA-0.75 are 181 μ s at 490 nm with $\tau_1 = 252$ μ s ($a_1 = 0.312$) and $\tau_2 = 99$ μ s ($a_2 = 0.688$) and 69 μ s at 610 nm with $\tau_1 = 108$ μ s ($a_1 = 0.199$), $\tau_2 = 43$ μ s ($a_2 = 0.44$) and $\tau_3 = 15$ μ s ($a_3 = 0.361$).

By choosing different silver loadings we are able to synthesize systems which contain only Ag₂S monomers ($x = 0.01$), Ag₂S and Ag₄S₂ clusters in different ratios ($0.01 < x < 2$), and mainly Ag₄S₂ ($x = 2$). The decay of the Ag₂S-luminescence strongly depends on the amount of Ag₄S₂. If only Ag₂S molecules are present, a nearly single exponential decay with a luminescence lifetime of about 300 μ s is observed (see Figure 10, top). With increasing silver sulfide content the luminescence lifetime of Ag₂S decreases and the decay can no longer be described by a single exponential function. Table 1 shows the luminescence lifetimes of Ag₂S as a function of silver loading. With increasing silver loading the Ag₄S₂ concentration increases and the luminescence lifetime of Ag₂S decreases. This effect is most likely due to energy transfer from Ag₂S (donor) to Ag₄S₂ (acceptor). The mechanism of this energy transfer is expected to be of the Förster type because the individual silver

sulfide particles are located in different α -cages therefore eliminating physical contact. A spectral overlap of the emission spectrum of Ag₂S and the excitation spectrum of Ag₄S₂ is a further indication that energy transfer is probable (see Figure 9).

Table 1 Luminescence lifetimes (τ_n) in μ s and their corresponding amplitudes (a_n) of Ag₂S as a function of silver loading x at 123 K. $\langle\tau\rangle$ is the average luminescence lifetime in μ s. Excitation wavelength = 320 nm, time window for detection = 100 μ s, detection of the green luminescence at 490 nm (Integration region 450-550 nm). The average lifetimes are mean values of three measurements.

x	$\tau_1 (a_1)$	$\tau_2 (a_2)$	$\langle\tau\rangle$
0.01	293 (1)	-----	297
0.1	341 (0.457)	117 (0.543)	276
0.5	304 (0.275)	94 (0.725)	210
0.75	252 (0.312)	99 (0.688)	178
1.25	217 (0.328)	68 (0.672)	152

Although the orange luminescence band can be described in a good approximation by a Gaussian curve and decays homogeneously, the decay behavior is not single exponential and a dependence on the excitation wavelength is observed. For example the average luminescence lifetime of Ag₂S-CaA-2 is 71 μ s (with $\tau_1 = 111$ μ s, $a_1 = 0.117$, $\tau_2 = 27$ μ s, $a_2 = 0.32$, $\tau_3 = 4$ μ s, $a_3 = 0.563$) after excitation at 440 nm and 55 μ s (with $\tau_1 = 83$ μ s, $a_1 = 0.193$, $\tau_2 = 30$ μ s, $a_2 = 0.316$, $\tau_3 = 9$ μ s, $a_3 = 0.491$) after excitation at 320 nm. This is probably due to a distribution of the same clusters but with slightly different environment, for example different positions in the α -cage and different coordination to water and co-cations. Another possibility is that these samples also contain a small amount of Ag₃S₂H particles (see mechanism of cluster growth) which may influence the luminescence decay behaviour by acting as a trap for the energy transfer. We conclude that the luminescence

lifetime of Ag₄S₂ clusters is much shorter than that of Ag₂S molecules and that most probably energy transfer from excited Ag₂S to Ag₄S₂ occurs.

Luminescence properties of Ag₂S-CaA-x as a function of temperature

Luminescence measurements at different temperatures reveal a different intensity and lifetime dependence of the two luminescence bands (see Figure 9). There is a stronger thermal quenching of the intensity of the orange luminescence band than of the green luminescence band. This can also be observed by looking at a sample under the UV lamp at different temperatures. The color of the luminescence then changes from bright orange to yellow to green with increasing temperature.

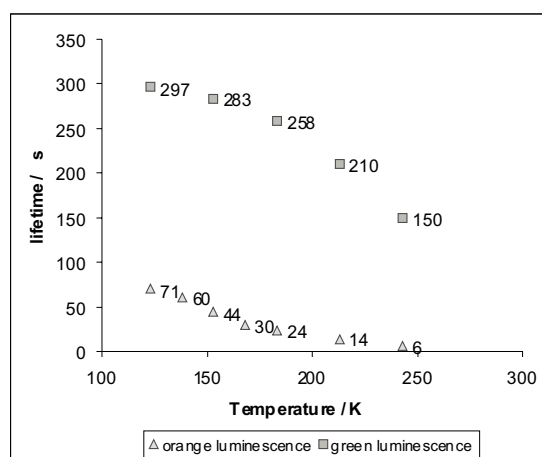


Fig. 11 Average luminescence lifetimes of Ag₂S (green luminescence) and Ag₄S₂ (orange luminescence) in μ s as a function of temperature. Excitation was performed at 320 nm for Ag₂S and at 440 nm for Ag₄S₂.

The luminescence lifetimes of the two bands have a different temperature dependence as shown in Figure 11. In the case of Ag₂S-CaA-0.01 where only single Ag₂S molecules are present, the electronic relaxation can be regarded as the sum of radiative and thermal relaxation since no other processes are involved. The measured lifetime τ is therefore the inverse of the sum

of the rate constant of the radiative relaxation k_L and of the rate constant of the thermal relaxation k_{IC} :

$$\tau = \frac{1}{k_{IC} + k_L} \quad (11)$$

where k_B is Boltzmann's constant, ΔE is the thermal quenching energy, and A is a pre-exponential factor. We then obtain the inverse lifetime τ^{-1} as a function of temperature:

$$\frac{1}{\tau} = A \exp\left(\frac{-\Delta E}{k_B T}\right) + k_L \quad (13)$$

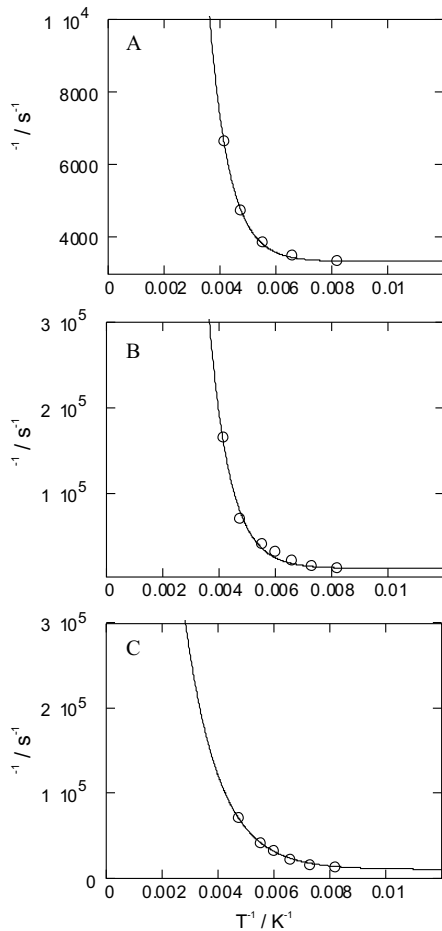


Fig. 12 Temperature dependence of the luminescence lifetime of Ag₂S and of Ag₄S₂. Experimental data (dots) and fit curve (line). A: Luminescence lifetime of Ag₂S with $\tau_0 = 300 \mu\text{s}$, $\Delta E = 11.54 \text{ kJ mol}^{-1}$, and $A = 1.003 \cdot 10^6 \text{ s}^{-1}$. B: Luminescence lifetime of Ag₄S₂ with $\tau_0 = 80 \mu\text{s}$, $\Delta E = 11.17 \text{ kJ mol}^{-1}$, and $A = 3.805 \cdot 10^7 \text{ s}^{-1}$. C: Luminescence lifetime of Ag₄S₂ with $\tau_0 = 100 \mu\text{s}$, $\Delta E = 6.88 \text{ kJ mol}^{-1}$, and $A = 2.982 \cdot 10^6 \text{ s}^{-1}$ in the temperature region 123-213 K.

The temperature dependence of k_{IC} can be described by the following equation:

$$k_{IC}(T) = A \exp\left(\frac{-\Delta E}{k_B T}\right) \quad (12)$$

k_L is the rate constant of the radiative relaxation and the inverse of the intrinsic lifetime τ_0 . If we plot the inverse lifetime τ^{-1} versus the inverse temperature T^{-1} , estimate the intrinsic lifetime to $300 \mu\text{s}$ ($k_L = 3333 \text{ s}^{-1}$) and fit the data to equation (13), we obtain $\Delta E = 11.54 \text{ kJ mol}^{-1}$ and $A = 1.003 \cdot 10^6 \text{ s}^{-1}$ (see Figure 12A).

To get the temperature dependence of the luminescence lifetime of Ag₄S₂ we choose a Ag₂S-CaA-2 sample which contains mainly Ag₄S₂ clusters and excited it at 440 nm where Ag₂S does not absorb. Figure 12C shows that a good fit is achieved only by using data between 123 and 213 K.

Influence of the co-cations on the luminescence of Ag₂S-MA and Ag₂S-MZK4

The co-cations influence not only the color of the silver sulfide-zeolite samples but also their luminescence properties. Looking at the luminescence spectra in Figure 13 we can distinguish different luminescent species. All samples except Ag₂S-KA-1 feature a band around 490 nm. The position of the maximum slightly depends on the co-cations and lies between 480 nm for Ag₂S-NaA and 495 nm for Ag₂S-SrA. Comparing the excitation spectra we conclude that this luminescence band is due to Ag₂S molecules. An assignment of the other luminescence bands is more difficult. The band around 610 nm which we assigned in the case of Ag₂S-CaA samples to Ag₄S₂ clusters is observed in every sample but its position and its width varies. This may be a consequence of the different neighboring co-cations or of

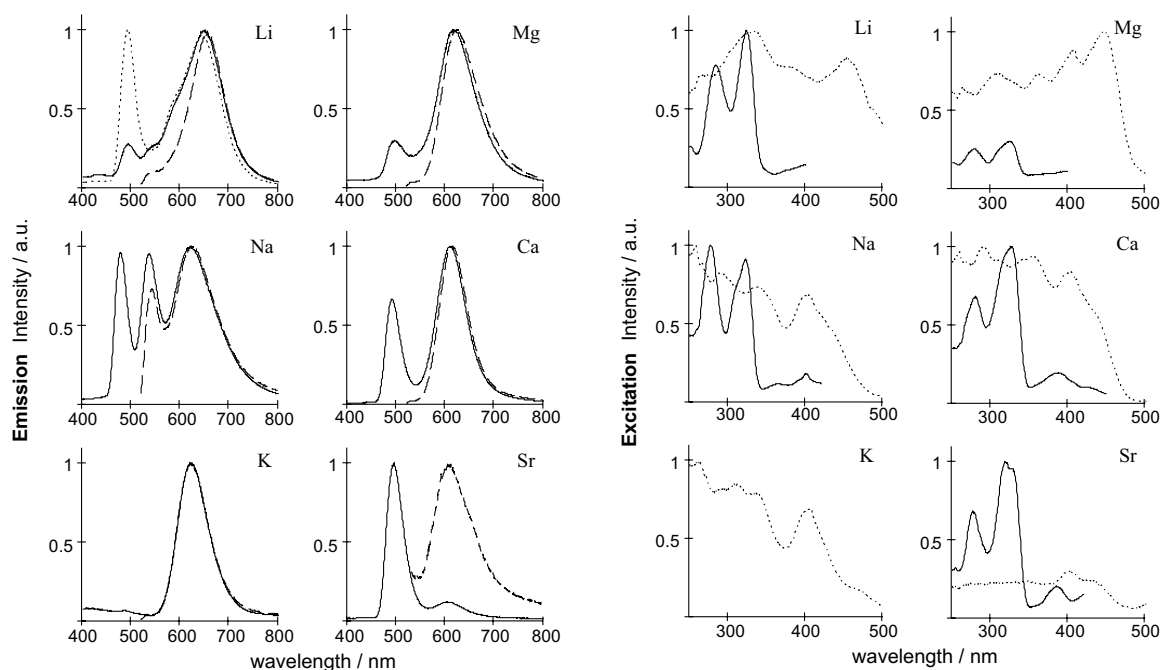


Fig. 13 Luminescence (left) and excitation (right) spectra of Ag₂S-MA-1 samples with M = Li, Na, K, Mg, Ca, and Sr at 80 K. The dotted line in the luminescence spectrum of "Li" corresponds to a Ag₂S-LiA-0.5 sample. Excitation was performed at 320 nm (solid line) and at 440 nm (dashed line). The spectra are scaled to the same height. Emission was observed at the maxima of the green luminescence band (solid line) and of the orange luminescence band (dotted line), respectively.

an overlap of the luminescence of different kind of (Ag₂S)_n clusters. The luminescence band of Ag₂S-KA-1 differs from the luminescence band of other sample that its maximum does not depend on the excitation wavelength. The excitation spectra of the orange luminescence do not supply much information because saturation effects especially below 400 nm complicate the spectral analysis. Nevertheless there are some similarities between Ca²⁺ and Sr²⁺ samples, between K⁺ and Mg²⁺ samples, and between Li⁺ and Na⁺ samples.

While in the case of K⁺, Mg²⁺, Ca²⁺, and Sr²⁺ samples the spectra can be assigned to one or two luminescent species, the luminescence spectra of Ag₂S-NaA-1 and Ag₂S-LiA-1 can be broken down into three and four components, respectively. This indicates that in Ag₂S-NaA and Ag₂S-LiA a larger variety of silver sulfide particles is present which is in agreement with the broad unstructured

absorption. Besides the luminescence bands of Ag₂S-NaA-1 at 480 nm and at 620 nm which again can be assigned to Ag₂S and Ag₄S₂, there is also a luminescence band at 540 nm. Its excitation spectrum consists of distinct absorption bands (see Figure 14A), suggesting a species with molecular properties. The thermal quenching of this luminescence band is much stronger compared to the other luminescence bands⁷ and its existence is related to the position of the Ag⁺ ions in dehydrated zeolites. Two observations were made: 1. Ag⁺-NaA is the only sample that turns yellow under dehydration already at an exchange level of 1 Ag⁺ per α -cage. For Ag⁺-KA and Ag⁺-LiA a higher exchange level is needed. 2. Luminescence spectra of Ag₂S-NaZK4 samples do not show a similar emission band (see Figure 15) and Ag⁺-ZK4-1 does not turn yellow under evacuation. The yellow color of dehydrated Ag⁺-exchanged zeolites was

attributed to Ag⁺-ions coordinated to the oxygens of the 4-ring.⁹ Ag⁺-ZK4-1 does not turn yellow because less cation sites are occupied than in zeolite A, so that all 4-ring positions are free. We conclude that the origin of the luminescence band at 540 nm of Ag₂S-NaA samples is most likely a small silver sulfide particle which is coordinated to the 4-ring oxygens even after rehydration of the zeolite. In Ag₂S-LiA-1 the same luminescence band is present but it is very weak and in contrast to Na-samples it cannot be observed at lower silver loadings. This indicates that only a very small number of Ag⁺ in LiA occupies the 4-ring position since no visible color change of Ag₁Li₁₁A under evacuation could be observed.

The long wavelength part (> 550 nm) of the luminescence spectrum of Ag₂S-LiA-1 consist of at least two overlapping emission bands. There is some difference in the excitation spectra at 580 nm and at 640 nm as shown in Figure 14B, suggesting two different luminescent species in Ag₂S-LiA. Excitation spectra of samples with other co-cations do not show such a dependence on the detection wavelength. The luminescence spectra in Figure 13 show that Ag₂S-LiA-1 emits at longer wavelengths than other samples after excitation at 440 nm. The lifetime of this luminescence is around 100 μs which is 30 - 40 μs longer than the luminescence lifetime of the other samples under the same conditions (see Table 2).

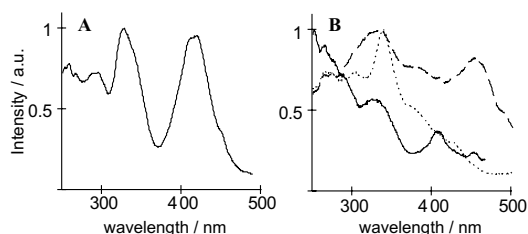


Fig. 14 A: Excitation spectrum of Ag₂S-NaA-1 at 540 nm. B: Normalized excitation spectra of Ag₂S-LiA-1 at 540 nm (solid line), at 580 nm (dotted line) and at 640 nm (dashed line).

Table 2 Luminescence lifetimes (τ_n) in μs and their corresponding amplitudes (a_n) of the orange luminescence band of Ag₂S-MA-1 at 123 K. Excitation was performed at 440 nm, the time window for detection was 10 μs, integration was done from 560 to 712 nm.

M	$\tau_1 (a_1)$	$\tau_2 (a_2)$	$\tau_3 (a_3)$	$\langle \tau \rangle$
Li	129 (0.234)	22 (0.455)	3 (0.311)	100
Na	88 (0.261)	22 (0.370)	3 (0.369)	68
K	103 (0.108)	31 (0.312)	6 (0.580)	60
Mg	83 (0.226)	24 (0.319)	2 (0.455)	64
Ca	190 (0.038)	48 (0.531)	9 (0.431)	72
Sr	134 (0.060)	32 (0.243)	4 (0.697)	71

Ag₂S-MZK4 samples look very similar to Ag₂S-MA samples. Figure 15 shows the luminescence spectra of Ag₂S-MZK4-1 with M = Na⁺, Ca²⁺, and Mg²⁺. The main difference is the missing luminescence band at 540 nm in Ag₂S-NaZK4 as mentioned above, the other luminescence bands are almost the same as in the corresponding Ag₂S-MA samples except for some spectral shifts.

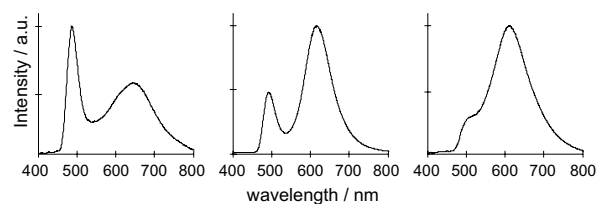


Fig. 15 Luminescence spectra of Ag₂S-NaZK4-1 (left), Ag₂S-CaZK4-1 (middle), and Ag₂S-MgZK4-1 (right) after excitation at 320 nm.

6 Conclusions

The optical properties of Ag₂S-zeolite materials are mainly influenced by the silver loading density and the co-cations and only to a small extent by the Si content of the zeolite (Zeolite A compared to ZK-4). By choosing different silver loadings in Ag₂S-CaA-x samples, we are able to

synthesize systems which contain only Ag₂S ($x = 0.01$), Ag₂S and Ag₄S₂ in different ratios ($0.01 < x < 2$), and mainly Ag₄S₂ ($x = 2$). These samples could be used for thermometry over a large temperature range (80 K and below - ~ 300 K) by measuring the luminescence intensity, the luminescence lifetimes, and the intensity ratio of the Ag₂S and Ag₄S₂ emission. An advantage of such a thermometer is that it can be placed anywhere because it does not have to be in contact with an electric device and it is insensitive to the environment because the luminescent silver sulfide particles are encapsulated in zeolites. Ag₂S-zeolites could be employed in addition to other luminescent nanoparticles or complexes which are suitable for thermometry.^{24,25} By arranging suitable Ag₂S-zeolites as monolayers it would be possible to measure the temperature difference of a surface with a high temperature resolution. With this arrangement one could get an imaging capability with high spatial resolution (μm). Another potential application would be a combination of Ag₂S-zeolites with AgCl for photocatalytic water splitting.^{21,26} The photochemical hydrogen production with suspensions of CdS was found to be increased by modifying the CdS powder with silver sulfide.²⁷

The luminescence lifetime of Ag₄S₂ is much shorter than that of Ag₂S and shows a more complex decay behavior. In mixed Ag₂S-Ag₄S₂ samples energy transfer from excited Ag₂S to Ag₄S₂ most probably occurs. A scheme of the involved energy levels and of the energy transfer is sketched in Figure 16. Both particles are excited with UV-light (320 nm). Ag₄S₂ can also be excited at lower energy (440 nm) most likely to another energy level. From the excited states radiationless relaxation into the LUMO occurs. Molecular orbital calculations state that the LUMO of Ag₄S₂ lies below the LUMO of Ag₂S while the HOMO is energetically equal.⁸ This is an explanation why the luminescence of Ag₄S₂ is red shifted

compared to the luminescence of Ag₂S. The same calculations give a very low oscillator strength for both HOMO-LUMO transitions in agreement with the large Stokes shift and the long luminescence lifetimes which were observed. In mixed Ag₂S-Ag₄S₂ systems the excited Ag₂S can either relax radiatively or non-radiatively to the ground state or it can transfer its energy to an excited state of Ag₄S₂.

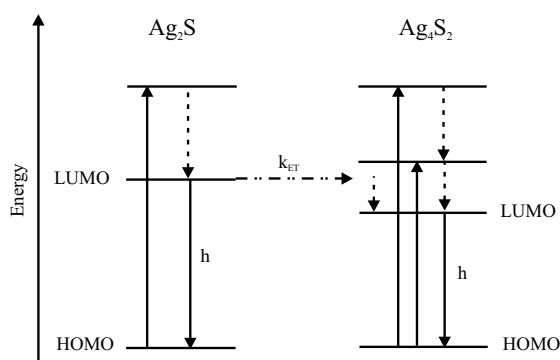


Fig. 16 Energy level diagram of Ag₂S and Ag₄S₂

It seems that the size and the amount of the co-cations, and thus the space available for silver sulfide particles in the α -cage, does not play an important role for the cluster growth. It is more likely that the co-cations influence the mobility of small silver sulfide particles during the cluster growth and the position and coordination of the final particles inside the zeolite cages. This might be due to different interactions of the co-cations with the zeolite framework, with the water molecules and with the silver sulfide clusters. However, the influence of the co-cations on the formation and on the optical properties of silver sulfide clusters in zeolites is not yet understood.

7 Acknowledgment

We acknowledge financial support by the Schweizerische Nationalfonds, project 2000-067684.02/1, by the Stiftung der Portland Cementfabrik Laufen, Baselland, Switzerland, and by the Schweizerische Bundesamt für Energiewirtschaft, project No

36846. We thank Beatrice Frey for EDX and SEM measurements.

8 References

- 1 L. Motte, M. P. Pileni, *Applied Surface Science*, 2000, **164**, 60-67.
- 2 K. Akamatsu, S. Takei, M. Mizuhata, A. Kajinami, S. Deki, S. Takeoka, M. Fujii, S. Hayashi, K. Yamamoto, *Thin Solid Films*, 2000, **359**, 55-60.
- 3 X. Qian, J. Yin, S. Feng, S. Liu, and Z. Zhu, *J. Mater. Chem.*, 2001, **11**, 2504-2506.
- 4 R. V. Kumar, O. Palchik, Y. Koltypin, Y. Diamant, A. Gedanken, *Ultrasonics Sonochemistry*, 2002, **9**, 65-70.
- 5 L. Armelao, R. Bertocello, E. Cattaruzza, S. Gialanella, S. Gross, G. Mattei, P. Mazzoldi, and E. Tondello, *J. Mater. Chem.*, 2002, **12**, 2401-2407.
- 6 G. D. Stucky and J. E. Mac Dougall, *Science*, 1990, **247**, 669- 677.
- 7 D. Brühwiler, R. Seifert, and G. Calzaferri, *J. Phys. Chem. B*, 1999, **103**, 6397-6399.
- 8 D. Brühwiler, C. Leiggener, S. Glaus and G. Calzaferri, *J. Phys. Chem. B*, 2002, **106**, 3770-3777.
- 9 R. Seifert, R. Rytz, and G. Calzaferri, *J. Phys. Chem. A*, 2000, **104**, 7473-7483.
- 10 R. Seifert, A. Kunzmann, and G. Calzaferri, *Angew. Chem. Int. Ed.*, 1998, **37**, 1521-1524.
- 11 D. W. Breck, *Zeolite Molecular Sieves* 1974, John Wiley & Sons
- 12 F. M. Higgins, N. H. De Leeuw, and S. C. Parker, *J. Mater. Chem.*, 2002, **12**, 124-131.
- 13 S. J. Hawkes, *J. Chem. Educ.*, 1996, **73**, 516-517.
- 14 P. Lainé, R. Seifert, R. Giovanoli, and G. Calzaferri, *New J. Chem.*, 1997, **21**, 453-460.
- 15 K. R. Franklin and R. P. Townsend, *J. Chem. Soc., Faraday Trans. 1*, 1985, **81**, 1071-1086.
- 16 A. Kunzmann, R. Seifert, and G. Calzaferri, *J. Phys. Chem. B*, 1999, **103**, 18-26.
- 17 D. W. Breck, W. G. Eversole, R. M. Milton, T. B. Reed, T. L. Thomas, *J. Am. Chem. Soc.*, 1956, **78**, 5963-5977.
- 18 M. Bärtsch, P. Bornhauser, G. Calzaferri, and R. Imhof, *J. Phys. Chem.*, 1994, **98**, 2817-2831.
- 19 P. Bornhauser and G. Calzaferri, *J. Phys. Chem.*, 1996, **100**, 2035-2044.
- 20 W. M. Meier and D. H. Olson, *Atlas of Zeolite Structure Type*, Second Edition 1987
- 21 G. Calzaferri, C. Leiggener, S. Glaus, D. Schürch, and K. Kuge, *Chem. Soc. Rev.*, 2003, **32**, 29-37.
- 22 G. Calzaferri, A. Kunzmann, P. Lainé, and K. Pfanner, *Imaging Science and Technology's 48th Annual Conference Proceedings*, 1995, 318-320.
- 23 A. A. Bagatur'yants, A. A. Safonov, H. Stoll, and H.-J. Werner, *J. Chem. Phys.*, 1998, **109**, 3096-3107.
- 24 S. Wang, S. Westcott, and W. Chen, *J. Phys. Chem. B*, 2002, **106**, 11203-11209.
- 25 N. Chandrasekharan and L. Kelly, *The Spectrum*, 2002, **15**, 1-7.
- 26 D. Schürch, A. Currao, S. Sarkar, G. Hodes, and G. Calzaferri, *J. Phys. Chem. B*, 2002, **106**, 12764-12775.
- 27 J.-F. Reber and M. Rusek, *J. Phys. Chem.*, 1986, **90**, 824-834.

3.2 Ag₂S-MA-x

Although the co-cations are not expected to be directly involved in the formation of silver sulfide clusters, they are somehow responsible for the nearest environment of the silver sulfide inside the zeolite cages. Depending on the co-cations the amount of water, the availability of coordination sites and the pore size (opening of the 8-ring) of the zeolite differ. In a series of experiments silver sulfide clusters were synthesized in different cation forms of zeolite A and silver loadings between 0.1 and 2 were chosen. The cations were alkaline and earth alkaline cations, namely Li⁺, Na⁺, K⁺, Mg²⁺, Ca²⁺, and Sr²⁺, which can be introduced by means of ion exchange before the synthesis of silver sulfide clusters. It was expected that within the defined silver loading range Ag₂S and Ag₄S₂ particles could be synthesized similar to what was observed in CaA.

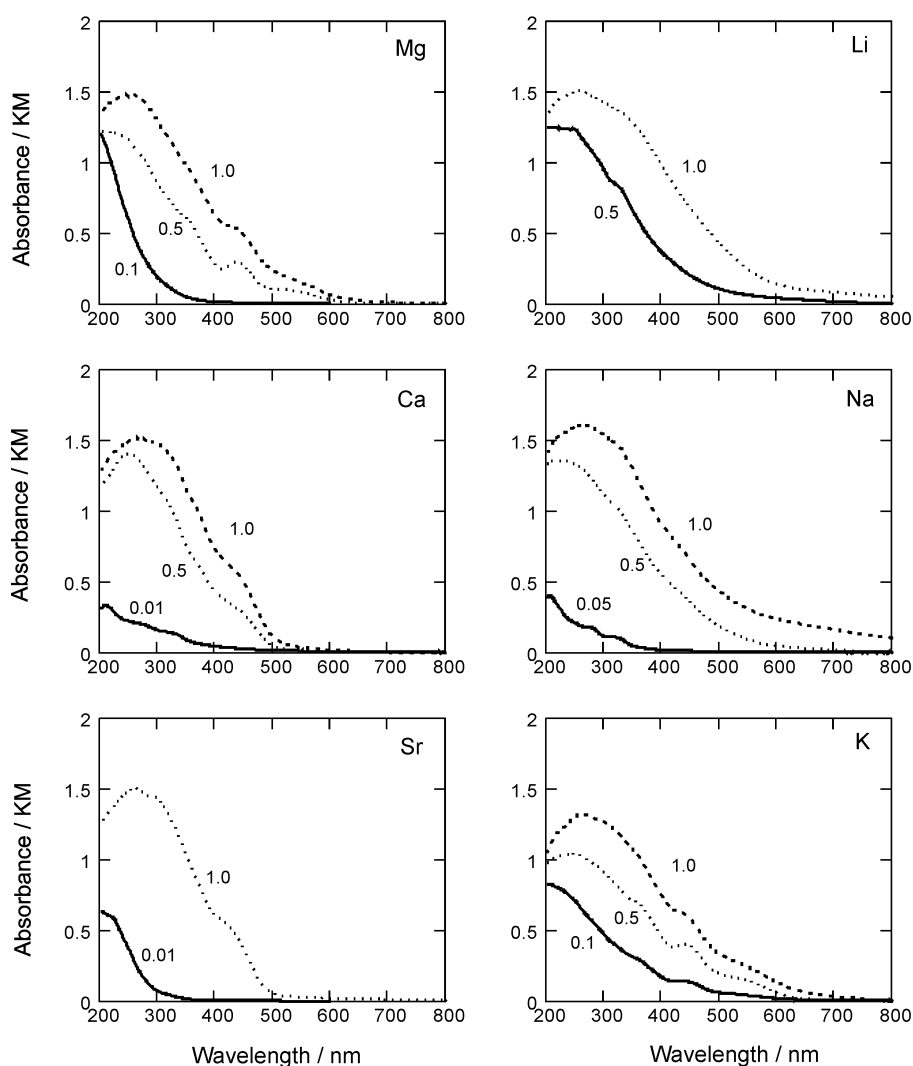


Figure 3.2.1: Diffuse reflectance spectra (Kubelka-Munk) of Ag₂S-MA-x with different co-cations and different silver loading. The value of x is indicated in the figures.

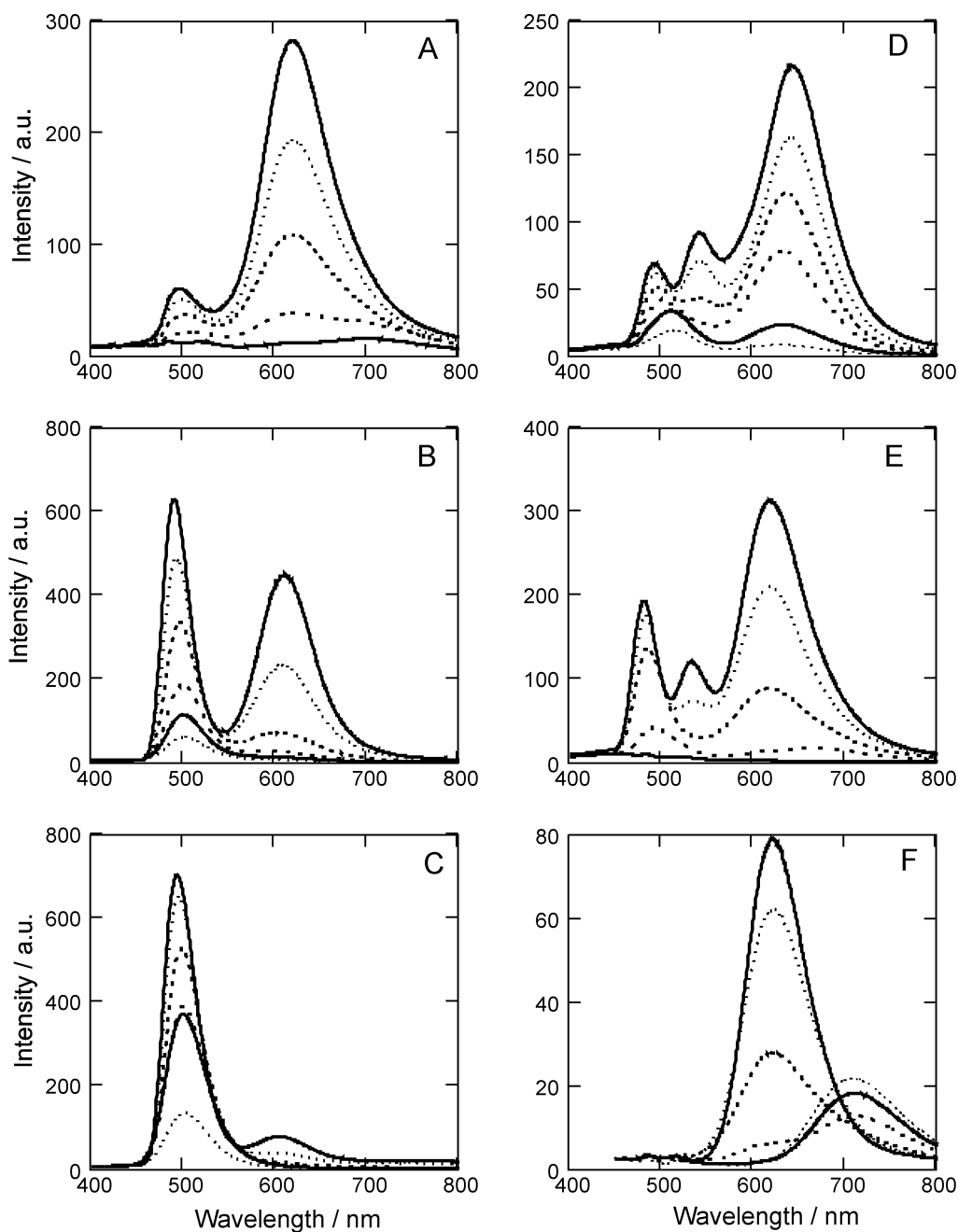


Figure 3.2.2: Luminescence spectra of Ag₂S-MA-x at different temperature (-190 °C, -150 °C, -100 °C, -50 °C, 0 °C, and +20 °C, decreasing intensity for A-E) upon excitation at 320 nm. A: Ag₂S-MgA-1, B: Ag₂S-CaA-0.75, C: Ag₂S-SrA-1, D: Ag₂S-LiA-1, E: Ag₂S-NaA-0.5, F: Ag₂S-KA-1.

3.2.1 Absorption

In general, samples with a low silver loading are colorless and become more and more colored with increasing silver loading. In Figure 3.2.1 the absorption spectra of samples with different co-cations and different silver loadings are shown. Depending on the co-cations the spectra are more or less structured. The mostly unstructured spectra belong to samples with Li⁺ and Na⁺ co-cations suggesting that these samples contain a larger variety of silver sulfide species than samples with other co-cations. The grayish color observed for some Ag₂S-NaA-x samples at higher silver loading could also be due to silver sulfide on the surface of the zeolite that absorbs in the whole visible range.

3.2.2 Luminescence

The differences of the luminescence properties depending on the co-cations are more significant than the differences observed in the absorption spectra. Figure 3.2.2 shows the temperature dependent luminescence spectra of samples with similar silver loading (0.5 - 1) and different co-cations. One can roughly distinguish between three types of spectra. 1. Spectra of samples containing divalent cations (A, B, and C) consist of two emission bands. 2. Spectra of samples containing Li⁺ and Na⁺ (D and E) consist of at least three emission bands. 3. Spectra of samples containing K⁺ show an additional emission band at elevated temperature. The reasons for these three types of spectra are not obvious and will be discussed in the following.

1. Spectra A - C: Ag₂S-MgA-x and Ag₂S-SrA-x reveal the same two luminescence bands as Ag₂S-CaA-x which were assigned to Ag₂S and Ag₄S₂. However, the relative intensities of the luminescence bands are quite different. We may assume that the amount of Ag₂S and Ag₄S₂ in all three samples is about the same. The similar absorbance supports this assumption. If this is correct, then the difference in the luminescence intensities could be due to cation dependent quenching mechanisms. Figure 3.2.3 shows the excitation spectra at the maxima of the two luminescence bands for the di-valent co-cations. In all of the three excitation spectra at 490 nm the typical transitions of Ag₂S at 280 nm and around 325 nm (double peak) can be recognized. In the case of Ag₂S-SrA-x there is also a clear transition at 386 nm which is predicted by theoretical reasoning of the Ag₂S molecule.^[17] The theoretical value of the oscillator strength of this transition is smaller than the oscillator strengths of the other transitions. The reason why this transition can be observed in Ag₂S-SrA-1 and not in Ag₂S-MgA-1 is not clear. From phenomenological observation one can state that it has something to do with the concentration of Ag₂S molecules because in Ag₂S-CaA-x samples it becomes more intense with increasing silver loading. The excitation spectra at 620 nm attributed to Ag₄S₂ are all noisy below 300

nm which is most probably due to saturation effects, and they show the same three transitions at 360 nm, 405 nm and 440 nm. The transition at 440 nm seems to be enhanced in Ag₂S-MgA-x compared to Ag₂S-CaA-x and Ag₂S-SrA-x.

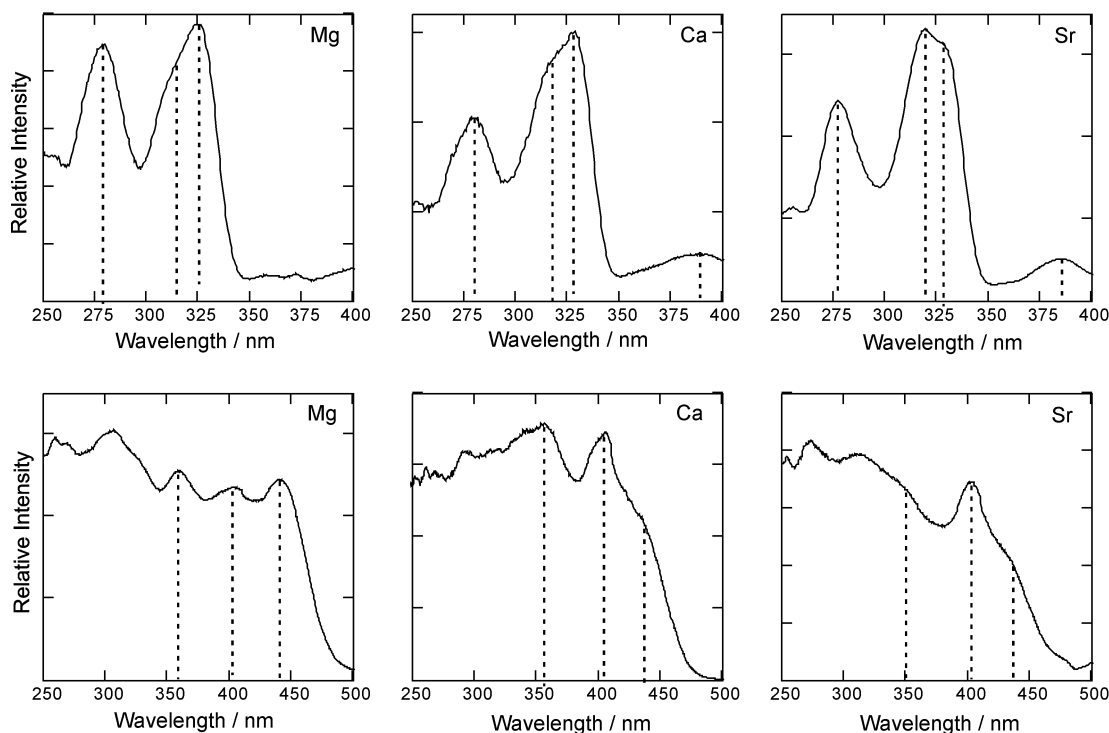


Figure 3.2.3: Excitation spectra at 490 nm (top) and at 620 nm (bottom) of Ag₂S-MA-x (M = Mg, Ca, Sr) at -190 °C.

The luminescence lifetimes of Ag₂S and Ag₄S₂ in Ag₂S-MA-1 (M = Mg, Ca, Sr) are shown in Table 3.2. The values are similar and lie within the normal deviation of data of different measurements. An exception is the luminescence lifetime of Ag₂S which is obviously shorter in Ag₂S-MgA-1 than in Ag₂S-CaA-1 and Ag₂S-SrA-1. We may argue that either there is a stronger quenching of the luminescence of Ag₂S in the presence of Mg²⁺, or energy transfer from Ag₂S to Ag₄S₂ is favored in Ag₂S-MgA-x compared to energy transfer in the other cation forms. Both explanations would be in accord with the different luminescence intensities of the spectra in Figure 3.2.2 (A,B,C). Ag₂S has the lowest luminescence intensity and the shortest luminescence lifetime in MgA. An argument for the enhanced energy transfer is given by the excitation spectra of Ag₄S₂ in Figure 3.2.3. The transition at 440 nm is stronger in MgA than in CaA or SrA leading to a larger spectral overlap between Ag₂S emission and Ag₄S₂ absorption. In SrA the opposite is

observed, the luminescence of Ag₂S is enhanced compared to the luminescence of Ag₄S₂.

Table 3.2: Luminescence lifetimes (τ) in μ s and the corresponding amplitudes (a) of Ag₂S and Ag₄S₂ in Ag₂S-MA-1 (M = Mg, Ca, Sr) at -150 °C. $\langle\tau\rangle$ is the average luminescence lifetime.

M	Ag ₂ S			Ag ₄ S ₂			
	$\tau_1 (a_1)$	$\tau_2 (a_2)$	$\langle\tau\rangle$	$\tau_1 (a_1)$	$\tau_2 (a_2)$	$\tau_3 (a_3)$	$\langle\tau\rangle$
Mg	176 (0.143)	42 (0.875)	97	83 (0.226)	24 (0.319)	2 (0.455)	64
Ca	207 (0.388)	52 (0.612)	163	97 (0.200)	42 (0.341)	11 (0.460)	66
Sr	224 (0.325)	52 (0.675)	168	134 (0.06)	32 (0.243)	4 (0.697)	71

For a detailed argumentation about energy transfer in Ag₂S-MgA-x and Ag₂S-SrA-x samples more and systematic work would be needed, similar as it was done in the case of Ag₂S-CaA-x.

2. Spectra D and E:

The luminescence spectra of Ag₂S-LiA-x and Ag₂S-NaA-x can be roughly divided into three bands at 480 nm, at 540 nm, and at 620 nm. The excitation spectra recorded at the maxima of the three luminescence bands are shown in Figure 3.2.4. The band at 480 nm again corresponds to single Ag₂S molecules as can be seen in the excitation spectra. The band at 540 nm is only observed in the presence of Li⁺ and Na⁺ as co-cations and is probably due to a silver sulfide species in the size regime between Ag₂S and Ag₄S₂. Its excitation spectrum reveals transitions around 280 nm, 320 nm, and 410 nm suggesting rather an Ag₂S particle. Another possibility is that the luminescence at 540 nm comes from Ag₃S₂H particles which are also involved in the cluster growth process. But then the question arises why they cannot be observed in samples with divalent cations. Besides a large amount of these species should also give a Ag/S ratio below 2 in the EDX data, which could not be confirmed for Ag₂S-NaA-x samples.^[10] So let us assume that one can distinguish between two different Ag₂S particles, one also observed in samples with divalent co-cations and one only observed in the presence of Li⁺ and Na⁺. The second has an additional absorption band at 410 nm and its luminescence is red shifted and stronger affected by temperature than the luminescence of the first Ag₂S. In the following discussion the two different Ag₂S are named Ag₂S(480) and Ag₂S(540) related to their emission wavelength. The luminescence lifetimes of Ag₂S(480) and Ag₂S(540) in

Ag₂S-LiA-1 are similar at -160 °C (see Table 3.3). Measurements at higher temperature were not possible because then the luminescence at 540 nm is too weak. The appearance of two electronically different Ag₂S has to be connected with the number of co-cations and their probability of occupying specific sites in the zeolite. In Na⁺-ZK4, which has less than 12 Na⁺ ions, Ag₂S(540) could not be observed. One can suggest that Ag₂S(540) is an Ag₂S molecule at a less favorable site in the zeolite than Ag₂S(480) and that it only appears if there are no other sites available. An example for such a less favorable site is a position near the 4-membered rings.

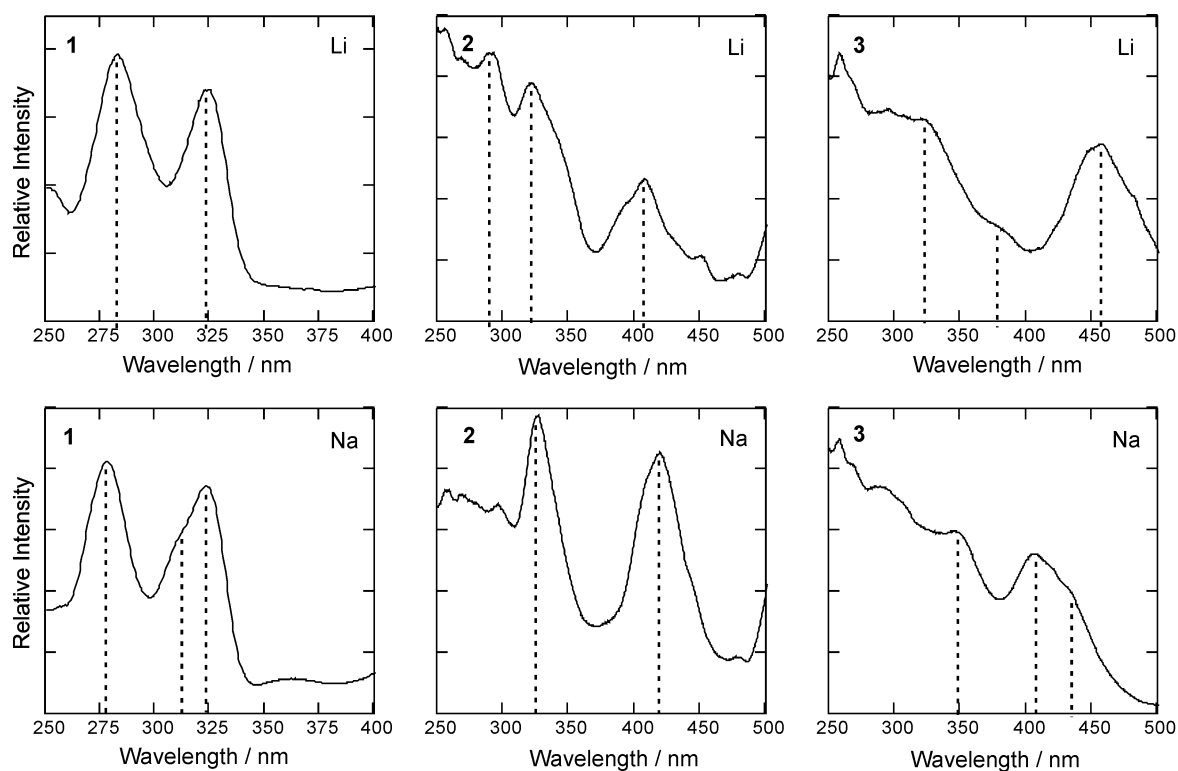


Figure 3.2.4: Excitation spectra of Ag₂S-LiA-1 (top) and Ag₂S-NaA-0.5 (bottom) recorded at different luminescence wavelengths (λ_{em}) at -190 °C. 1) $\lambda_{em} = 480$ nm, 2) $\lambda_{em} = 540$ nm, 3) $\lambda_{em} = 620$ nm.

The luminescence around 620 nm can again be assigned to Ag₄S₂ in the case of Ag₂S-NaA-x. However, in the case of Ag₂S-LiA-x this luminescence can be broken down into two overlapping bands. This is more clearly demonstrated in the spectra in Figure 3.2.5 (chapter 3.2.3). One can assume an equilibrium between two different forms of Ag₄S₂, one being similar to what is observed in Ag₂S-NaA-x and the other one having red shifted electronic spectra.

Table 3.3: Luminescence lifetimes (τ) in μ s and the corresponding amplitudes (a) of Ag₂S-LiA-1 at -160 °C after excitation at 320 nm. $\langle\tau\rangle$ is the average luminescence lifetime.

λ_{em}	$\tau_1 (a_1)$	$\tau_2 (a_2)$	$\tau_3 (a_3)$	$\langle\tau\rangle$
480 nm	406 (0.032)	129 (0.150)	6 (0.818)	208
540 nm	506 (0.030)	135 (0.181)	6 (0.789)	247

3. Spectra F:

Ag₂S-KA-x samples show a deep red photoluminescence at room temperature which is not observed in samples with other co-cations. In the temperature dependent luminescence spectra in Figure 3.2.2 one can see that the “normal” luminescence band at low temperature is replaced by a luminescence band at 710 nm at elevated temperature. This phenomenon is known as luminescence thermochromism and will be discussed in detail in chapter 4.

3.2.3 Stability

All samples are stable under ambient conditions in a sense that the silver sulfide clusters stay inside the zeolite cages. However, depending on the co-cations some changes of the luminescence with time can be observed. The most obvious changes happen in Ag₂S-LiA-x and in Ag₂S-NaA-x samples while in Ag₂S-CaA-x there are only little changes. Examples of luminescence spectra of Ag₂S-LiA-1, Ag₂S-NaA-1, and Ag₂S-CaA-0.75 at different times after the synthesis are shown in Figures 3.2.5 - 3.2.7.

One can imagine that the silver sulfide clusters are not in a rigid position in the α -cage and that they change their coordination sphere until they reach an energetically favorable position. Depending on the co-cations which are competing for coordination sites of the zeolite lattice and for the water molecules this can take more or less time. Also the diffusion rate of small species such as AgSH may be influenced by the co-cations. It also has to be considered that the reactions leading to cluster growth, which are described in chapter 2.4 (Equations 2.4.1-2.4.4), are equilibria. The presence of co-cations was not taken into account, but may have some effect on the kinetics to establish these equilibria.

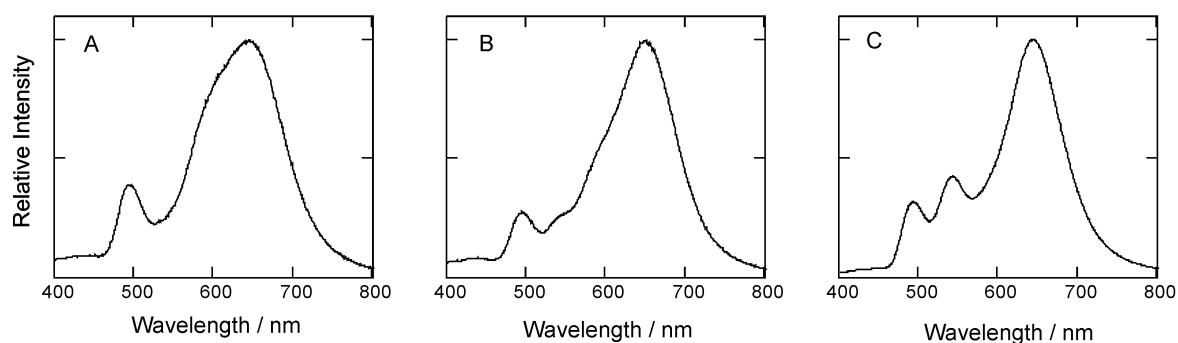


Figure 3.2.5: Luminescence spectra of Ag₂S-LiA-1 at different times after the synthesis. A) after one week, B) after 2 months, C) after 15 months. The spectra were measured at -190 °C upon excitation at 320 nm.

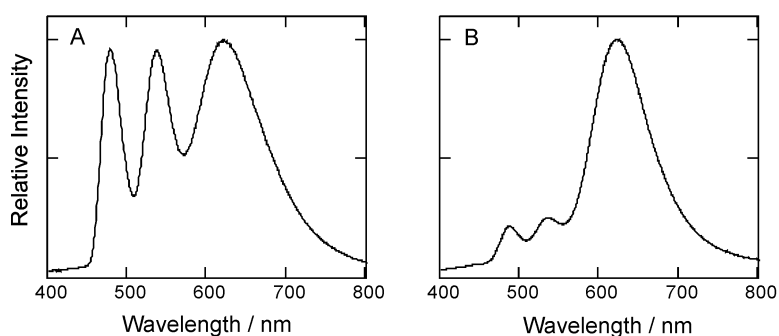


Figure 3.2.6: Luminescence spectra of Ag₂S-NaA-1 at different times after the synthesis. A) after 3 weeks, B) after 17 months. The spectra were measured at -190 °C upon excitation at 320 nm.

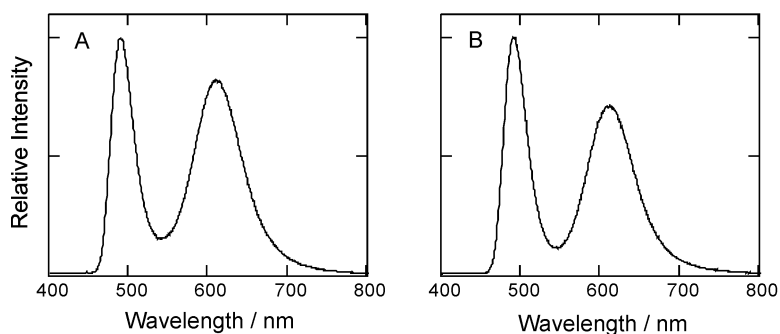


Figure 3.2.7: Luminescence spectra of Ag₂S-CaA-0.75 at different times after the synthesis. A) after 2 weeks, B) after 3 months. The spectra were measured at -190 °C upon excitation at 320 nm.

3.3 Conclusions

The optical properties of Ag₂S-zeolite A materials can be tuned by varying the amount of silver sulfide and the co-cations. The color of these materials ranges from white over different kind of yellow and orange to brown. All samples show photoluminescence in the visible, the color and the intensity of which is influenced by several factors. However, the reasons for the influence of the co-cations on the optical properties of silver sulfide clusters are not yet understood.

The size of the silver sulfide clusters depends on the initial silver loading of the zeolite. The two smallest silver sulfide clusters that we propose being stabilized inside the α -cage are the Ag₂S monomer and the Ag₄S₂ cluster. The luminescence properties of these species were studied in detail in Ca²⁺-exchanged zeolite A. Over a silver loading range of $x = 0.01 - 2$ samples containing Ag₂S and Ag₄S₂ in the same zeolite crystal were obtained. The ratio of Ag₂S and Ag₄S₂ is given by the silver loading and can therefore be varied at the beginning of the synthesis. Upon excitation with UV light Ag₂S emits at 490 nm and Ag₄S₂ at 610 nm, while Ag₄S₂ can also be excited at longer wavelengths ($\lambda \leq 500$ nm). Time-resolved luminescence measurements at different temperatures yield an intrinsic luminescence lifetime around 300 μ s for Ag₂S and around 100 μ s for Ag₄S₂ in zeolite A. Considering all spectroscopic results one can say that Ag₂S and Ag₄S₂ can both be excited to short-lived excited states from where fast radiationless relaxation to the first excited state occurs, followed by a long-lived luminescence. This is in agreement with MO calculations which predict a weak oscillator strength for the HOMO-LUMO transitions of Ag₂S and Ag₄S₂. In samples containing Ag₂S and Ag₄S₂ the excited Ag₂S can either relax radiatively or non-radiatively to the ground state or it can transfer its energy to an excited state of Ag₄S₂. The mechanism of this energy transfer is expected to be of the Förster type.

The same two species are also found in zeolite A with other co-cations and in ZK-4. In the presence of Li⁺ and Na⁺ co-cations an additional luminescence band at 540 nm is observed. Its existence is related to 4-ring coordinated Ag⁺ in dehydrated zeolite A and its excitation spectrum indicates a particle with molecular properties similar to Ag₂S. Our suggestion is that the luminescence at 540 nm is due to Ag₂S molecules located near the 4-ring, which is a less favorable position, and that this position is only occupied if no other coordination is possible.

The next larger silver sulfide clusters may have the stoichiometries Ag₆S₃ and Ag₈S₄. They are supposed to be responsible for the brown color of samples with increasing silver

loading and for the red shift of the luminescence, which correlates with decreasing luminescence lifetimes.

The luminescence properties of all Ag₂S-Zeolite A samples strongly depend on the temperature which makes them potential materials for thermometry. Most interesting are Ag₂S-CaA-x (with $0.01 > x > 2$) showing a different thermal quenching of the Ag₂S and Ag₄S₂ luminescence and Ag₂S-KA-x samples showing luminescence thermochromism.

4. Monolayers of Zeolite A Containing Luminescent Silver Sulfide Clusters

For future applications of Ag_2S -zeolite A materials it is a big advantage to have the zeolite crystals arranged as monolayers. For example if one would like to create a sensor for water or for specific cations it is much easier to study the optical changes on a monolayer. With a monolayer of zeolite A microcrystals containing silver sulfide clusters, which show luminescence changes with temperature, one could map surface temperatures with a high spatial resolution. Another possibility to make use of Ag_2S -zeolite A monolayers is in the field of photocatalytic water splitting which is another current project in our group.^[49,50] Thin AgCl layers can act as photocatalysts in the presence of a small excess of silver ions. In the photocatalytic reaction water is oxidized to O_2 and protons, and Ag^+ is reduced to silver upon irradiation. The reduced silver species are then reoxidized, which makes the system catalytic.^[51,52] The photoactivity of the system extends from the UV to the visible region due to silver clusters adsorbed on the surface. This process is known as self-sensitization. The photoactivity of AgCl layers was enhanced by modification with gold colloids.^[53] The modification of the same layers with Ag_2S - or Ag^+ -zeolites could have a similar effect. On the one hand the silver sulfide clusters may act as photosensitizers due to their absorption in the visible. On the other hand the active surface area of the photoanode is increased by the presence of the zeolites, so that a higher O_2 production rate is expected.

The publication “*Monolayers of Zeolite A containing Luminescent Silver Sulfide Clusters*” in chapter 4.1 reports the synthesis of Ag_2S -zeolite A monolayers on quartz, and two special optical phenomena of these materials in the presence of potassium co-cations, namely luminescence thermochromism and laser action, are described. In chapter 4.2 and 4.3 some additional information about these phenomena will be given, and in chapter 4.4 the preparation of zeolite monolayers on other substrates and their use in photocatalytic water splitting experiments will be discussed.

4.1 Publication

“Monolayers of Zeolite A containing Luminescent Silver Sulfide Clusters”

ChemPhysChem **2004**, 5, 1593-1596.

Claudia Leiggner and Gion Calzaferri*

Department of Chemistry and Biochemistry, University of Bern, Freiestrasse 3, CH-3000 Bern 9, Switzerland

Luminescence thermochromism is an optical phenomenon which was first observed in copper(I) complexes.^[1] Recently also silver and gold compounds were found to be among the few good examples showing luminescence thermochromism.^[2,3] We have reported how luminescent silver sulfide species can be synthesized in the cavities of zeolite A.^[4] The color of the luminescence of these materials changes with temperature due to a stronger thermal quenching of the luminescence of Ag_4S_2 than of the luminescence of Ag_2S . The synthesis of these new species is based on the

observation that thin layers of Ag^+ -loaded zeolite A can be reversibly activated (dehydrated) at room temperature.^[5] We now describe a new procedure for preparing very stable, high-quality zeolite A monolayers on quartz and similar substrates, and we report the first example of an in situ “ship-in-a-bottle”^[6] cluster synthesis on such monolayers. To our surprise we observed that, in the presence of potassium co-cations, luminescence thermochromism occurs.

The preparation and properties of monolayers of zeolite crystals were

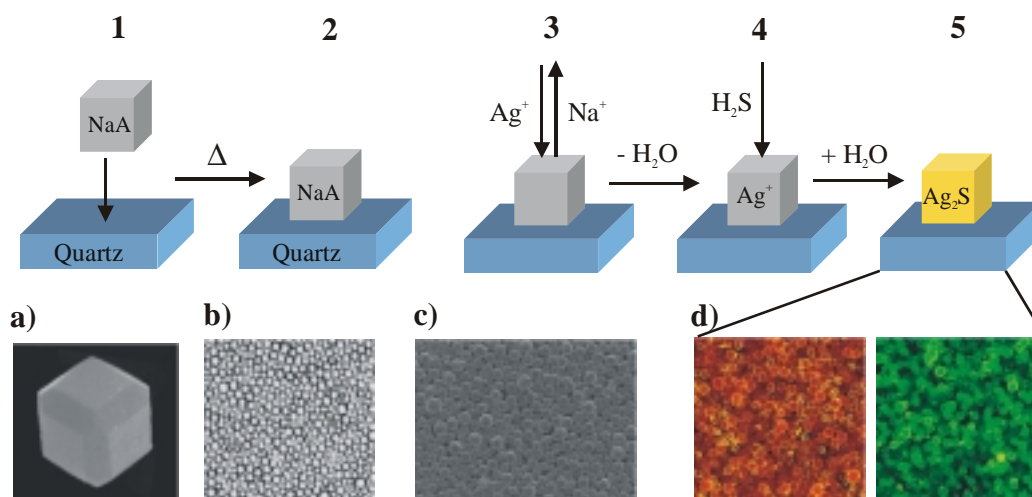


Figure 1: Formation of stable zeolite A monolayers on quartz and subsequent “ship-in-a-bottle” synthesis of luminescent silver sulfide clusters, step 1-5. a) Electron micrograph of a single zeolite A crystal with an edge length of 3 μm . b) Optical microscopic image of a monolayer of zeolite A crystals, seen in transmission. c) Electron micrograph of a monolayer of zeolite A crystals with an edge length of about 3-4 μm . d) True color optical microscopic images of luminescent zeolite A monolayers containing Ag_4S_2 (orange) and Ag_2S (green).

described in 1995^[7] and later substantially expanded by several groups.^[8] We found that the procedure explained in Figure 1 is very convenient for preparing stable zeolite A monolayers, which can afterwards successfully be modified, for example, by means of a "ship-in-a-bottle" synthesis.

First zeolite A crystals are deposited as monolayers on quartz (or another appropriate substrate) by sedimentation at room temperature, step 1. In the next step 2, the physisorbed crystals were fixed by heating the layer up to 600 °C. The layers are stable in aqueous environment, so that in 3 the insertion of Ag⁺ into zeolite A by means of ion-exchange could be carried out in a well-controlled way. Then the layers were dried under high vacuum at room temperature to remove water from the zeolite cages. The samples were now ready for exposure to H₂S(g), which diffused into the zeolite cages and reacted with Ag⁺ yielding AgSH and a proton, step 4. The samples were then rehydrated in step 5 so that AgSH became sufficiently mobile and the desired (Ag₂S)_n clusters were formed and stabilized in the α -cages of zeolite A. It was experimentally easy to vary the amount of exchanged Ag⁺ precisely. This allows control of the size of the clusters, so that for example either green luminescent zeolites containing Ag₂S monomers or orange luminescent zeolites containing Ag₄S₂ may be obtained.

The cations compensate the negative charge of the zeolite framework and are usually Na⁺ ions due to the synthesis conditions of zeolite A. The cations occupy specific positions in the framework and may also be exchanged with other cations. We found that the co-cations can also be exchanged after the silver sulfide synthesis if the silver sulfide content is not too high. In the presence of K⁺ as co-cations a new phenomenon appears, which corresponds to what is known as luminescence thermochromism. We observed that zeolite

A samples containing K⁺ and silver sulfide show, at room temperature, a bright deep-red photoluminescence with its maximum emission at 710 nm. Figure 2 shows the luminescence spectra of K⁺-zeolite A containing silver sulfide with a concentration of one Ag⁺ per a-cage. With decreasing temperature the luminescence band at 710 nm becomes weaker and is replaced by an orange luminescence at 620 nm. This process is completely reversible, which is a prerequisite for luminescence thermochromism. The luminescence decay at 620 nm fits to a three-exponential function with the lifetimes $\tau_1 = 110 \mu\text{s}$, $\tau_2 = 26 \mu\text{s}$, and $\tau_3 = 5 \mu\text{s}$ at $-150 \text{ }^\circ\text{C}$, with the amplitudes $a_1 = 0.126$, $a_2 = 0.438$, and $a_3 = 0.437$, resulting in an average luminescence lifetime of 67 μs . The fractional contribution of the components is defined as Equation (1).

$$f_j = \frac{a_j \cdot \tau_j}{\sum_i a_i \cdot \tau_i} \quad (1)$$

The values obtained are $f_1 = 0.505$, $f_2 = 0.415$, and $f_3 = 0.08$. The position of the orange luminescence band at 620 nm, its excitation spectrum, and its decay behavior indicate that it comes from Ag₄S₂ clusters.^[4] The luminescence band at 710 nm has a completely different excitation spectrum, as shown in Figure 3.

There are different reasons for assuming that a temperature-dependent equilibrium and not a thermally stimulated luminescence or energy transfer is responsible for this luminescence thermochromism. First, we can exclude the thermally activated population of an energy level of the same compound because the excitation spectra observed at 620 nm and at 710 nm are too different. Second, the luminescence at 710 nm is not observed at temperatures below $-100 \text{ }^\circ\text{C}$. If the species that emit at 710 nm

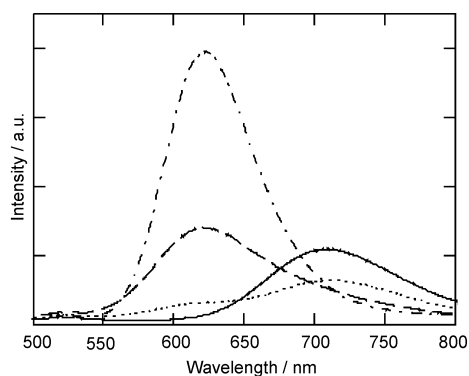


Figure 2: Luminescence spectra of $\text{Ag}_2\text{S-KA-1}$ at different temperatures after excitation at 320 nm. $T = 22^\circ\text{C}$ (solid line), -50°C (dots), -100°C (dash), and -190°C (dash-dot).

were also present at low temperature, they would be expected to show luminescence after excitation at a suitable wavelength also at low temperature. Besides, the luminescence lifetime of the 710 nm band decreases with increasing temperature (see Table 1), while the intensity increases. This observation can only be explained as follows: The increasing intensity is due to the favored formation of the red luminescent form at elevated temperature, however, the luminescence lifetime decreases because of stronger thermal quenching. In other words, at room temperature the amount of the red luminescent form is higher than at -50°C , but its luminescence lifetime is shorter than at low temperatures due to thermal quenching. So one can consider equilibrium between two luminescent forms $X(L_1)$ – see Equation (2) – which stands for the orange emitting species (620 nm) and $B(L_2)$, which corresponds to the red emitting species (710 nm).



The observation that the red luminescence at 710 nm only occurs in samples containing K^+ indicates that it is due to specific interaction between K^+ and silver sulfide. In fact, on exchanging Li^+ in a $\text{Ag}_2\text{S-LiA-0.5}$

Table 1. Luminescence lifetimes of the red luminescence (710 nm) in μs . $\langle\tau\rangle$ is the average luminescence lifetime.

$T[^\circ\text{C}]$	τ_1	a_1	f_1	τ_2	a_2	f_2	$\langle\tau\rangle$
0	71	0.487	0.799	17	0.513	0.201	61
-10	109	0.504	0.874	16	0.496	0.126	97
-30	131	0.665	0.875	37	0.335	0.124	119
-50	197	0.595	0.948	16	0.405	0.052	187^[a]

[a] A better fit is achieved by using three components ($\tau_1 = 286 \mu\text{s}$, $a_1 = 0.305$, $\tau_2 = 126 \mu\text{s}$, $a_2 = 0.306$, $\tau_3 = 16 \mu\text{s}$, $a_3 = 0.389$) resulting in an average lifetime of $227 \mu\text{s}$.

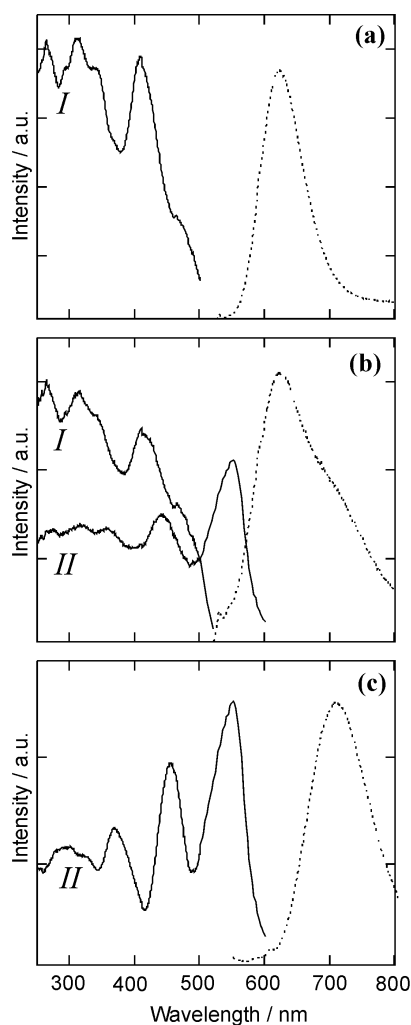


Figure 3: Luminescence (dots) and excitation (solid line) spectra of $\text{Ag}_2\text{S-KA-1}$ at different temperatures. (a) -190°C , (b) -100°C , and (c) 20°C . Excitation was performed at 440 nm. Excitation spectra were measured at 620 nm (I) and at 710 nm (II).

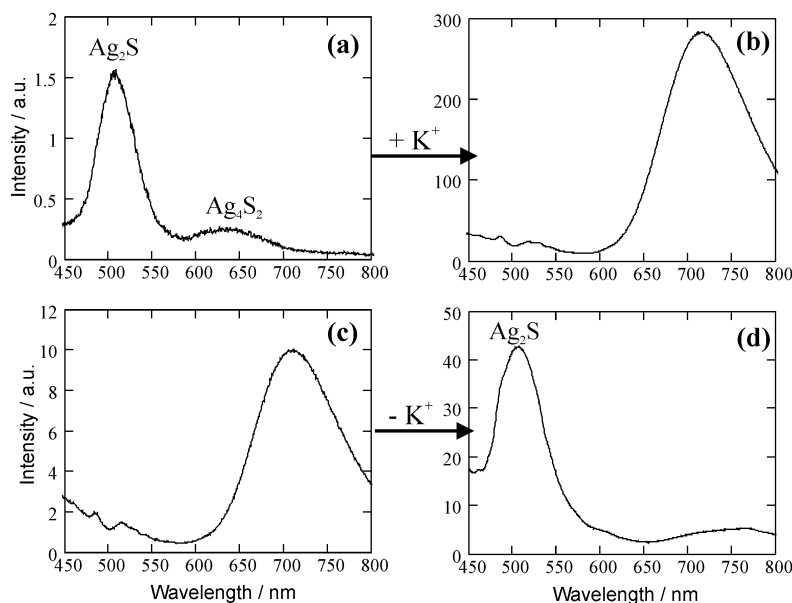
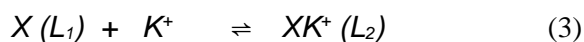


Figure 4: Luminescence spectra of a) $\text{Ag}_2\text{S-LiA-0.5}$, b) $\text{K}^+\text{-Ag}_2\text{S-LiA-0.5}$, c) $\text{Ag}_2\text{S-KA-0.1}$, and d) $\text{Ca}^{2+}\text{-Ag}_2\text{S-KA-0.1}$ at 20°C after excitation 320 nm.

sample for K^+ the band at 710 nm appears and the two other bands, assigned to Ag_2S (500nm) and Ag_4S_2 (620nm) disappear (Figure 4). If K^+ is exchanged for Ca^{2+} the opposite happens: The band at 710 nm disappears and a band at 500 nm rises. This means that the luminescence at 710 nm is due to the formation of K^+ -silver sulfide clusters. Equilibrium (2) can then be written as Equation (3)



where X stands for Ag_2S or Ag_4S_2 . XK^+ is stabilized at elevated temperature while at low temperature ($T < -100^\circ\text{C}$) the interaction between K^+ and silver sulfide is so weak that only the luminescence of Ag_2S and Ag_4S_2 is observed.

The refractive index of zeolites is in the same range as that of quartz. This index is expected to vary to some extent depending on the co-cations, the water content, and the silver sulfide loading. Thus optical effects

observed in tiny glass fibers, due to total internal reflection, are expected to appear in zeolite crystals as well. Taking into account these effects, one may ask if a zeolite crystal can also be considered as a microresonator.^[9] We now report some observations we made when exciting a layer of zeolite A crystals containing silver sulfide clusters and K^+ as co-cations with a pulsed laser. At room temperature such crystals show a deep red photoluminescence. The light emission is enhanced at the corners of the cubic crystals, as illustrated in the confocal luminescence microscopy image on the right side of Figure 5. A layer of $\text{Ag}_2\text{S-zeolite}$ crystals was excited with 5 ns laser pulses at 450 nm. The excitation power was increased in several steps, as shown in the inset of Figure 5. Up to an excitation power of 90 MWcm^{-2} , the measured emission spectra matched the fluorescence spectra. Above this intensity, two new peaks started to appear, one at 590 nm that stems from the 620 nm band which is otherwise only observed at low temperature (see

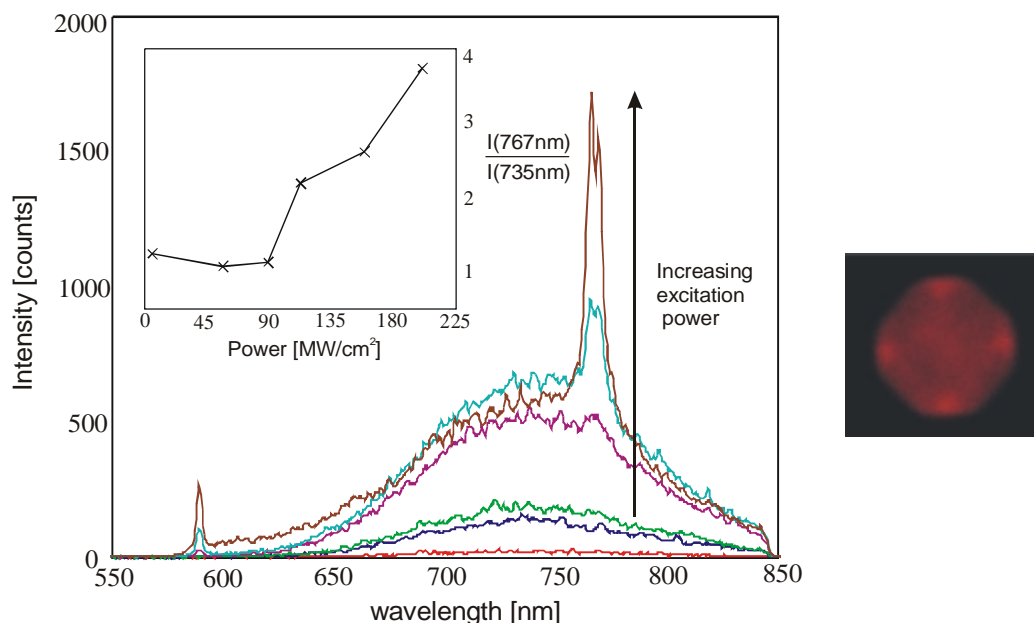


Figure 5: Luminescence spectra of a layer of K^+ - Ag_2S -zeolite A crystals at increasing excitation power. The sample was excited at 450 nm with a pulsed laser (5 ns pulses). The inset shows the ratio between the intensity at 767 nm and 735 nm. On the right is a confocal microscopy image showing a single luminescent K^+ - Ag_2S -zeolite A crystal with an edge length of 3000 nm, excited with an Argon laser at 488 nm at room temperature.

Figure 2) and a more intense one at 767 nm. The ratio of the intensity of the new peak at 767 nm and the fluorescence band at 735 nm indicate a threshold at about 90 MWcm^{-2} . These observations are remarkable and it would be challenging to find out if these properties could be used to develop a new kind of laser material.

In summary, very stable high quality zeolite A monolayers have been prepared by deposition of zeolite A crystals on quartz and on other substrates, followed by thermal fixation. These layers have been demonstrated to be suitable for a "ship-in-a-bottle" synthesis, exemplified on silver sulfide clusters. Zeolites containing green luminescent Ag_2S and orange luminescent Ag_4S_2 show a remarkable change in their luminescence color with temperature due to a stronger thermal

quenching of the green luminescence than of the orange luminescence. However, only in the presence of K^+ do the samples show a real luminescence thermochromism, which suggests a specific interaction between K^+ and silver sulfide. This interaction is strongest at room temperature, resulting in a deep-red luminescence at 710 nm and becomes weaker with decreasing temperature until only the luminescence of Ag_2S and Ag_4S_2 is observed. K^+ can also be added after the silver sulfide synthesis and the detection of the red luminescence is then a proof of the presence of potassium ions. The reason for the specific influence of the K^+ is not yet understood. There are similarities to observations made on gold(I) complexes.^[10] The procedures and observations reported in this Communication have the potential to promote the development of a challenging

class of materials for example, for electro-optical applications.^[9]

Experimental Section

Zeolite A was synthesized and characterized according to ref.[8a] yielding crystals of the composition $\text{Na}_{12}[(\text{AlO}_2)_{12}(\text{SiO}_2)_{12}] \cdot 27 \text{H}_2\text{O}$. After the synthesis all Na^+ ions were exchanged for K^+ ions by suspending the zeolites three times in a 0.5 M KNO_3 solution and then washing three times with double-distilled water. Zeolite A monolayers were prepared by depositing a drop of an aqueous suspension of zeolite A on a quartz plate (diameter = 8mm) and let it dry slowly, similar to the procedure described in ref.[8a]. An important condition for obtaining high quality monolayers is a narrow size distribution of the zeolite crystals. The physisorbed crystals were fixed by heating the layers at 600° C for 24 h.

The synthesis of silver sulfide clusters in zeolite A can be divided in 4 steps: 1) Insertion of a defined amount of Ag^+ by means of ion exchange, 2) dehydration of the zeolites in vacuum, 3) reaction with H_2S , 4) rehydration and cluster growth. Details can be found in refs.[4].

For the cation exchange after the synthesis of silver sulfide, the samples were suspended two times in a corresponding aqueous nitrate solution during 20 min and then washed with bidistilled water.

The following abbreviations are used: NaA for zeolite A ($\text{Na}_{12}[(\text{AlO}_2)_{12}(\text{SiO}_2)_{12}]$) and KA for zeolite A when all Na^+ are exchanged by K^+ . $\text{Ag}_2\text{S-KA-x}$ means KA containing silver sulfide while x denotes the number of Ag^+ per α -cage and is therefor proportional to the total silver sulfide content. $\text{Ca}^{2+}\text{-Ag}_2\text{S-KA-x}$ stands for a $\text{Ag}_2\text{S-KA-x}$ sample that was exchanged with Ca^{2+} after the silver sulfide synthesis and $\text{K}^+\text{-Ag}_2\text{S-LiA-x}$ for a $\text{Ag}_2\text{S-LiA-x}$ sample that was exchanged with K^+ after the synthesis. Confocal fluorescence microscopy was performed with a fluoview FV300, Olympus, accessory-equipped with an argon laser operating at 488 nm. For a detailed description of the equipment used for measuring the absorption spectra and the stationary and

time-resolved luminescence data we refer to ref.[4c].

Acknowledgements

This work is part of the Schweizerische Nationalfonds project 2000-067684.02/1. We also acknowledge the Stiftung der Portland Cementfabrik Laufen, Baselland (Switzerland), and the Schweizerische Bundesamt für Energiewirtschaft, project no. 36846, for financial support, and we thank Dr. Dominik Brühwiler for many useful discussions.

Keywords: clusters · host-guest systems · microresonators · photoluminescence · thermochromism · zeolites

- [1] a) H. D. Hardt, *Naturwissenschaften* **1974**, *61*, 107. b) K. R. Kyle, C. K. Ryu, J. A. DiBenedetto, and P. C. Ford, *J. Am. Chem. Soc.* **1991**, *113*, 2954. c) P. C. Ford, E. Cariati, and J. Bourassa, *Chem. Rev.* **1999**, *99*, 3625.
- [2] P. Fischer, B. Lucas, M. A. Omary, C. L. Larochelle, and H. H. Patterson, *J. Solid State Chem.* **2002**, *168*, 267.
- [3] a) Z. Assefa, M. A. Omary, B. G. McBurnett, A. A. Mohamed, H. H. Patterson, R. J. Staples, and J. P. Fackler, *Inorg. Chem.* **2002**, *41*, 6274. b) Y. Lee, J. E. McGarrah, R. J. Lachicotte, and R. Eisenberg, *J. Am. Chem. Soc.* **2002**, *124*, 10662.
- [4] a) D. Brühwiler, R. Seifert, G. Calzaferri, *J. Phys. Chem. B* **1999**, *103*, 6397. b) D. Brühwiler, C. Leiggenger, S. Glaus, and G. Calzaferri, *J. Phys. Chem. B* **2002**, *106*, 3770; c) C. Leiggenger, D. Brühwiler, and G. Calzaferri, *J. Mater. Chem.* **2003**, *13*, 1969.
- [5] a) R. Seifert, A. Kunzmann, G. Calzaferri, *Angew. Chem.* **1998**, *110*, 1603; *Angew. Chem. Int. Ed.* **1998**, *37*, 1521; b) R. Seifert, R. Rytz, G. Calzaferri, *J. Phys. Chem. A* **2000**, *104*, 7473.
- [6] a) G. Meyer, D. Wöhrle, M. Mohl, G. Schulz-Ekloff, *Zeolites* **1984**, *4*, 30; b) A.

- Corma, H. Garcia, *Eur. J. Inorg. Chem.* **2004**, 1143.
- [7] a) J. Li, K. Pfanner, G. Calzaferri, *J. Phys. Chem.* **1995**, *99*, 2119. b) G. Calzaferri, M. Lanz, J. Li, *J. Chem. Soc. Chem. Commun.* **1995**, 1313.
- [8] a) P. Lainé, R. Seifert, R. Giovanoli, and G. Calzaferri, *New J. Chem.* **1997**, *21*, 453; b) S. Mintova, B. Schoeman, V. Valtchev, J. Sterte, S. Mo, T. Bein, *Adv. Mater.* **1997**, *9*, 585; c) K. Ha, Y.-J. Lee, H. J. Lee, and K. B. Yoon, *Adv. Mater.* **2000**, *12*, 1114; d) A. Kulak, Y.-J. Lee, Y. S. Park, and K. B. Yoon, *Angew. Chem.* **2000**, *112*, 980; *Angew. Chem. Int. Ed.* **2000**, *39*, 950; e) K. Ha, Y.-J. Lee, D.-Y. Jung, J. H. Lee, and K. B. Yoon, *Adv. Mater.* **2000**, *12*, 1614; f) L. Huang, Z. Wang, J. Sun, L. Miao, Q. Li, Y. Yan, D. Zhao, *J. Am. Chem. Soc.* **2000**, *122*, 3530.
- [9] a) G. Calzaferri, S. Huber, H. Maas, and C. Minkowski, *Angew. Chem.* **2003**, *115*, 3860; *Angew. Chem. Int. Ed.* **2003**, *42*, 3732; b) G. Calzaferri, M. Pauchard, H. Maas, S. Huber, A. Khatyr, T. Schaafsma, *J. Mater. Chem.* **2002**, *12*, 1.
- [10] V. W. Yam, C. K. Li, and C. L. Chan, *Angew. Chem.* **1998**, *110*, 3041; *Angew. Chem. Int. Ed.* **1998**, *37*, 2857.

4.2 Luminescence thermochromism of $\text{Ag}_2\text{S-KA-x}$

Luminescence thermochromism of silver sulfide clusters in K^+ -zeolite A is not limited to samples with a silver loading of $x = 1$. It also occurs in samples with other silver loadings as demonstrated in the luminescence spectra in Figure 4.2.1. At silver loadings of $x = 0.1$ and $x = 0.5$ the luminescence bands of Ag_2S and Ag_4S_2 at low temperature can be recognized, however their luminescence is quite weak. The reasons for that are not yet understood. According to the luminescence spectra it is not clear if only Ag_4S_2 or also Ag_2S particles are involved in the thermal equilibrium. The question arises what actually happens to the silver sulfide clusters when they interact with K^+ and why no similar effects could be observed in the presence of the other investigated co-cations. To answer these questions absorption and luminescence spectroscopy are not sufficient and one may have to consider other analytical methods.

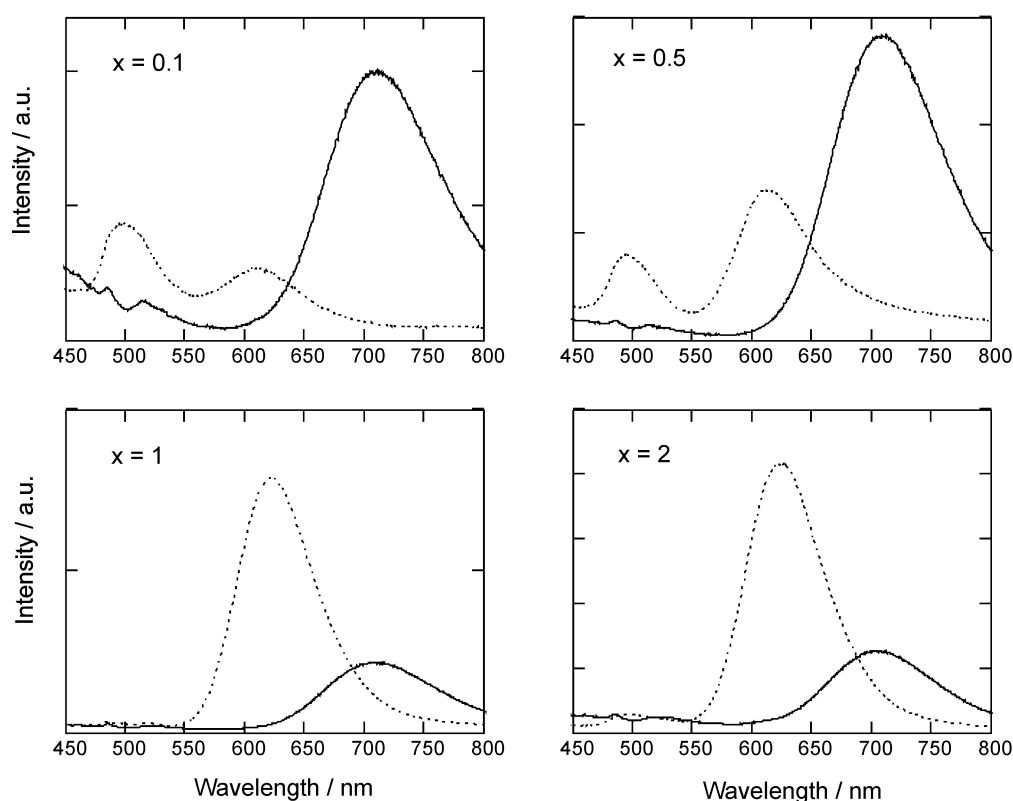


Figure 4.2.1: Luminescence spectra of $\text{Ag}_2\text{S-KA-x}$ with different x at room temperature (solid line) and at $-190\text{ }^\circ\text{C}$ (dots) upon excitation at 320 nm .

4.3 Laser action

Amplified spontaneous emission and laser action have been observed in other zeolites loaded with organic dyes e.g. zeolite L^[54] and AlPO₄-5^[55], in different kind of materials providing microcavities such as semiconductor quantum dots^[56], and InGaAs microdisks.^[57] A prerequisite for laser action is that the laser-active dye is inside a resonator. Zeolites can be expected to act as resonators. The light emitted by the fluorophore circulates inside the zeolite due to total internal reflection at the edges of the zeolite, until the gain required to overcome the lasing threshold is reached. This seems also to be true for luminescent silver sulfide clusters in zeolite A. Similar results as for Ag₂S-KA-x (chapter 4.1) were obtained by investigating Ag₂S-CaA-2 containing to a great extent orange luminescent Ag₄S₂ clusters. The main difference is that in Ag₂S-CaA-2 several laser modes are observed as shown in Figure 4.3.1.

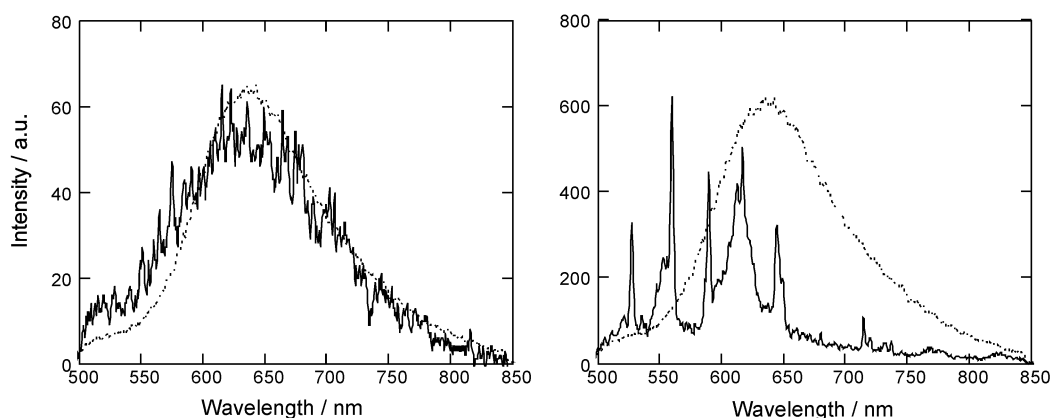


Figure 4.3.1: Luminescence spectra of Ag₂S-CaA-2 upon excitation with a pulsed laser (1 pulse per spectrum) at 440 nm. *Left*: normal excitation. *Right*: Focussed laser pulse (increased excitation power). The dotted spectra shown for comparison were measured of the same sample without focussing and with 100 scans (100 pulses per spectrum) and are scaled to the same height.

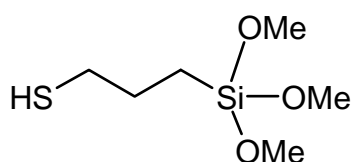
Green luminescent zeolite A crystals containing Ag₂S may also show a similar behavior, because the electronic structure of Ag₂S is at least a three level system with a long-lived excited state as well. The reason why no laser experiments on these samples were made so far is, that the excitation wavelength has to be in the UV and the excitation power of the laser available for these experiments is not high enough in the UV to overcome the lasing threshold of the samples.

4.4 Zeolite A monolayers on different substrates

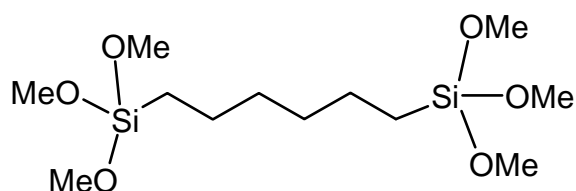
For the synthesis of silver sulfide clusters in zeolite A, monolayers of physisorbed crystals on quartz are stable enough, especially when they have been heated up to 600 °C. The heating may have two effects. First, water molecules between the zeolite and the quartz surface are removed, leading to a closer contact of the zeolites and the quartz. Second, a few covalent bonds between the OH-groups on the zeolite surface and OH-groups on the quartz surface may be built at 600 °C, which is near the melting point of quartz. However, in this case one cannot talk of a complete covalent binding of zeolite crystals to a substrate, because the zeolites can be removed by ultrasonic treatment. For covalent binding the zeolite crystals to a substrate one has either to modify the external surface of the zeolite or the surface of the substrate or both. Yoon et al. have used different kind of silanes to achieve covalent binding of zeolite A and ZSM-5 on glass.^[58]

Another approach to link zeolites to a substrate is described in Ref. [59], where dye-loaded zeolite L crystals were modified on the external surface with a covalently bound dye (ATTO680) and arranged on a silicon semiconductor. It could be shown that after excitation of the dye inside the zeolite, excitation energy transfer to the external dye and to the silicon occurred. Such photonic antennae systems offer new possibilities of developing, for example, more efficient solar cells.^[60] One can also consider a similar approach for Ag₂S-zeolite A systems to trap the excitation energy of the silver sulfide clusters on the external surface of the zeolite. The task then would be to find a suitable dye to modify the surface and as small as possible zeolite A crystals would be an advantage.

For the application of zeolite A monolayers in photocatalytic water splitting or any electrochemical experiments, they have to be prepared on conducting substrates. In first experiments glass supports with a thin gold or SnO layer were used. The idea was to bind the zeolite crystals with a silane to the conducting layer and is illustrated in Figure 4.4.1. For the gold layer 3-mercapto-trimethoxysilane and for the SnO layer 1,6-bis-trimethoxysilyl-hexane were used.



3-mercapto-trimethoxysilane



1,6-bis-trimethoxysilyl-hexane

The silanes were diluted in toluene and deposited on the substrate. Zeolite monolayers were prepared as described in chapter 4.1 and then fixed to the silane by heating at 110 °C for 3 h. Afterwards silver sulfide clusters were synthesized in the common way, taking care that the silver loading was $x > 2$. Finally the Ag_2S -zeolite A monolayers were loaded again with silver ions in the stoichiometric ratio of 2 Ag^+ per 1 Ag_2S unit.

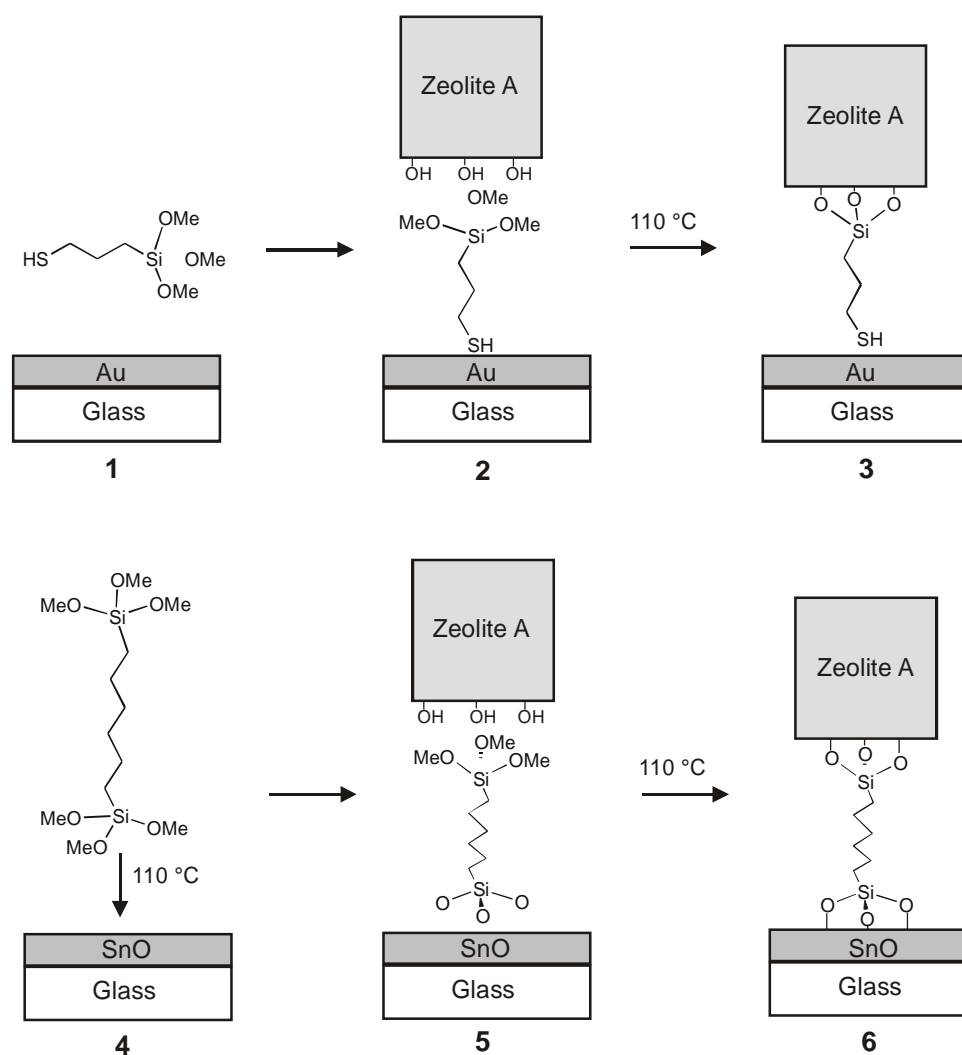


Figure 4.4.1: Scheme of the preparation of zeolite A monolayers on gold-coated glass (1-3) and on SnO-coated glass (4-5). 1: Deposition of the silane from toluene at room temperature. 4: Deposition of the silane from toluene at 110 °C. 2/5: Preparation of zeolite A monolayers. 3/6: Heating of monolayers at 110 °C in air.

To improve the mechanical stability of the layer it was coated with a very thin polymer layer (PVA) before the experiments. Then 150 nm of silver were deposited on the top of the $\text{Ag}^+/\text{Ag}_2\text{S}$ -zeolite A layer by means of physical vapor deposition (PVD). The silver layer was then electrochemically oxidized to AgCl in 0.2 M KCl. With this kind of zeolite-modified AgCl electrode photoelectrochemical experiments were carried out similar to the experiments described in Refs. [53,61]. Upon illumination of the electrode the O_2 production and the photocurrent were measured. First results showed an oxygen production rate of around 500 nmol/h which is similar to gold colloids modified AgCl electrodes. The photocurrent was a bit lower with 9 to 11 μA instead of 14 μA . The signals were stable for several cycles and over more than 60 hours. This is a remarkable improvement compared to previous experiments with Ag^+ -zeolite A modified electrodes, which showed an immediately decrease of the signals after the first cycle.^[61,62] One reason for this rapid decrease of the O_2 signal was the lack of electrical contact between reduced silver clusters on the surface of the zeolites and the conducting substrate. It seems that this problem can be prevented by the presence of silver sulfide clusters inside the zeolites.

In another experiment smaller zeolite A crystals were used. For that purpose crystals with an edge length of $\leq 1\mu\text{m}$ were synthesized as described in chapter 6.1 (synthesis procedure 3) and monolayers were prepared in the same way as it was done for the large crystals. Figure 4.4.2 shows the SEM image of such a monolayer on SnO-coated glass. The problem with these small crystals was that they formed aggregates instead of homogeneous layers. Photoelectrochemical experiments with this kind of monolayers containing $\text{Ag}^+/\text{Ag}_2\text{S}$ -clusters revealed, so far, weaker O_2 -signals than the corresponding layers with large crystals. This may be due to worse contact of the aggregated crystals with the conducting surface. To avoid aggregation of small zeolite crystals one could try to suspend them in other solvents than water and try to use surfactants before sedimentation, or one would have to develop another preparation method for the small crystals than for the large crystals.

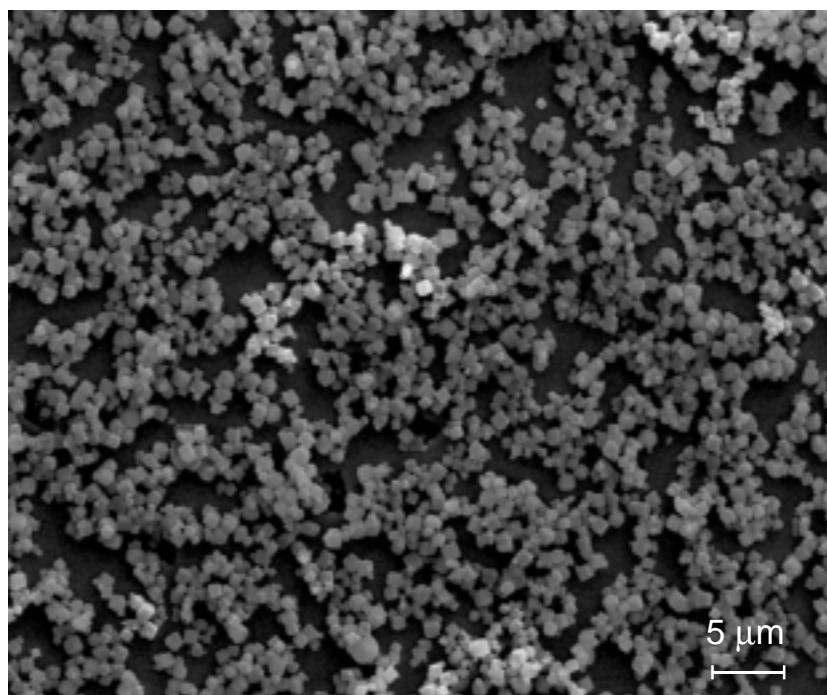


Figure 4.4.2: SEM image of a monolayer of small zeolite A crystals (synthesis procedure 3) on SnO-coated glass.

4.5 Conclusions

It was shown that it is possible to prepare high quality zeolite A monolayers on different substrates which can be afterwards successfully loaded with silver sulfide clusters. This was first demonstrated on Ca^{2+} -zeolite A monolayers on quartz. The silver sulfide loading was proved by the luminescence of the layers which is typical for Ag_2S and Ag_4S_2 in Ca^{2+} -zeolite A. The same principle was extended for preparing Ag_2S -zeolite A modified AgCl-electrodes for photocatalytic water splitting. First experiments with $\text{Ag}^+/\text{Ag}_2\text{S}$ -CaA monolayers showed promising results. In further experiments one could vary the silver loading and the co-cations or one could even try to load monolayers of disk-shaped zeolite L crystals with silver sulfide. The synthesis of silver sulfide clusters in the channels of zeolite L will be discussed in chapter 5.

Silver sulfide clusters in zeolite A show luminescence thermochromism in the presence of potassium co-cations. All Ag_2S -KA-x samples ($0.1 \leq x \leq 2$) reveal a luminescence band at 710 nm that is strongest at room temperature and becomes weaker with decreasing temperature until it completely disappears. The disappearance of this luminescence goes simultaneously with a rise of the luminescence bands of Ag_2S and Ag_4S_2 . We propose a thermal equilibrium between two different luminescent forms of silver sulfide clusters. One form is observed at low temperature and is similar to Ag_2S and Ag_4S_2 in samples with other co-cations. The second form is stable at room temperature and is probably due to specific interaction between potassium cations and silver sulfide. The observation, that the luminescence at 710 nm disappears by exchanging K^+ with other cations and that it reappears by exchanging other cations with K^+ , supports this idea. However, at the moment we do not have a suggestion what such a $\text{K}^+(\text{Ag}_2\text{S})_n$ -cluster could look like and why the other investigated co-cations do not have a similar effect on the luminescence of silver sulfide clusters.

Zeolite A crystals can act as microresonators for the luminescence of silver sulfide clusters. Ag_2S -zeolite A samples showing luminescence at room temperature start lasing upon excitation with a pulsed laser and high excitation power. This could be demonstrated for red luminescent Ag_2S -KA-x samples and orange luminescent Ag_2S -CaA-x samples.

5. Silver Sulfide Clusters in other Zeolites

In principle the same synthesis procedure of silver sulfide cluster could also be applied for other ion-exchangeable materials having a cavity structure. Depending on the size of the cavities, larger silver sulfide clusters or clusters having a different geometry and other properties than those in zeolite A are expected. In the following experiment zeolite L was used as a host.

5.1 Zeolite L

Zeolite L is like zeolite A a crystalline aluminosilicate, but its framework consists of one-dimensional channels. In Figure 5.1.1 the framework of zeolite L with the crystallographically identified cation positions is shown. Only the cations located in position D are exchangeable at room temperature. Nevertheless, this is enough to produce silver sulfide clusters inside the channels of zeolite L.

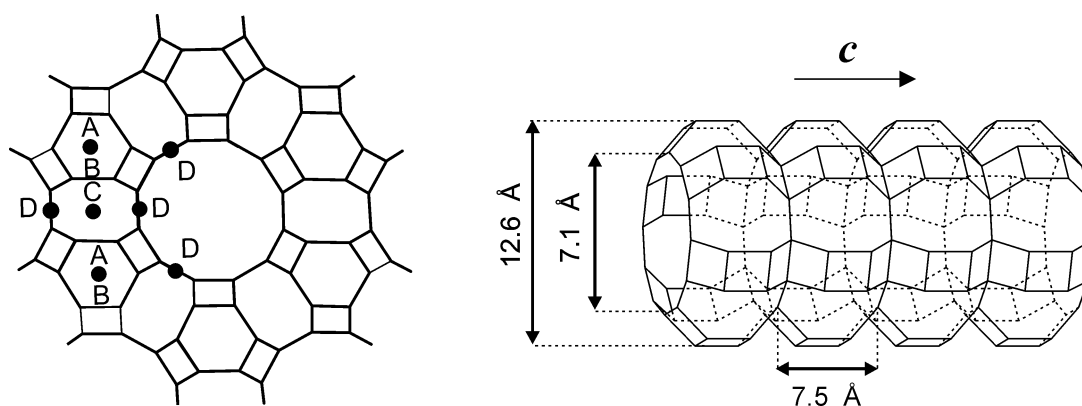


Figure 5.1.1: Framework of zeolite L with the different cation positions (A-D). View along the channels (left) and perpendicular to the channels (right).

Ag₂S-zeolite L samples with silver loadings of 0.01, 0.5, and 1 Ag⁺ per unit cell were synthesized in the same way as it was done for zeolite A. At a silver loading of 0.01 the samples are colorless and show a weak luminescence at 495 nm (see Figure 5.1.2), which can be assigned to isolated Ag₂S molecules. The luminescence and the excitation spectra are the same as in zeolite A indicating that Ag₂S has about the same geometry in zeolite L. Samples with a higher silver loading have a yellowish color but are also a bit gray. This is probably due to the formation of bulk silver sulfide at the entrances of the channels on the base of zeolite L. However, these samples show a bright green to yellow photoluminescence after cooling with liquid nitrogen. In contrast to Ag₂S-zeolite A

samples the color change of the luminescence with increasing silver sulfide content is not due to the appearance of a second luminescence band, but is caused by a red shift of the band at 495 nm and the rise of a broad shoulder in the red part of the spectrum. The excitation spectrum shifts as well with increasing silver loading, but the transitions stay the same. The typical luminescence band around 610 nm assigned to Ag₄S₂ cannot be observed in the investigated zeolite L samples. It seems that the formation of Ag₄S₂ particles, which are observed in zeolite A, is not favored in zeolite L. The reason for that is probably the different framework of the zeolites. While a small molecule like Ag₂S finds similar coordination sites in both zeolites, the geometry of clusters such as Ag₄S₂ may be more influenced by the shape of the zeolite cavities. Also the absorption spectrum of Ag₂S-zeolite L with a silver loading of 1 Ag⁺/u.c. looks quite different than the corresponding spectrum of zeolite A (Figure 5.1.3). The absorption bands at 280 nm and at 320 nm typical for Ag₂S can be still recognized and there is another clear transition at 400 nm. The appearance of this transition correlates with the red shift of the luminescence. A possible interpretation of this observation is that from a certain silver loading on ($x \approx 0.5$) interaction between neighboring Ag₂S molecules occur. This interaction causes changes in the electronic spectra, but its not that strong that the Ag₂S molecules loose their identity, so one cannot talk of the formation of a larger silver sulfide particle.

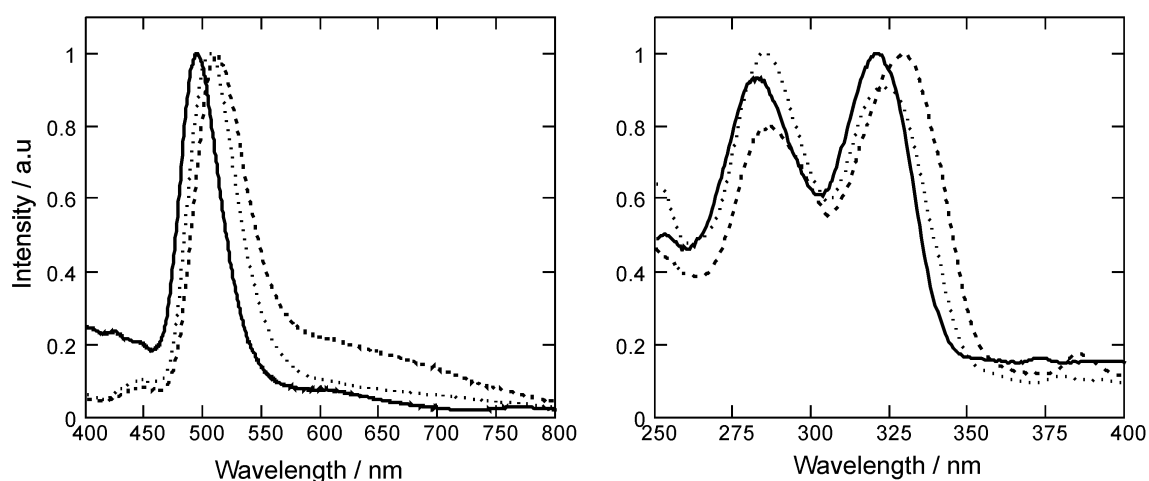


Figure 5.1.2: Luminescence (left) and excitation (right) spectra of Ag₂S-zeolite L with different silver loading at -190 °C upon excitation at 320 nm. The spectra are scaled to the same height. The silver loadings are 0.01 (solid line), 0.5 (points), and 1 (dash) Ag⁺/u.c.

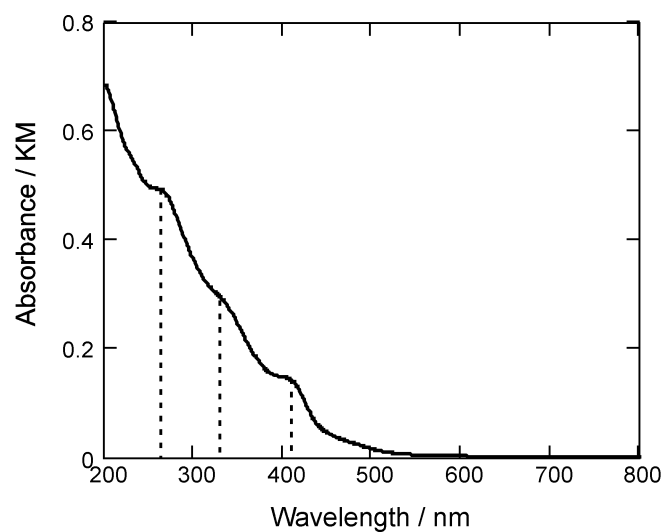


Figure 5.1.3: Diffuse reflectance spectrum of Ag₂S-Zeolite L with a silver loading of 1 Ag⁺/u.c. KM stands for the Kubelka-Munk function.

It would be interesting to see what happens if one goes to higher silver loadings than 1 Ag⁺/ u.c. Theoretically the silver sulfide particles could be aligned to each other through a whole channel forming something like a molecular wire. This kind of material could be highly interesting, but is difficult to realize. First one has to make sure that the silver ions are equally distributed over all channels after ion exchange. One has to consider that the diffusion in zeolite L is limited to one dimension and hence the ion exchange process may be slower than in zeolite A. An equally exchanged sample could probably be obtained by a longer and stepwise ion exchange. The second problem is the formation of silver sulfide at the entrances of the channels which hinders the diffusion of H₂S into the zeolite.

6. Experimental

6.1 Synthesis of zeolite A

In this work three different synthesis procedures have been used to obtain crystals of different size and morphology. Most of the experiments were carried out with crystals from synthesis procedure 1, which yields large crystals with a nice shape. The product of procedure 2 is ZK-4. ZK-4 has the same framework as zeolite A but a lower Al content and hence less charge compensating cations. Procedure 3 was developed for small crystals with an edge length of about 1 μm or less. All products were characterized by SEM, XRD, and EDX (Energy Dispersive X-ray Analysis).

In all procedures two solutions (*A*) and (*B*) are prepared separately in Teflon flasks, (*A*) containing Si- and (*B*) containing Al-precursors, then the solutions are combined forming a gel. Heating the gel for several hours leads to crystallization. The size and the morphology of the crystals depend on the composition of the starting gel. The Si source of procedure 1 is tetra-ethoxysilane, while in procedures 2 and 3 SiO_2 is used. Very fine powder of SiO_2 is obtained as follows:

72.86 g of di-isopropylamine was diluted in 75 ml doubly distilled water and stirred for 1 h until the solution was clear. Under vigorous stirring 150 g of $\text{Si}(\text{OEt})_4$ (tetra-ethoxysilane) was added and the mixture was stirred for 48 h. The white product was separated by centrifugation and suspended in 400 ml ethanol. The suspension was stirred for 1 h and then filtrated (glass frit, pore size 4). The product was washed twice with ethanol and dried in vacuum at 100 °C for 2-3 h. Thermogravimetric analysis gives a lost of 20% at 800 °C.

Procedure 1 ^[63]

(*A*): 5.93 g of NaOH was dissolved in 150 ml doubly distilled water and 7.721 g of $\text{Si}(\text{OEt})_4$ (tetra-ethoxysilane) was added. The mixture was refluxed under $\text{N}_2(\text{g})$ at 60 °C for 3 h.

(*B*): 5.93 g of NaOH was dissolved in 150 ml doubly distilled water and 2 g of Al-wire was added. The mixture was refluxed under $\text{N}_2(\text{g})$ at 90 °C for 3 h.

The solutions were cooled to room temperature before (*A*) was added to (*B*). The gel was stirred for 15 min at room temperature and then for 16 h under reflux at 90 °C. The mixture was filled in a beaker for sedimentation of the product. The supernatant was removed and the product was washed three times with 250 ml boiling doubly distilled water. Then the product was washed with ethanol, filtrated (pore size 4) and dried at 80 °C.

Product: $\text{Na}_{12}[(\text{AlO}_2)_{12}(\text{SiO}_2)_{12}]$, cubic crystals of different size (average 3-5 μm) with chamfered edges, nearly no intergrowth. The SEM image is shown in Figure 6.1.1.

Procedure 2: ZK-4 ^[35]

(A) 4.34 g of SiO_2 and 25.74 g of tetra-methyl-ammoniumhydroxide (TMAOH) were dissolved in 57 ml doubly distilled water at 90 °C for 2 h with constant stirring.

(B) 0.962 g of Al-wire, 2 g of NaOH, and 6.435 g of TMAOH were dissolved in 50 ml doubly distilled water at 90 °C for 3 h.

The solutions were cooled to room temperature before (A) was added to (B). The gel was stirred for 15 min at room temperature and then for 24 h under reflux at 90 °C. The product was separated by centrifugation and was washed three times with boiling doubly distilled water. After washing with ethanol the product was first dried at 80 °C and then the TMA ions were destroyed by calcination at 500 °C in air. The remaining protons were exchanged with Na^+ by suspending the zeolites three times for 15 min in 0.1 M NaNO_3 solution.

Product: $\text{Na}_9[(\text{AlO}_2)_9(\text{SiO}_2)_{15}]$, cubic crystals with sharp edges, average size 1-2 μm , intergrowth. The SEM image is shown in Figure 6.1.2.

Procedure 3: small crystals

(A) 0.6225 g of SiO_2 and 4.47 g of tetra-methyl-ammoniumhydroxide (TMAOH) were dissolved at 90 °C under $\text{N}_2(\text{g})$ for 2 h with constant stirring.

(B) 0.5 g of Al-wire, 0.6 g of NaOH, and 5.328 g of TMAOH were dissolved at 90 °C under $\text{N}_2(\text{g})$ for 4 h.

The solutions were cooled to room temperature before (A) was added to (B). The gel was stirred for 2 days at room temperature. For crystallization the gel was filled into Polypropylene flasks and placed in a rotating oven at 100 °C for three days. The product was separated by centrifugation and was washed three times with boiling doubly distilled water. After washing with ethanol the product was first dried at 80 °C and then the TMA ions were destroyed by calcination at 500 °C in air. The remaining protons were exchanged with Na^+ by suspending the zeolites three times for 15 min in 0.1 M NaNO_3 solution.

Product: $\text{Na}_{12}[(\text{AlO}_2)_{12}(\text{SiO}_2)_{12}]$, cubic crystals with slightly rounded edges, size $\leq 1 \mu\text{m}$, few intergrowth. The SEM image is shown in Figure 6.1.3.

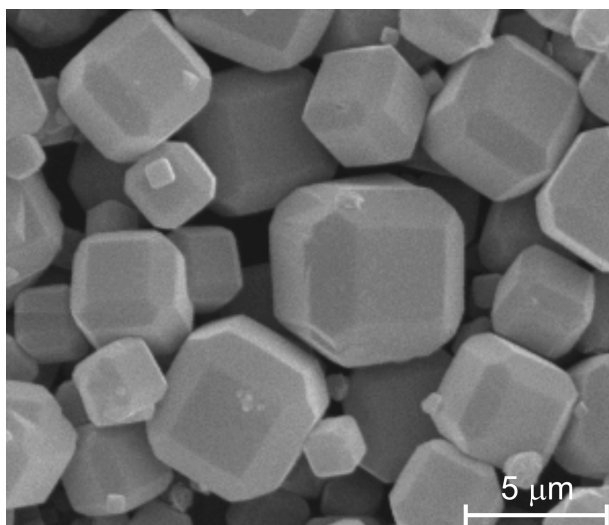


Figure 6.1.1: SEM image of the synthesis product of procedure 1.

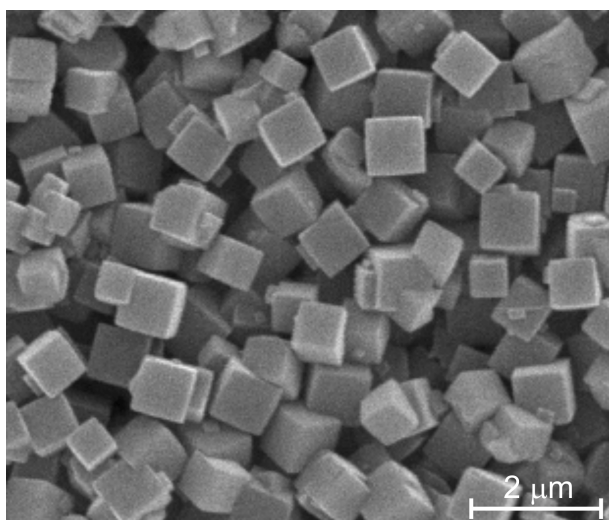


Figure 6.1.2: SEM image of the synthesis product of procedure 2.

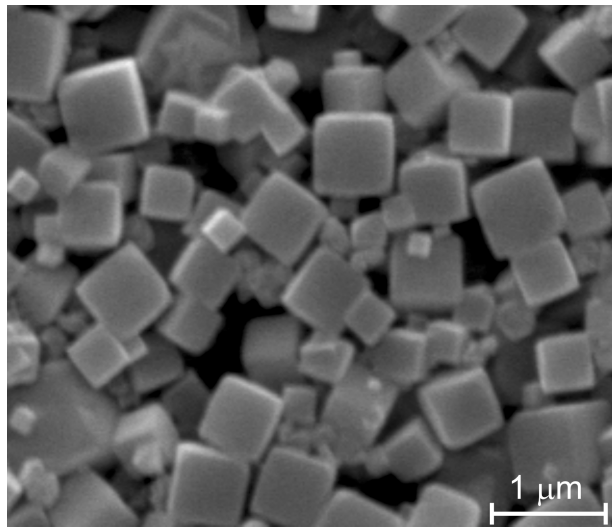


Figure 6.1.3: SEM image of the synthesis product of procedure 3.

6.2 Synthesis of silver sulfide clusters

500 mg of NaA were suspended in 20 ml of a 0.5 M $M(\text{NO}_3)_n$ solution ($M = \text{Li}, \text{K}, \text{Mg}, \text{Ca}, \text{Sr}$) for 20 min. After centrifugation this step was repeated twice. Then the zeolites were washed three times with doubly distilled water and dried at 80 °C. The product is MA where M^{n+} are the charge compensating cations $\text{Li}^+, \text{Na}^+, \text{K}^+, \text{Mg}^{2+}, \text{Ca}^{2+},$ or Sr^{2+} .

The synthesis of silver sulfide clusters is divided into four steps:

1. Ag^+ exchange

120 mg of MA were suspended in 10 ml of the corresponding 0.01 M $M(\text{NO}_3)_n$ solution. Then the desired amount of 0.1 M AgNO_3 solution was added and the suspension was stirred for 2 h in the dark. The samples were washed twice with doubly distilled water, filled in small quartz vessels and dried at room temperature over night.

2. Dehydration

The samples were placed into the vacuum system described in Figure 6.2.1. The procedure for evacuation of the system is the following:

- switch on pump 1, open the valves v_1 and v_2 , switch a to position 1, then open b and d .
- switch on detector 1 (D1) and wait until the pressure is 1 mbar.
- close b , switch a to position 2, open c
- wait until the pressure is about 10^{-2} mbar, then switch on pump 2.

The zeolites are dried in dynamic vacuum for 2-3 days until the pressure in the system is about $2\text{-}3\cdot 10^{-6}$ mbar.

3. Exposure to H_2S

The samples are exposed to H_2S gas for one hour, then the excess H_2S is trapped with liquid nitrogen, and the whole system is flooded with nitrogen gas. To remove the trapped H_2S the system is exposed to a continuous nitrogen flow for 75 min and the emitted H_2S is oxidized in a FeCl_3 solution. The following procedure is used:

- close d
- open e and evacuate the trap for liquid nitrogen
- open f and evacuate the hose
- close c and a and switch off the pumps
- switch off detector D1
- switch on detector D2 and calibrate it to 0 Torr
- add 60 Torr of H_2S gas

- open *d* and wait for 1 h
- add liquid nitrogen to the trap until D2 shows nearly 0 Torr
- open the N_2 gas and *g* until the pressure in the systems equals the pressure outside
- open *h* and leave the system under nitrogen flow for 75 min
- evacuate the system over night as described before

4. Rehydration

All valves are closed and the pumps are switched off. The system is flooded with nitrogen gas until the pressure inside equals the pressure outside. The samples are removed and stored under ambient conditions.

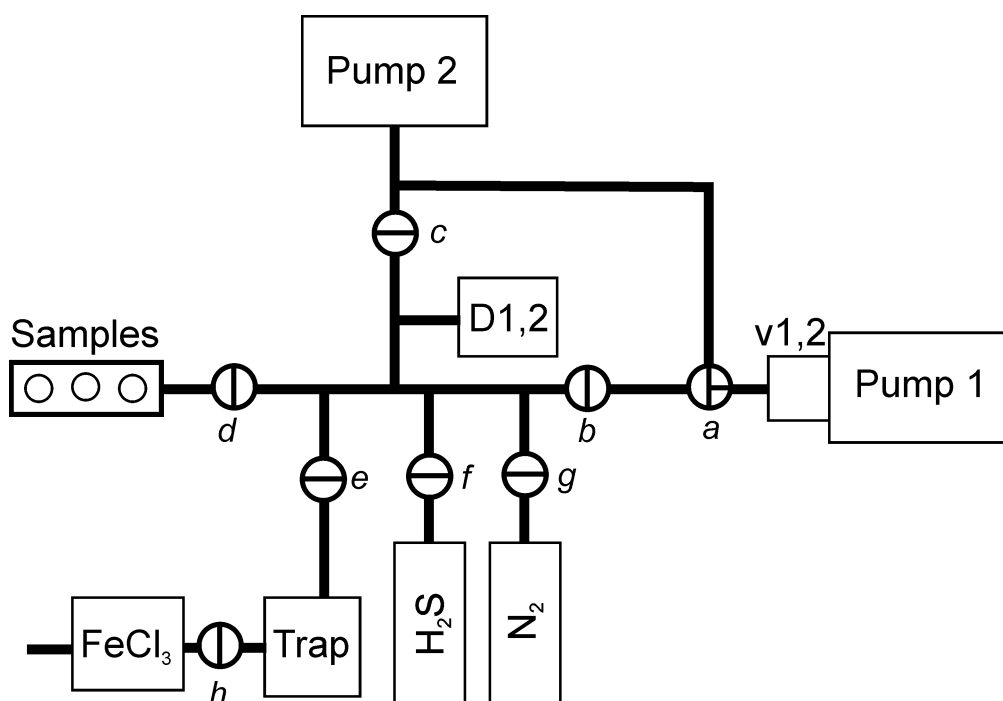


Figure 6.2.1: Scheme of the vacuum system. *Sample*: sample holder for three samples; *Pump 1*: rotary slide-valve oil pump ; *Pump 2*: turbo molecular pump; *D1,2*: pressure gauges 1 = Balzers PKR 250 with device TPG 251A for pressure < 10 mbar, 2 = MKS Baratron with device 111A for pressure > 1 Torr; N_2 gas bomb; H_2S gas bomb; *Trap*: liquid nitrogen trap; $FeCl_3$ solution; *a-h*: valves.

6.3 Spectroscopy

6.3.1 Sample preparation

Ag₂S-MA-x:

All samples were synthesized as described in chapter 6.2. For spectroscopy the final products were prepared on quartz plates and measured in their fully hydrated state. For that purpose the samples were suspended in doubly distilled water, dropped on a clean quartz plate, and then let dry in air at room temperature.

Ag_xK_{12-x}A:

80 mg of KA were suspended in 8 ml of 0.01 M KNO₃ solution. A calculated amount of 0.1 M AgNO₃ solution was added and the suspension was stirred for 2 h in the dark. The silver exchanged zeolite was washed three times with 10 ml of doubly distilled water. Then it was suspended in 0.5 ml of doubly distilled water and transferred into a cylindrical quartz cuvette with a vacuum adapter. The cuvette was connected to the vacuum system and the water was slowly evaporated at 5 mbar. The zeolite was further dried in high vacuum (10⁻⁶ mbar) for about 80 h. Then the cuvette was sealed with a burner and separated from the vacuum system under airtight conditions.

6.3.2 Absorption spectra

Absorption and diffuse reflectance spectra were recorded on a Perkin Elmer Lambda 900 (UV/VIS/NIR) spectrophotometer with an integrating sphere. The diffuse reflectance spectra were converted into absorption spectra by applying the Kubelka-Munk function.^[64]

$$F(R_{\infty}) = \frac{(1 - R_{\infty})^2}{2R_{\infty}} = \frac{K}{S} \quad (6.3.1)$$

where R_{∞} is the diffuse reflecting power, K is the absorption coefficient, and S is the scattering coefficient.

6.3.3 Luminescence spectra

Steady-state luminescence spectra were recorded on a Perkin Elmer LS 50B luminescence spectrometer equipped with an Oxford PE1704 cryostat and a thermostat which allows measurements at temperatures between -195 °C (liquid nitrogen) and room temperature.

6.3.4 Time-resolved luminescence spectra

Measuring method:

The same measuring method as in Ref. [10] was used. A scheme of the experimental setup for time-resolved luminescence measurements is shown in Figure 6.3.1. It is built up of the following components: Vibrant Laser System, Optical Multichannel Analyzer (OMA), Digital Delay (DG535), Digitizing Oscilloscope (TEK), Polychromator with detector, PC with GPIB interface, OR-Gatter, sample holder (SH), quartz fiber (Q), cutoff filter (F), photodiode (D), beam splitter (BS), beam lift (BL), and shutter (S).

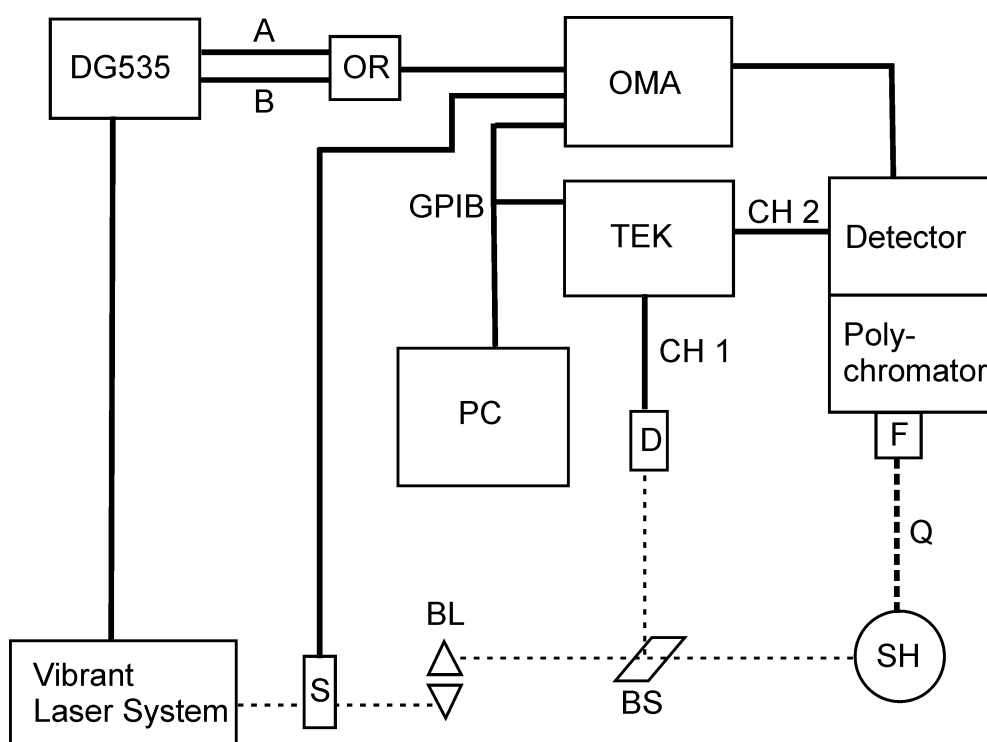


Figure 6.3.1: Scheme of the setup for time-resolved luminescence measurements. The light (----) and the electric signals (—) are shown. The components are described in the text.

The system allows to record spectra at different times after the excitation of the sample with a pulsed laser. The Vibrant Laser System consists of a NdYAG laser and an OPO. The OPO is pumped with the third harmonic of the NdYAG laser (355nm) and the output wavelength can be tuned in the visible (410-690 nm) and in the UV (250-300nm, 320-380 nm) via a computer. The pulse length is 5 ns. The flash lamp runs with a frequency of 10

Hz and the frequency of the Q-switch can be selected between 1, 2, 5, and 10 Hz. For time-resolved measurements a frequency of 1 Hz is used. The spectra are recorded on an Optical Multichannel Analyzer (OMA 1460) equipped with a gated detector (Parc EG&G model 1455R-700-HQ). The emission light of the sample is collected in a quartz fiber and transferred to the polychromator. The filter F selectively cuts off the laser emission light and can be exchanged depending on the excitation wavelength. Different grating positions of the polychromator can be chosen for different spectral ranges. The detector consists of a diode array of 1024 photodiodes giving 1024 points of intensity in the spectrum. The detection time (gate) can be tuned between 100 ns and 10 ms. The OMA is triggered by the laser system via the Digital Delay and the OR-Gatter. The trigger signals induce the OMA for light measurements (A, spectra) and dark measurements (B, background). The shutter (S) is opened by an electric signal induced by the OMA before each measurement and closed at the end of the measurement. The TEK records the laser pulses (CH 1) and the gate (CH 2) during the measurement. The time and the intensity of the laser pulse and the gate width are important for the evaluation of the data. Time resolved spectra are measured by recording a series of spectra at different delays after the excitation pulse. This means that the gate stays the same during a series of measurements, but the onset of the gate shifts in time (see Figure 6.3.2).

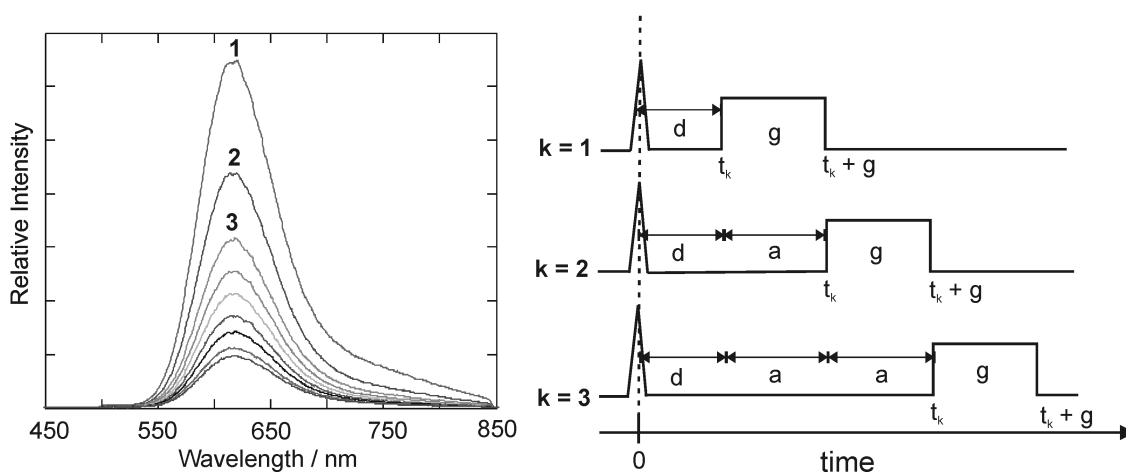


Figure 6.3.2: *Left:* time-resolved spectra recorded with a gate width of 10 μ s and a delay increment of 10 μ s. *Right:* Scheme of a series of gated measurements. The laser pulse sets the time $t = 0$, g is the gate, d is the delay, and a is the delay increment.

The whole process is controlled by a program (laser.exe) running on a PC that is connected via a GPIB interface with the OMA and the TEK. The program is based on DOS and allows to change the settings (gate, grating position, number of spectra and so

on). It also reads the measured data of the OMA and the TEK and saves them as an ASCII file. The handling of the program is described below.

The samples were measured in a special sample holder described in Ref. [65]. The chamber of the sample holder can be evacuated by a vacuum pump and can be cooled with liquid nitrogen. A thermostat allows measurements at different temperatures. The Ag₂S-MA-x samples were all measured in their hydrated state and at temperatures between -150 °C and room temperature. This was achieved by evacuating the chamber down to 10 mbar and then cooling with liquid nitrogen. Typically 19 time-resolved spectra per measurement were taken (memory j) while one spectrum is the sum of 100 individual spectra at the same delay (number of scans i). The values for the gate width (g) and for the delayincrement (a) have to be chosen in a way that one obtains a complete decay curve.

Program "laser.exe"

1. Start program
2. Change the settings
 - f: choose filename (max 8 characters)
 - u: choose between ns, μ s, and ms
 - g: gate width
 - d: delay
 - a: delayincrement
 - i: number of scans
 - j: memory (number of spectra k)
3. Enter "o" for initializing the OMA (the settings are transfer to the OMA) and wait
4. Enter "x" to start the measurement

Data evaluation:

The data were evaluated with two Mathcad programs written by Dominik Brühwiler. The programs fit the data to a multi-exponential decay curve where the number of exponents equals the number of lifetimes. The number of exponents and the spectral range for the evaluation can be chosen by the user. The following fitting function is used:

$$E_k = \int_{t_k}^{t_k + g} \sum_{n=1}^m A_n \exp\left[-\frac{t}{\tau_n}\right] dt \quad (6.3.2)$$

where E_k is the relative intensity of measurement k , t_k is the time at the beginning of measurement k , g is the gate width, m is the number of exponents, A_n are the amplitudes, and τ_n are the corresponding luminescence lifetimes.

The luminescence intensity as a function of time is obtained by integration of every spectrum over a desired spectral range, usually over the whole luminescence band.

The luminescence decay of Ag_2S and Ag_4S_2 in the same sample can be analyzed separately by choosing a suitable integration region, respectively. An example is given in Figure 6.3.3, where the integration region for Ag_2S is from 450 nm to 530 nm and the integration region for Ag_4S_2 is from 580 nm to 720 nm, resulting in two different decay curves. Another method is to fit every time-resolved spectrum to two gaussian curves and then plot the intensity of the gaussian curves as a function of time. This method takes more time and the resulting decay curves and lifetimes are the same. It shows, however, that just spectral separation of the two luminescence bands is enough.

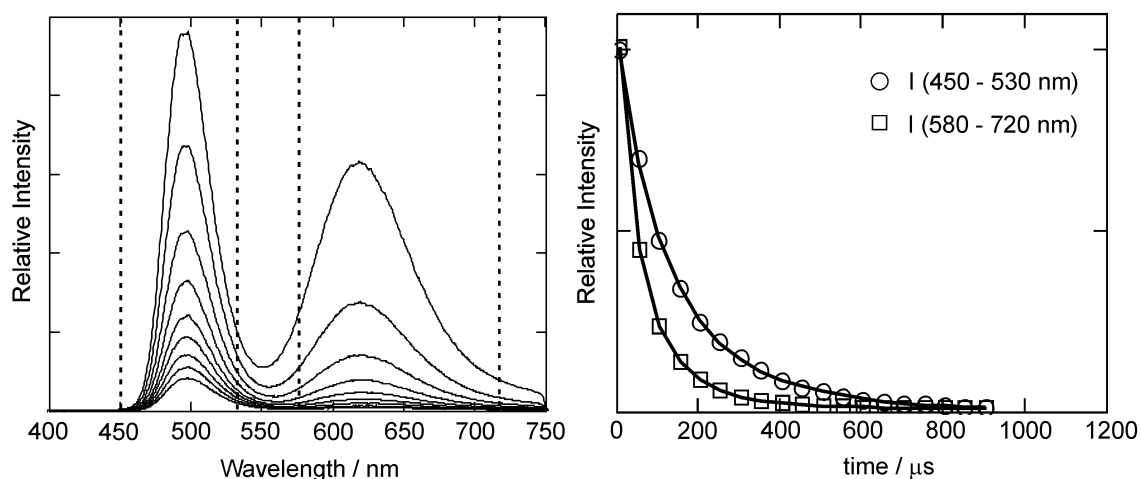


Figure 6.3.3: *Left:* time-resolved luminescence spectra of Ag_2S and Ag_4S_2 in zeolite A. The dotted lines indicate the integration regions for each luminescence band which are 450 - 530 nm and 580 - 720 nm. *Right:* Corresponding luminescence decay curves of the two luminescence bands.

The average luminescence lifetime is calculated by the following formula:

$$\langle \tau \rangle = \frac{\sum a_n \cdot \tau_n^2}{\sum a_n \cdot \tau_n} \quad (6.3.3)$$

where τ_n are the luminescence lifetimes and a_n are the corresponding amplitudes.

6.3.5 Laser experiments

Laser experiments on $\text{Ag}_2\text{S-KA-x}$ and $\text{Ag}_2\text{S-CaA-x}$ samples were carried out at room temperature. The samples were prepared as thin layers on quartz plates and fixed in a cuvette sample holder. The laser beam was focussed with a lens giving a spot of less than 1 mm^2 on the sample. Tuning of the laser power was achieved by using different optical transmission filters in front of the sample. Typically one scan per spectrum was taken due to the fast destruction of the sample at high laser power.

6.4 Preparation of zeolite A monolayers

6.4.1 Size separation of zeolite A crystals

The preparation of homogeneous zeolite A monolayers requires crystals of about the same size. However, the size distribution of the synthesis product is often quite broad (1 - 8 μm). It was found that crystals of different size can be separated to a certain extent by fractional sedimentation.^[30,63] The idea behind is that large crystals sediment faster than small crystals. For that purpose a column containing small glass tubes is used. A scheme of this column is shown in Figure 6.4.1. The column is filled with 0.01 M NaNO_3 solution and a suspension of zeolite A in water/ethanol (1:1) is put on the top of the column. The sediment is collected in a plastic hose at the end of the column. The sedimentation takes about 2-3 days. The hose is cut away, stored for 2 h at $-20\text{ }^\circ\text{C}$, and then cut into pieces giving fractions A - F. Fraction A consists of the largest crystals and fraction F of the smallest crystals as can be seen on the electron microscopy images in Figure 6.4.2.

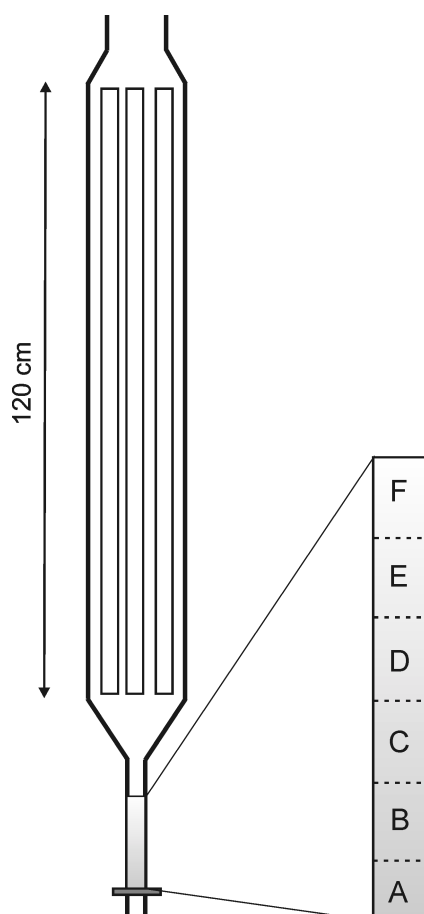


Figure 6.4.1: Scheme of the column used for fractional sedimentation of zeolite A crystals.

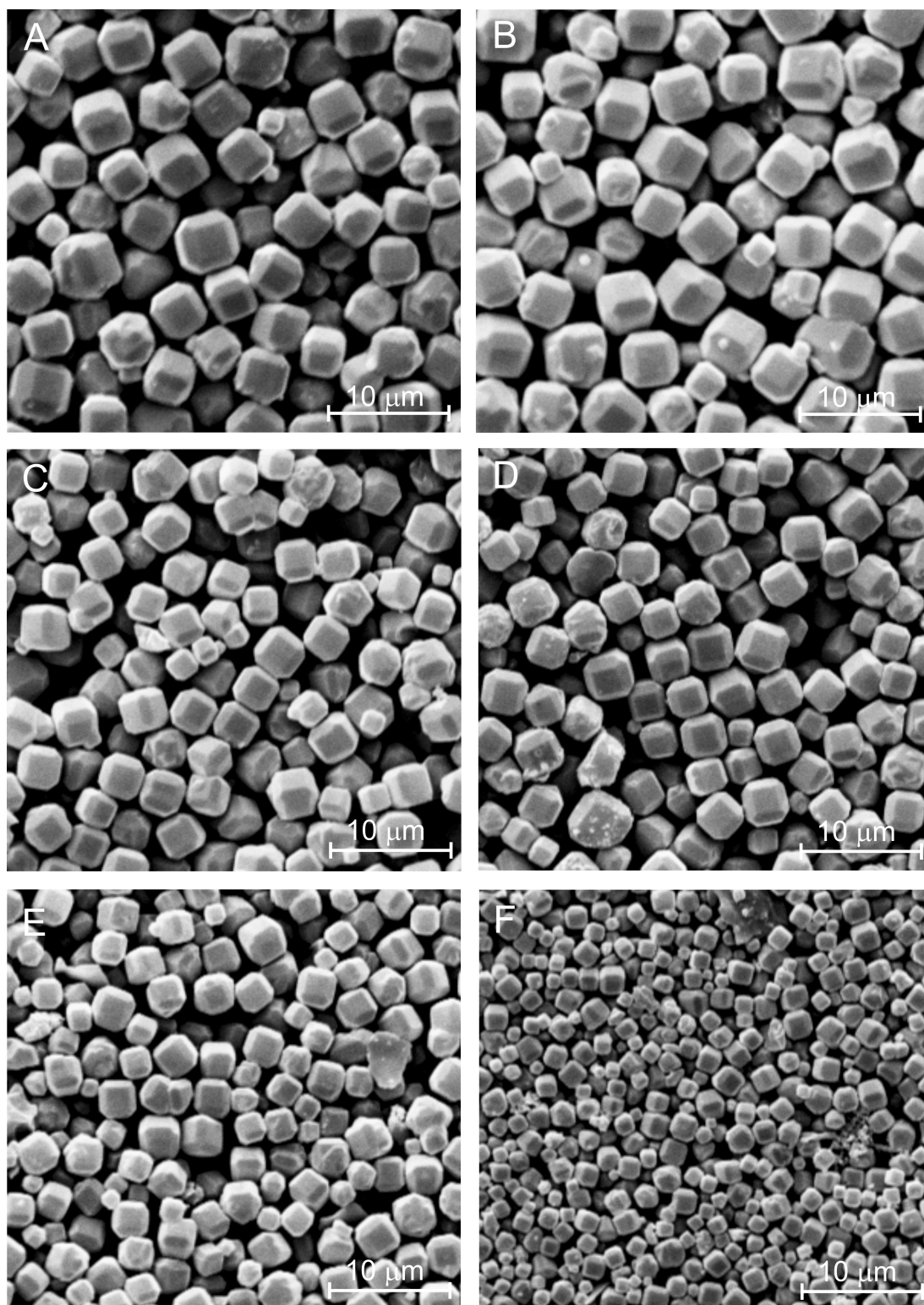


Figure 6.4.2: SEM images of the fractions A to F of the size separation showing crystals of different size. The largest crystals are found in the first fraction (A) at the bottom of the hose, and the smallest in the last fraction (F).

6.4.2 Preparation of monolayers

The best monolayers were obtained by using crystals of a medium size (fraction C - E). The zeolites were suspended in doubly distilled water. The concentration of the suspension was 3 - 5 mg of zeolite per 1 ml of water depending on the average crystal size. 50 -150 μl of the suspension was dropped on the clean substrate. The water was slowly evaporated in a chamber in the presence of a saturated aqueous KNO_3 solution, ensuring an atmosphere of approximately 92% humidity.

6.5 Ag^+/K^+ ion exchange isotherms

The experiments were carried out with a special equipment represented in Figure 6.5.1, consisting of a double-walled vessel with a thermostat and two electrodes connected to a voltmeter. The working electrode is a silver sulfide electrode and the reference electrode is a double junction Ag/AgCl electrode. The measured voltage is proportional to the Ag^+ concentration in solution. Ion exchange isotherms were obtained by measuring the voltage in a suspension of K^+ -zeolite A after the addition of different amounts of AgNO_3 solution and further evaluation of the data by a Mathcad program.^[28,66]

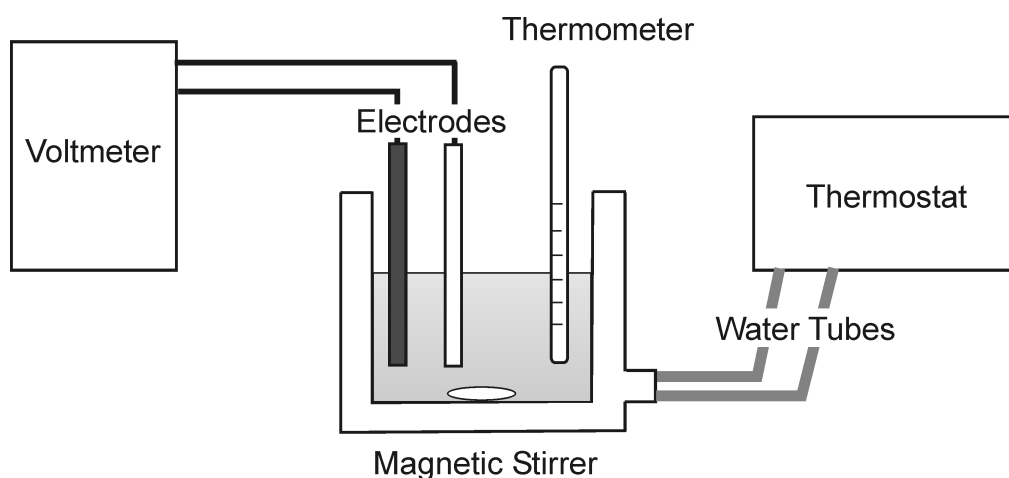


Figure 6.5.1: Scheme of the equipment used for measuring ion exchange isotherms. The double-walled vessel in the middle of the scheme contains the zeolite suspension and a magnetic bar. The space between the walls is filled with distilled water from the thermostat.

6.5.1 Experimental

Ion exchange isotherms were measured at five different temperatures, 25 °C, 30 °C, 35 °C, 40 °C, and 45 °C. The temperature was set by the thermostat and controlled with a thermometer dipped in the solution. For every temperature a calibration function was measured, which was necessary for the data evaluation. In all experiments the vessel was wrapped in aluminum foil preventing photoreduction of Ag^+ and helping to keep the temperature constant.

Calibration function: 100 ml of 0.1 M KNO_3 solution was filled into the double-walled vessel and heated up to the desired temperature. First, 4 μl of 0.1 M AgNO_3 solution was added with constant stirring and the voltage was measured right afterwards. This step was repeated several times, giving at the end 19 measured values. The volumes of 0.1 M AgNO_3 solution added at every step are listed below.

Measurement #	Added Volume 0.1 M AgNO_3	Total Volume 0.1 M AgNO_3
1-5	4 μl	4 μl - 20 μl
6-9	20 μl	40 μl - 100 μl
10-16	100 μl	200 μl - 800 μl
17-19	500 μl	1300 μl - 2300 μl

Ion exchange: 100 mg of KA were suspended in 100 ml of 0.1 M KNO_3 solution and filled into the double-walled vessel. The suspension was heated up to the desired temperature with constant stirring. 0.5 ml of 0.1 M AgNO_3 solution was added and the suspension was stirred for 20 min before the voltage was measured. It turned out that after 20 min the equilibrium is achieved. This step was repeated eleven times giving twelve data points at the end.

7. Conclusions and Outlook

Zeolite A is a suitable material to host small silver sulfide clusters. The clusters are synthesized by means of a “ship-in-a-bottle” synthesis and their size is limited by the dimensions of the α -cage leading to quantum sized silver sulfide clusters as guest species. The two smallest species found in zeolite A are the Ag_2S monomer and the Ag_4S_2 cluster, while the largest cluster is expected to have an approximate stoichiometry of Ag_8S_4 . Compared to the band gap of bulk silver sulfide, which is around 1 eV, the energy gap between HOMO and LUMO of the silver sulfide clusters is blue shifted and is around 2.5 eV (490 nm) for Ag_2S and around 2 eV (610 nm) for Ag_4S_2 . This is consistent with theory and means that the electronic properties of the silver sulfide clusters are only little affected by the zeolite framework. The electronic structure of these host-guest systems can thus be regarded as a superposition of the electronic structures of the zeolite and of the silver sulfide clusters. It was, however, found that the co-cations influence the optical properties of silver sulfide clusters to a certain extent. The most obvious influence was observed in the presence of potassium co-cations which are supposed to interact specifically with silver sulfide.

The optical properties of the otherwise colorless zeolite A crystals change completely by the presence of the silver sulfide clusters. The amount and the size of the clusters can be varied in a well controlled way during the synthesis, resulting in differently colored materials, which all show photoluminescence in the visible. The color of the luminescence ranges from blue-green (Ag_2S monomer) over different kind of yellow and orange to red depending on the size and on the ratio of the differently luminescent clusters.

Excited Ag_2S can transfer its excitation energy to Ag_4S_2 . One can imagine that the excitation energy could also be transferred to the external surface of the zeolite if suitable acceptors are there. In zeolite L this was done by modifying the external surface with different dye molecules and monodirectional energy transfer from the dyes inside the zeolite to the outside or the other way round was observed.^[60,67,68] In zeolite A three-dimensional energy transfer would be expected.

The optical properties are sensitive to water, to co-cations, and to temperature. So one can consider a zeolite A crystal containing silver sulfide clusters as a microsensor. A clear change of the samples color occurs upon addition of silver ions to yellow Ag_2S -CaA samples, which afterwards become orange. The most obvious changes of the luminescence properties are observed after addition of potassium ions. How sensitive these systems really are to small amounts of Ag^+ and K^+ has to be checked in further

experiments. The strong temperature dependence of the luminescence of all Ag_2S -zeolite A materials could be used for thermometry. The change of the luminescence with temperature is in all samples reversible. The most interesting samples for luminescence thermometry are Ag_2S -CaA containing Ag_2S and Ag_4S_2 and Ag_2S -KA. In Ag_2S -CaA the color of the luminescence changes with temperature due to a stronger thermal quenching of the luminescence of Ag_4S_2 than of Ag_2S . The ratio of the two luminescence bands can be measured over a large temperature range (from $-190\text{ }^\circ\text{C}$ or below up to room temperature). For a more narrow temperature range Ag_2S -KA samples may be suited. These samples show luminescence thermochromism, which means that around $-50\text{ }^\circ\text{C}$ a new luminescence band at 710 nm appears and becomes stronger with increasing temperature and the low-temperature luminescence disappears.

One step towards potential applications of these materials was done by developing a method to arrange the zeolite A crystals as monolayers on different substrates. It could be shown that it is possible to prepare first the zeolite monolayers and then load the zeolites with silver sulfide. The same method was used to modify AgCl electrodes for photocatalytic water splitting. First experiments showed promising results, so that it is worth to continue this work.

Another potential application of these luminescent host-guest systems could be in biotechnology. Coupling inorganic nanoparticles to biomolecules for diagnostics and analytical tests attracts a lot of current interest.^[69] Luminescent nanoparticles coupled via a linker molecule to a specific protein allow, for example, very sensitive detection of antibody-antigen recognition. By means of confocal microscopy one can also observe the diffusion of labeled biomolecules to their receptors. Compared to organic dyes used as luminescent labels, inorganic compounds are expected to be more stable against photobleaching and their usually long luminescence lifetimes allow time-delayed fluorescence measurements, which can be used to suppress the autofluorescence of biological matrices. So far, mainly CdS nanoparticles^[70,71] and CdSe /core-shell (shell ZnS or CdS) nanoparticles^[72,73] have been applied as luminescent biological labels. Luminescent zeolite A nanocrystals would be a nontoxic alternative. The zeolite surface could, for example, be modified by silanes, which are discussed in Ref. [69] as typical linker molecules, and which have been used to couple SiO_2 -coated nanoparticles to biomolecules. In Figure 7.1.1 the structures of two potential linker molecules are shown.

A prerequisite for the use of zeolites as biological labels is that one has zeolite crystals in the nanometer-scale. The synthesis of nano-sized zeolite crystals has already been realized for zeolite L.^[74] This task could probably also be fulfilled for zeolite A by further developing the synthesis procedure 3 (chapter 6.1) and/or by finding a suitable method for

size-separation of these small crystals e.g. by fractional centrifugation. To be competitive with the current luminescent labels the Ag_2S -zeolite A materials have to be highly luminescent. It was shown in this work that the luminescence intensity at room temperature depends on the co-cations, hence they have to be considered.

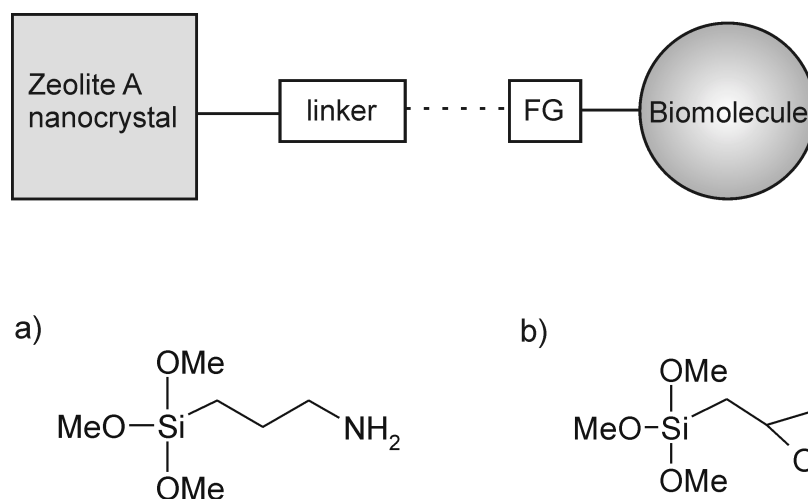


Figure 7.1.1: Schematic representation of a method to couple zeolite A nanocrystals and biomolecules. FG stands for the functional coupling group of the biomolecule. In a) and b) two potential linker molecules are shown.

Although Ag_2S -zeolite A materials show many interesting optical properties, some of the mechanisms behind are not yet understood. Using additional analytical methods may give a deeper insight. It would be worth, for example, to find a method to investigate the interaction of the co-cations with the silver sulfide clusters. Some information may be obtained by IR and Raman spectroscopy. The IR transitions are expected to be at low frequency, similar to what was observed in $\text{Ag}_2\text{S-B}_2\text{S-Ge}_2\text{S}$ glasses, where the vibrations of Ag^+ are at 110 cm^{-1} .^[75] So KBr as a matrix and also monolayers on quartz or on ZnSe are not suited. A possibility would be to prepare thin self-supporting wafers of zeolite A as described in Ref. [33]. Another possibility is to analyze the samples by means of extended x-ray absorption fine structure spectroscopy (EXAFS). EXAFS data give information about the nearest neighbors of an atom and about bond lengths. It would even help to determine the structure and the position of the silver sulfide clusters in zeolite A.

8. References

- [1] a) L. Brus, *J. Phys. Chem.* **1986**, *90*, 2555. b) M. Nirmal, L. Brus, *Acc. Chem. Res.* **1999**, *32*, 407.
- [2] Y. Wang, N. Herron, *J. Phys. Chem.* **1991**, *95*, 525.
- [3] J. Nanda, S. Sapra, D.D. Sarma, N. Chandrasekharan, G. Hodes, *Chem. Mater.* **2000**, *12*, 1018.
- [4] A. van Dijken, E. A. Meulenkaamp, D. Vanmaekelbergh, A. Meijerink, *J. Lumin.* **2000**, *87-89*, 454.
- [5] F. W. Wise, *Acc. Chem. Res.* **2000**, *33*, 773.
- [6] a) D. T. Talapin, S. Haubold, A. L. Rogach, A. Kornowski, M. Haase, H. Weller, *J. Phys. Chem. B* **2001**, *105*, 2600; b) T. Vossmeier, L. Katsikas, M. Giersig, I. G. Popovic, K. Diesner, A. Chemseddine, A. Eychmüller, H. Weller, *J. Phys. Chem.* **1994**, *98*, 7665.
- [7] S. K. Poznyak, D. V. Talapin, E. V. Shevchenko, H. Weller, *Nano Lett.* **2004**, *4*, 693.
- [8] S. F. Wuister, A. van Houselt, C. de Mello Donega, D. Vanmaekelbergh, A. Meijerink, *Angew. Chem. Int. Ed.* **2004**, *43*, 3029.
- [9] D. Brühwiler, R. Seifert, G. Calzaferri, *J. Phys. Chem. B* **1999**, *103*, 6397.
- [10] Dominik Brühwiler, PhD thesis **2001**, University of Bern.
- [11] Stephan Glaus, PhD thesis **2002**, University of Bern.
- [12] L. Motte, M. P. Pileni, *Applied Surface Science* **2000**, *164*, 60.
- [13] K. Akamatsu, S. Takei, M. Mizuhata, A. Kajinami, S. Deki, S. Takeoka, M. Fujii, S. Hayashi, K. Yamamoto, *Thin Solid Films* **2000**, *359*, 55.
- [14] X. Qian, J. Yin, S. Feng, S. Liu, and Z. Zhu, *J. Mater. Chem.* **2001**, *11*, 2504.
- [15] R. V. Kumar, O. Palchik, Y. Koltypin, Y. Diamant, A. Gedanken, *Ultrasonics Sonochemistry* **2002**, *9*, 65.
- [16] L. Armelao, R. Bertoncello, E. Cattaruzza, S. Gialanella, S. Gross, G. Mattei, P. Mazzoldi, and E. Tondello, *J. Mater. Chem.* **2002**, *12*, 2401.
- [17] D. Brühwiler, C. Leiggenger, S. Glaus, G. Calzaferri, *J. Phys. Chem. B* **2002**, *106*, 3770.
- [18] S. T. King, *J. Catalysis* **1996**, *161*, 530.
- [19] S. M. Kanan, C. P. Tripp, R. N. Austin, H. H. Patterson, *J. Phys. Chem. B* **2001**, *105*, 9441.

-
- [20] M. Anpo, M. Matsuoka, K. Hanou, H. Mishima, H. Yamashita, H. H. Patterson, *Coordination Chemistry Reviews* **1998**, 171, 175.
- [21] J. Weitkamp, A. Raichle, Y. Traa, *Appl. Cat. A* **2001**, 222, 277.
- [22] W. Sachtler, *Acc. Chem. Res.* **1993**, 26, 383.
- [23] D. Brühwiler, G. Calzaferri, *Microporous and Mesoporous Materials* **2004**, 72, 1-23.
- [24] K. Kuge, G. Calzaferri, *Microporous and Mesoporous Materials* **2003**, 66, 15.
- [25] M. Wark, G. Schulz-Ekloff, N. I. Jaeger, *Bulg. Chem. Comm.* **1998**, 30, 129.
- [26] A. A. Demkov, O. F. Sankey, *J. Phys.: Condens. Matter* **2001**, 13, 10433.
- [27] D. W. Breck, *Zeolite Molecular Sieves*, **1974** John Wiley & Sons, Inc., p. 83-92; 530-540.
- [28] M. Meyer, C. Leiggenger, G. Calzaferri, in preparation
- [29] D. W. Breck, W. G. Eversole, R. M. Milton, T. B. Reed, T. L. Thomas, *J. Am. Chem. Soc.* **1956**, 78, 5963.
- [30] Roland Seifert, PhD thesis **1999**, University of Bern
- [31] M. Ralek, P. Jiru, O. Grubner, H. Beyer, *Collect. Czech. Chem. Commun.* **1962**, 27, 142.
- [32] T. Sun, K. Seff, *Chem. Rev.* **1994**, 94, 857.
- [33] J. Baumann, R. Beer, G. Calzaferri, B. Waldeck, *J. Phys. Chem.* **1989**, 93, 2292.
- [34] R. Seifert, A. Kunzmann, G. Calzaferri, *Angew. Chem. Int. Ed.* **1998**, 37, 1521.
- [35] R. Seifert, R. Rytz, G. Calzaferri, *J. Phys. Chem. A* **2000**, 104, 7473.
- [36] G. Calzaferri, R. Giovanoli, I. Kamber, V. Shklover, R. Nesper, *Res. Chem. Intermed.* **1993**, 19, 31.
- [37] J. J. Pluth, J. V. Smith, *J. Phys. Chem.* **1979**, 83, 741.
- [38] J. J. Pluth, J. V. Smith, *J. Am. Chem. Soc.* **1980**, 102, 4704.
- [39] P. Junod, *Helv. Phys. Act.* **1959**, 32, 567.
- [40] S. Miyatani, *J. Phys. Soc. Japan* **1968**, 24, 328.
- [41] S. Kitova, J. Eneva, A. Panov, *J. Imag. Sci. Tech.* **1994**, 38, 484.
- [42] a) T. Tani, *J. Imag. Sci. Tech.* **1995**, 39, 386; b) T. Tani, *J. Imag. Sci. Tech.* **1998**, 42, 135.
- [43] A. P. Marchetti, K. Lushington, R. Baetzold, *J. Phys. Chem. B* **2003**, 107, 136.
- [44] A. Corma, H. Garcia, *Eur. J. Inorg. Chem.* **2004**, 1143-1164.

- [45] A. Fukuoka, N. Higashimoto, Y. Sakamoto, M. Sasaki, N. Sugimoto, S. Inagaki, Y. Fukushima, M. Ichikawa, *Catalysis Today* **2001**, *66*, 23.
- [46] D. Sendor, U. Kynast, *Adv. Mater.* **2002**, *14*, 1570.
- [47] Claudia Leiggenger, Diploma thesis **2001**, University of Bern
- [48] Th. Förster, *Z. Naturforschung* **1949**, *4a*, 321.
- [49] D. Schürch, A. Currao, S. Sarkar, G. Hodes, G. Calzaferri, *J. Phys. Chem. B* **2002**, *106*, 12764.
- [50] Vanga Raja Reddy, PhD thesis in preparation, University of Bern.
- [51] M. Lanz, D. Schürch, G. Calzaferri, *J. Photochem. Photobiol. A: Chem.* **1999**, *120*, 105.
- [52] a) G. Calzaferri, D. Brühwiler, S. Glaus, D. Schürch, A. Currao, C. Leiggenger, *J. Imag. Sci. Technol.* **2001**, *45*, 331; b) A. Currao, V. R. Reddy, M. van Veen, R. E. I. Schropp, G. Calzaferri, *Photochem. Photobiol. Sci.* **2004**, *3*, 1017.
- [53] A. Currao, V. R. Reddy, G. Calzaferri, *ChemPhysChem* **2004**, *5*, 720.
- [54] Gion Calzaferri, Claudia Leiggenger, Stefan Huber, Dominik Brühwiler, and Arantzazu Zabala Ruiz, *Proceedings European Coatings Conference, Smart coatings III, Berlin, June 7-8, 2004*, 93-109.
- [55] I. Braun, G. Ihlein, F. Laeri, J. U. Nöckel, G. Schulz-Ekloff, F. Schüth, U. Vietze, O. Weiss, D. Wöhrle, *Appl. Phys. B* **2000**, *70*, 335.
- [56] a) A. V. Malko, A. A. Mikhailovsky, M. A. Petruska, J. A. Hollingsworth, H. Htoon, M. G. Bawendi, V. I. Klimov, *Appl. Phys. Lett.* **2000**, *81*, 1303; b) V. I. Klimov, A. A. Mikhailovsky, S. Xu, A. Malko, J. A. Hollingsworth, C. A. Leatherdale, H.-J. Eisler, M. G. Bawendi, *Science* **2000**, *290*, 314.
- [57] S. L. McCall, A. F. J. Levi, R. E. Slusher, S. J. Pearton, R. A. Logan, *Appl. Phys. Lett.* **1992**, *60*, 289.
- [58] a) K. Ha, Y.-J. Lee, H. J. Lee, and K. B. Yoon, *Adv. Mater.* **2000**, *12*, 1114; b) A. Kulak, Y.-J. Lee, Y. S. Park, and K. B. Yoon, *Angew. Chem.* **2000**, *112*, 980; *Angew. Chem. Int. Ed.* **2000**, *39*, 950; c) K. Ha, Y.-J. Lee, D.-Y. Jung, J. H. Lee, and K. B. Yoon, *Adv. Mater.* **2000**, *12*, 1614.
- [59] S. Huber, G. Calzaferri, *ChemPhysChem* **2004**, *5*, 239.
- [60] G. Calzaferri, S. Huber, H. Maas, C. Minkowski, *Angew. Chem.* **2003**, *115*, 3860; *Angew. Chem. Int. Ed.* **2003**, *42*, 3732.
- [61] David Schürch, PhD thesis **2002**, University of Bern.
- [62] G. Calzaferri, C. Leiggenger, S. Glaus, D. Schürch, K. Kuge, *Chem. Soc. Rev.* **2003**, *32*, 29.

- [63] P. Lainé, R. Seifert, R. Giovanoli, G. Calzaferri, *New J. Chem.* **1997**, 21, 453.
- [64] H. H. Perkampus, *UV-VIS Spectroscopy and its applications*, Springer ISBN 3-540-55421-1, p. 95- 101.
- [65] Andreas Kunzmann, PhD thesis **1996**, University of Bern.
- [66] Marc Meyer, PhD thesis **2005**, University of Bern.
- [67] Huub Maas, PhD thesis **2003**, University of Bern.
- [68] T. Ban, D. Brühwiler, G. Calzaferri, *J. Phys. Chem. B* **2004**, 108, 16348.
- [69] C. M. Niemeyer, *Angew. Int. Ed.* **2001**, 40, 4128.
- [70] a) R. Mahtab, H. H. Harden, C. J. Murphy, *J. Am. Chem. Soc.* **2000**, 122, 14; b) R. Mahtab, J. P. Rogers, C. J. Murphy, *J. Am. Chem. Soc.* **1995**, 117, 9099.
- [71] M. L. Curri, A. Agostiano, G. Leo, A. Mallardi, P. Cosma, M. Della Monica, *Mater. Sci. Eng. C* **2002**, C 22, 449.
- [72] W. C. Chan, S. Nie, *Science* **1998**, 281, 2016.
- [73] M. Bruchez, M. Moronne, P. Gin, S. Weiss, A. P. Alivisatos, *Science* **1998**, 281, 2013.
- [74] A. Zabala Ruiz, D. Brühwiler, T. Ban, G. Calzaferri, *Monatsh. Chem.* **2005**, in press.
- [75] Q. Mei, J. Saienga, J. Schrooten, B. Meyer, S. W. Martin, *J. Non-Crystalline Solids* **2003**, 324, 264.

9. Summary

Due to the fast development of nanotechnology, the synthesis and characterization of nanosized semiconductor particles continues to attract considerable interest. While much work has been done on a large number of different semiconductor clusters, quite little is known about the properties of small silver sulfide species. In our group a synthesis procedure has been developed, which yields very stable host-guest systems where the host material is zeolite A and the guests are silver sulfide species in the molecular size regime. Zeolite A provides a suitable cavity structure for the in situ synthesis of silver sulfide clusters and prevents further aggregation of the small clusters into larger ones or bulk. The smallest silver sulfide particle found in zeolite A is the Ag_2S monomer. This was the first time that Ag_2S monomers could be stabilized in a way that spectroscopic investigations became possible.

This thesis gives a deeper insight into the optical properties of Ag_2S -zeolite A systems. It was found that these materials emit visible light when they are irradiated with UV light. The color of the emitted light depends on the size of the silver sulfide clusters. Ag_2S monomers emit green light, while the color of the emission of the dimers, Ag_4S_2 , is orange. It is possible to synthesize samples containing Ag_2S and Ag_4S_2 in the same zeolite crystals, resulting in a yellow colored emission. The presence of larger silver sulfide clusters than Ag_4S_2 leads to a red-shift of the emission. Within this work it was tried to find explanations for the processes inside these systems and to investigate the influences on their optical properties. It was found that some of these materials are sensitive to environmental changes such as temperature, water, and specific cations by reversibly changing their optical properties. A single zeolite A crystal containing Ag_2S and Ag_4S_2 particles can, for example, be regarded as a tiny luminescent thermometer because the color of the emitted light changes with temperature. The reason for that is a stronger thermal quenching of the luminescence of Ag_4S_2 than of the luminescence of Ag_2S . The results obtained from time-resolved luminescence spectroscopy on these systems indicate that electronically excited Ag_2S can transfer its excitation energy to a neighboring Ag_4S_2 . An overview of the luminescence properties of Ag_2S and Ag_4S_2 in zeolite A has been published in the *Journal of Materials Chemistry* (*J. Mater. Chem* **2003**, 13, 1969). On exchanging the charge compensating cations of zeolite A for potassium ions a new phenomenon appears, which corresponds to what is known as luminescence thermochromism. We observed that zeolite A samples containing K^+ and silver sulfide show, at room temperature, a bright deep-red photoluminescence with its maximum

emission at 710 nm, suggesting a specific interaction of K^+ with the silver sulfide clusters. This interaction is strongest at room temperature and becomes weaker with decreasing temperature until only the luminescence of Ag_2S and Ag_4S_2 is observed. K^+ can also be added after the silver sulfide synthesis and the detection of the red luminescence is then a proof of the presence of potassium ions.

The observations reported in this PhD thesis show that Ag_2S -zeolite A systems have the potential to be among a challenging class of materials for the development of new optoelectronic devices. One step towards this direction was done by finding a method to arrange zeolite A crystals as monolayers on different substrates. It could be shown that it is possible to prepare first the zeolite monolayers and then successfully load the zeolites with silver sulfide in a well controlled way. The preparation of these luminescent zeolite A monolayers has been reported in *ChemPhysChem* (2004, 5, 1593). The same principle was extended for preparing Ag_2S -zeolite A modified AgCl-electrodes for photocatalytic water splitting. First experiments, in which AgCl-electrodes were combined with Ag^+/Ag_2S -zeolite A monolayers, have shown promising results.

List of Publications

Dominik Brühwiler, Claudia Leiggener, and Gion Calzaferri

Silver Ions and Quantum-Sized Silver Sulfide Clusters in Zeolite A

Proceedings of the 13th International Zeolite Conference, Montpellier, France, July 8–13, **2001**, Elsevier electronic form (number of pages 6).

Dominik Brühwiler, Claudia Leiggener, Stephan Glaus, and Gion Calzaferri

Luminescent Silver Sulfide Clusters

J. Phys. Chem. B **2002**, *106*, 3770-3777.

Gion Calzaferri, Dominik Brühwiler, Stephan Glaus, David Schürch, Antonio Currao, and Claudia Leiggener

Quantum-Sized Silver, Silver Chloride and Silver Sulfide Clusters

J. Imaging Science and Technology **2001**, *45*, 331-339.

Gion Calzaferri, Claudia Leiggener, Stephan Glaus, David Schürch, and Ken'ichi Kuge

The Electronic Structure of Cu⁺, Ag⁺, and Au⁺ Zeolites

Chem. Soc. Rev. **2003**, *32*, 29-37.

Claudia Leiggener, Dominik Brühwiler, and Gion Calzaferri

Luminescence Properties of Ag₂S and Ag₄S₂ in Zeolite A

J. Mater. Chem. **2003**, *13*, 1969-1977.

Gion Calzaferri, Stephan Glaus, Claudia Leiggener, and Ken'ichi Kuge

Electronic Structure of Zeolite Stabilized Ions and Quantum Dots

Host-Guest Systems Based on Nanoporous Crystals, Eds. F. Laeri, F. Schüth, U. Simon, and M. Wark, Wiley-VCH **2003**, ISBN 3-527-30501-7, p. 424-450.

Gion Calzaferri, Claudia Leiggener, Stefan Huber, Dominik Brühwiler, and Arantzazu Zabala Ruiz

Supramolecular Organization of Dyes and Quantum Dots in Zeolites: Light Harvesting Host-Guest Antenna Systems

Proceedings European Coatings Conference, Smart coatings III, Berlin, June 7-8, **2004**, 93-109.

Claudia Leiggener and Gion Calzaferri

Monolayers of Zeolite A containing Luminescent Silver Sulfide Clusters

Chem.Phys.Chem. **2004**, *5*, 1593-1596.

Gion Calzaferri, Olivia Bossart, Dominik Brühwiler, Stefan Huber, Claudia Leiggener,
Marieke van Veen, and Arantzazu Zabala Ruiz

**Light-harvesting Host-Guest Antenna Materials for Quantum Solar Energy
Conversion Devices**

Proceedings IPS15 Comptes Rendus, Chimie, special issue.

Conference Contributions

Oral presentations

Third International Conference on Inorganic Materials, 7.-10. September 2002, Konstanz, Germany

Fall Meeting 2002 of the Swiss Chemical Society, 17. October 2002, Basel, Switzerland

SGPP-Graduate Student Symposium 2003 (Swiss Group for Photochemistry and Photobiology), 11./12. April 2003, Fribourg, Switzerland

Particles 2003 (Imaging, Printing and marking applications of Particle Technology), 23.-26. August 2003, Toronto, Canada

Poster presentations

UPS 2001, International Conference on Unconventional Photoactive Systems, 4. – 8. September 2001, Les Diablerets, Switzerland

Séminaire Hors-Ville de 3ème Cycle en Chimie Physique, 16.-20. September 2002, Champéry, Switzerland

HRSM & EPA Summer School "New Perspectives in Photochemistry", 28. June - 2. July 2003, Egmond aan Zee, Holland

Fall Meeting 2003 of the Swiss Chemical Society, 9. October 2003, Lausanne, Switzerland

Perspectives of Photochemistry in the New Millenium (Tetranational Symposium Austria-Germany-Hungria-Switzerland), 7.-11. March 2004, Bad Gastein, Austria

IPS-15 (15th International Conference on Photochemical Conversion and Storage of Solar Energy), 4.-9. July 2004, Paris, France

Curriculum Vitae

Name: Leiggener
First Name: Claudia
Date of birth: 19. Mai 1976
Place of birth: Bern
Place of origin: Ausserberg (VS)

Education

1983 – 1992: Primar- und Sekundarschule in Bern
1992 – 1996: Literargymnasium Kirchenfeld, Bern; Matura Typus B
1996 – 2001: Studies in chemistry at the Department of Chemistry and Biochemistry, University of Bern
2001: Diploma in chemistry, diploma thesis under the supervision of Prof. Dr. Gion Calzaferri
2001 – 2004: PhD thesis in physical chemistry under the supervision of Prof. Dr. Gion Calzaferri

Assistance

2001: Teaching assistant in the practical course "Qualitative anorganische Analyse" for pharmacists
2001 – 2004: Teaching assistant in the practical course "Physikalische Chemie II" for chemists
2002 – 2003: Teaching assistant in the practical course "Photochemie" for chemists

Diploma thesis

"Herstellung und Eigenschaften grössenquantisierter Silbersulfid-Cluster in Zeolith A", 2001

PhD thesis

"Luminescent Silver Sulfide Clusters in Zeolite A", 2004